Atmospheric Sciences Research Center
University at Albany
State University of New York
100 Fuller Road
Albany, NY 12222

TO: John Ritter
NASA Langley Research Center

NASA Scientific and Technical Information Facility
P. O. Box 8757
Baltimore and Washingto International Airport, MD 21240

FROM: David R. Fitzjarrald
Atmospheric Sciences Research Center
State University of New York, Albany

SUBJECT: **Final Report NAG1692**
Measurement of the Amazon forest canopy interaction with the atmosphere.

We have now completed work on this project. Data have been submitted to the GTE ABLE Archive. Rather than submit a separate report, we are enclosing copies of two papers that have been submitted for publication in the Journal of Geophysical Research. These papers are: "Daytime turbulent exchange between the Amazon forest and the atmosphere" and "Nocturnal exchange between rain forest and atmosphere," by myself, K. E. Moore, and coauthors.

DAYTIME TURBULENT EXCHANGE BETWEEN THE AMAZON FOREST AND THE ATMOSPHERE

by

David R. Fitzjarrald and Kathleen E. Moore
Atmospheric Sciences Research Center
State University of New York at Albany

Osvaldo M. R. Cabral
Centro Nacional de Pesquisa da Seringueira e Dendé-EMBRAPA
Manaus, Amazonas, Brazil

José Scolar[1]
Instituto Astronômico e Geofísico
Departamento de Meteorologia
Universidade de São Paulo
São Paulo, SP, Brazil

Antônio O. Manzi and Leonardo D. de Abreu Sá
Instituto de Pesquisas Espaciais
São José dos Campos, SP, Brazil

[1]Current affiliation: Instituto de Pesquisas da Meteorologia, Universidade Estadual de São Paulo, Bauru, SP, Brazil

ABSTRACT

Detailed observations of turbulence just above and below the crown of the Amazon rain forest during the wet season are presented. The forest canopy is shown to remove high frequency turbulent fluctuations while passing lower frequencies. Filter characteristics of turbulent transfer into the Amazon rain forest canopy are quantified. Simple empirical relations that relate observed turbulent heat fluxes to horizontal wind variance are presented. Changes in the amount of turbulent coupling between the forest and the boundary layer associated with deep convective clouds are presented both as statistical averages and as a series of case studies. These convective processes during the rainy season are shown to alter the diurnal course of turbulent fluxes. In wake of giant coastal systems, no significant heat or moisture fluxes occur for up to a day after the event. Radar data is used to demonstrate that even small raining clouds are capable of evacuating the canopy of substances normally trapped by persistent static stability near the forest floor . Recovery from these events can take more than an hour, even during mid-day. In spite of the ubiquitous presence of clouds and frequent rain during this season, the average horizontal wind speed spectrum is well described by dry CBL similarity hypotheses originally found to apply in flat terrain. Diurnal changes in the sign of the vertical velocity skewness observed above and inside the canopy are shown to be plausibly explained by considering the skewness budget.

1. Introduction

Much of the concern in forest-atmosphere interaction to date has been in determining the heat, moisture, and momentum budgets over forests (Hutchison and Hicks, 1985). The desire among atmospheric chemists to determine natural sources and sinks of radiatively active trace gases in forests has increased interest in understanding the mechanisms of mass transport between the canopy and the atmosphere. Although transports of the trace gases are often inferred by analogy with those of heat and momentum, for example, these sources and sinks are concentrated in the upper canopy, while sources deeper in the forest may also be important to trace gases. Only a small number of observational studies of the turbulent properties of the canopy and above-canopy layers in forest environments anywhere have been published, and few of these have been conducted in the large tropical rain forests.

The structure of the Amazon rain forest is such that little (1-3%) of incident solar radiation reaches the forest floor (Shuttleworth, et al., 1984b). Because in rain forests there is a dense canopy cover formed by the tallest trees, much of the short-wave radiation is absorbed and long wave radiation emitted to the atmosphere in the upper 20% of the canopy. Thus, the heat budget during the daytime refers mainly to processes occurring near canopy top. The presence of leaves in the same layer also means that the moisture flux is concentrated there, though it is possible that momentum flux may be felt through a somewhat deeper layer. The result of radiative heating is that between forest floor and upper canopy there is nearly always a layer that is statically stable in the mean, both day and night, as illustrated in Fig. 1, and this circumstance poses great difficulties for the use of simple flux-gradient models of deep canopy exchange processes. Other important atmospheric constituents do not have sources and sinks coincident in the upper canopy. For example, carbon dioxide is absorbed during the daytime in the foliar upper canopy but is emitted primarily by decay processes at the forest floor. Thus, for example, to understand exchange processes that accomplish the diurnal cycle of CO_2 emission (see Fan *et al.* , 1989) or nitrogen oxide emission (Bakwin *et al.* , 1989), it is necessary to consider processes that lead to coupling through the entire canopy layer.

In this paper we examine mechanisms associated with the turbulent exchange of heat, momentum, and moisture between the Amazon forest and the lower atmosphere during the wet season, with the aim to relate these mechanisms to transports of trace gases into or out of the canopy. In earlier work during the Amazon dry season (Fitzjarrald *et al.* , 1988), we studied the properties of the surface layer just above the Amazon forest canopy. In addition, we also consider the coupling between the atmosphere and the mid-canopy level. Since fluxes of the thermodynamic quantities are largest during the day and because of fundamental differences in the static stability

regimes within and just above the canopy, we discuss the daytime situation in this paper, deferring the nocturnal case to a companion paper (Fitzjarrald and Moore, this volume). The weak daytime stable layer near the forest top is thin, bounded below by a more stable layer and above by the convective surface layer, and it is fragile, being punctured at intervals by penetrating gusts. The nocturnal stable layer in the canopy is an extension of the stable boundary layer that reaches above 300 m (Martin *et al.*, 1988).

Because of the continuing need by modellers for knowledge of the bulk properties (roughness and displacement lengths, transport resistances) of different surfaces, it is customary to study forest-atmosphere relations in terms of structural characteristics inferred from profile observations. It is often difficult to determine momentum and temperature gradients just above the canopy and, for various reasons, they do not always follow the same logarithmic laws essential to application of the hypothesis that the canopy top acts just like a plane surface displaced upwards. Direct observation of fluxes is preferable to inferring them from gradients.

Though perfect knowledge of the bulk properties in principle allows one to estimate the response of the forest to given forcing, it is arguably just as important to gather information on what this forcing is, especially when one is dealing with a data-sparse region such as the Amazon forest during such a chaotic period as the wet season. The distinction between forcing and response is only a useful prototype, and one expects it to be most applicable when one considers processes such as storm outflows or convective boundary layer eddies that do not depend directly on details of the surface. At the scale of shear-dominated turbulence just above the canopy, the prototype does not work as well. Fortunately, recent work (Hunt *et al.*, 1988; Kaimal, 1978) shows that large and small scale turbulence in the surface layer may be described as statistically nearly independent distributions. In this paper we aim to describe the atmospheric forcing and then consider the forest "response", the fluxes at canopy top and motions within the canopy that result from the winds above.

In section 2, we present the experimental design for micrometeorological measurements in ABLE-2b and discuss the site, instrumentation, data analysis techniques and available data. In section 3, we present summary results of statistics for the four-week period of the experiment, illustrating modulation of the surface layer winds by both diurnal cycles and by large scale convective cloud systems. From average daytime data we identify dominant scales of motion. In this section we also consider relevant differences between the surface layer above the Amazon forest canopy and the more extensively studies plane surface layers. In section 4, we focus on the vertical coupling of the layer just above the canopy and that just below the crown. Turbulent fluctuations inside the canopy are considered as filtered versions of fluctuations above. In section 5 we address the response of the forest to cloud convective downdrafts through a series of case studies. The aim is to relate radar echo passage near the tower to gusts observed at canopy top. Then these gusts are related to the degree and depth of mixing into the canopy. In section 6, we identify relationships between directly measured turbulent fluxes and simpler, more readily available measurements.

Conclusions and suggestions for future work are in section 7.

2. Experimental design and execution

Our selection and deployment of instrumentation was guided by a desire to document transient mixing episodes associated with raining convection and to study the statistical properties of the vertical coupling between the atmosphere just above the forest and the air below the canopy crown. Thus, our focus included processes that occur on the order of seconds to minutes, and it was necessary to record data at more frequent intervals than in previous field campaigns. The primary observations presented here were made at the 45-m micrometeorological tower at the Ducke Forest Reserve (2°57'; S, 59°57'W). Shuttleworth *et al.* (1984a) and Sá *et al.* (1986) present descriptions of the vegetation near the site. Trees in the region have an approximate height of 35m, varying from 20 to 42 m, with plant density of approximately 3000 trees/ha (Shuttleworth *et al.*, 1984a). The dense canopy is not layered but is continuous from the 3-5 m tall palms to the tallest trees at about 35 m. Occasional emergent trees reach 40 m or more in height.

Instrumentation. Observations presented in this paper were made by four automatic Portable Automated Mesonet (PAM) stations located on towers just above the rain forest canopy, by the 3-cm radar operated at Eduardo Gomes airport near Manaus, Amazonas, Brazil. Details of the PAM network location and the operating characteristics of the radar are given in Garstang *et al.* (1989). In this paper we draw on time series of horizontal winds and rainfall amount from the PAM stations, and constant altitude plan-position indicator (CAPPI) echo images from the radar. Profile measurements of wind speed, temperature and humidity at the Ducke tower were made at the levels indicated in Table 1 and incident solar and net radiation were observed at canopy top by the team from the Instituto de Pesquisas Espaciais (INPE). Because of some technical difficulties with the net radiation measurement during the day, we do not discuss the heat budget here. Heat balance estimates at Ducke Forest have been presented previously by Shuttleworth *et al* (1984a), Sá *et al.* (1986), and Fitzjarrald *et al.* (1988). The radiation and profile instruments and the data acquisition system are the same as those described by Shuttleworth *et al.* (1985) with two modifications. First, the data were acquired at five-minute instead of the previously used twenty-minute interals, and wind speed sensors at 30m, 25m, and 13m were replaced by Thornthwaite low-threshold cup anemometers.

Sets of rapid-response turbulence instruments, identical to those discussed in Fitzjarrald *et al.* (1988) were installed at 45 m (level 1), 39 m (level 2), and 20 m (level 3). Each set of instruments consisted of a Campbell Scientific vertical sonic anemometer with fine-wire thermocouple and a Campbell Scientific krypton hygrometer. Instrument response characteristics and appropriate references were given in Fitzjarrald *et al.* (1988). At the 45 m level a Gill propeller-vane anemometer was operated. Data acquisition was done using the Campbell Scientific Datalogger, to calculate and record moments, fluxes, and average quantities. The Datalogger sampled each sensor at 2 second intervals. Raw data from thirteen fast channels were also recorded at 10 Hz onto the

hard disk of a PDP 11/73. These data were backed up twice daily to floppy disks. The thirteen signals included w, T, and q at three levels, wind speed and direction from the Gill anemometer, and two signals from the Harvard group, from their fast-response ozone and carbon dioxide instruments. Details of these instruments are presented by Fan *et al.* (1989). Despite the difficulty of operating during the rainy season, a total of 138 hours of raw data were collected during the experiment. Data from the Gill anemometer were recorded by the Datalogger for three weeks continuously. Because the sonic anemometers were damaged by rain, there are long periods when only one of the above-canopy instruments were operating. Turbulent moment data presented in this paper were calculated by defining fluctuation to be the deviation from a centered, five-minute running mean filter operating on the raw, ten-herz signal. A summary of the instrument locations is given in Table 1.

3. Temporal variation and diurnal cycles.

On days without strong convection, strong daytime surface heat flux leads to rapid convective boundary layer growth and cloud formation (Martin *et al.*, 1988). After noon, appreciable cloud development occurs, and satellite images of the region show diurnal pulsing in cloud amount. During the wet season, the diurnal pattern may be enhanced or disrupted by large organized cloud systems (Greco *et al.*, 1989). In this section we examine how these large systems punctuate the diurnal wind signal at the Ducke site. The longest time series we have are horizontal wind measurements from the Gill anemometer at Ducke tower and the four PAM stations. Average winds speeds during the wet season are light, with twenty minute averaged wind speeds rarely exceeding 4 m/s over the three week period shown in Fig. 2. Enhanced daytime turbulent mixing at canopy top leads to a stronger diurnal signal in σ_u than in the mean wind. It is clear that at the beginning of the experiment and the last twelve days show the most pronounced diurnal signal. Two periods with rainfall followed by very light winds and little diurnal variation (day 114 and days 120-123) were identified by Greco *et al.* as being dominated by large systems that propagated from the coast. Menzel *et al.* (1989) found from satellite analysis that large cirrus shields are left in the wake of these systems, and it seems reasonable that reduced solar radiation and evaporation of rainfall from leaves could reduce how convective the above canopy layer can be during these periods. This results in relatively long periods of time during which little turbulent exchange is likely to occur from the canopy. Techniques to estimate fluxes during these disturbed periods are discussed in section 6 below.

It is clear that after day 121 (1 May), diurnal changes in σ_u are pronounced, and the solar radiation record indicates that the average onset of appreciable convective cloudiness was approximately 11 LST. The average wind speed shows a drop in the afternoon (Fig. 3). The PAM stations also recorded the maximum gust in one-minute periods, but this also showed no afternoon increase.One might expect enhanced wind speed or σ_u due to the presence of convective clouds. Indeed, it is at this time of day that downdrafts from raining clouds were observed to occur. It

appears that these events, though potentially important to total transport out of the canopy (see section 5 below), are sufficiently infrequent to make a mark on the wind averages. The standard deviation in solar radiation does increase somewhat during the afternoon, reflecting the onset of convective cloudiness.

c. Characteristic turbulent scales. The spectrum of horizontal wind fluctuations in the atmospheric surface layer is broad in comparison with that of vertical velocity fluctuations. Kaimal (1978) showed that this broadening results from the influence of large eddies on the scale of z_i, the height of the convective boundary layer. Højstrup (1982) presented universal curve fits of spectra of horizontal wind fluctuations within and above the convective surface layer as a linear combination of a low wave number contribution from large eddies, whose size is determined by z_i, and a high wave number contribution from mechanical turbulence produced by shear near the surface. This is in accordance with the concept of statistical separation of the convective and mechanical contributions to horizontal velocity variance, recently emphasized by Hunt (1988). Over a nearly plane surface in the absence of significant cloud effects, one would therefore expect the horizontal wind speed spectrum above the forest canopy during the daytime to show the influence of CBL eddies in like manner. In the equatorial trough over the Amazon rain forest during the wet season, presence of variance partition based on the dry CBL scaling laws would seem unlikely. On the other hand, one observes convectively mixed layers in disturbed conditions in areas removed from the direct influence of cloud drafts in both the oceanic and continental equatorial tropics (Martin *et al.*, 1988; Fitzjarrald and Garstang, 1981).

Are eddies from the dry CBL in contributing to the daytime maximum in σ_u presented above (Fig. 3b)? An average daytime total wind speed spectrum was found using the one minute averaged wind data from each of the PAM stations for twelve days (Fig. 4). Taylor's hypothesis was used to convert from frequency to wavenumber, though we recognize that this may produce some distortion at the lowest wavenumbers. Except for transient periods near local clouds, the wind direction usually did not change significantly during the day, and we have used the total wind speed in this calculation rather than the along wind component. Similar spectra were obtained using the data from the other three PAM stations. An example of the high wavenumber end of the spectrum, based on data from the Gill anemometer at the micrometeorological tower at Ducke for a single afternoon, shows the expected inertial subrange law above wavenumbers of approximately 0.01 m^{-1}. At lower wavenumbers, a broad peak is seen, similar to that seen in the Minnesota and Kansas experiments (Kaimal, 1978). Højstrup's (1982) model spectrum that fits the Minnesota data for typical daytime values of z_i = 1.2 km, $z \to 0$, $-z_i/L = 12$, is included for comparison. Note that the spectrum here is scaled by σ_u^2 rather than by u_*^2. The empirical relation between these quantities (see Section 6 below) was used to convert the Højstrup spectrum to this normalization. The observed averaged spectrum agrees remarkably well with the model spectrum, and this indicates that the spectral peaks near 0.001 and near 0.003 m^{-1} probably correspond to the convective and the mechanical eddy scales, respectively. This is a surprising result. Despite the presence of active,

raining convection on many days, the scales of motion that produce horizontal wind speed variance on the average are the same as those seen over flat prairie during dry conditions.

What are the differences between the daytime surface layer above the Amazon and that seen in Kansas (i.e., a plane convective surface layer)? In the absence of nearby deep convective cloud activity in the daytime, a well-mixed convective boundary layer (CBL) develops over the Amazon (Martin *et al.*, 1988), just as is observed over flat terrain (Stull, 1988) and we have demonstrated that, in average, horizontal velocity spectra behave as they do over flat terrain. However, the layer just above the forest top, the canopy surface layer, does exhibit significantly different properties from the convective plane surface layer. Canopy surface layers are characterized by enhanced importance of turbulent transports of eddy fluxes and variances. For example, Maitani (1978), showed that the eddy transport of turbulent kinetic energy is negative over a rice canopy, while the same quantity is observed to be positive in plane surface layers. (Note, however, that the sign of the *transport* of TKE is downward in each instance). Raupach *et al.* (1980) observed a constant flux layer in which turbulent transports were important just above a model canopy top in the wind tunnel. They referred to this layer as the *roughness sublayer*, distinguishing it from a more conventional constant flux layer above, in which transports are less important. In contrast to the development of observational micrometeorology in the plane surface layer, much of the work above canopies has treated the neutral case, arguably an observational anomaly over the Amazon forest and probably elsewhere, as the time series of σ_u presented earlier (Fig.2b) indicates. Fitzjarrald *et al.* (1988) demonstrated that a similar roughness sublayer, with constant heat flux but appreciable buoyant and transport terms, exists over the Amazon forest, and showed that buoyancy production terms in the vertical velocity variance and heat flux budgets cannot be ignored.

We gain insight into the difference between plane and canopy surface layers and can estimate the height at which the boundary layer returns to its "normal", convective state by considering the properties of the third moment of the vertical velocity fluctuation, $\overline{w^3}$, or its normalized form, the vertical velocity skewness ($Sk_w = \overline{w^3}/\sigma_w^3$). Vertical velocity skewness is typically observed to be negative above and within plant canopies (i. e. Fitzjarrald *et al.*, 1988) and positive in convective plane surface layers (Chiba, 1978). At some level above the canopy, Sk_w changes sign, and it seems reasonable to regard this level to be a measure of the beginning of the "equivalent plane surface" layer. That $Sk_w < 0$ above canopies is due simply to the fact that there is something *below* the "surface" in canopy layers, and there can be downward turbulent transport of vertical velocity variance [we can write $\overline{w^3} = \overline{w\,(w^2)}$]. The skewness sign difference also persists at night, when all signs invert. These differences may be simply understood by following reasoning recently presented by Hunt *et al.* (1988, Appendix A). Hunt *et al.* combined the pressure-gradient and dissipation terms, assuming that they act to inhibit the growth of skewness over a relaxation time T_L . The approximate skewness budget can then be written as:

$$\overline{w^3}/T_L \approx (g/\Theta_o)\,\overline{w^2\theta} - \alpha\,\overline{w^2}\,\overline{\partial w^2/\partial z}\ , \qquad (1)$$

where Θ_o is a reference potential temperature, g the acceleration of gravity, α is a proportionality constant (=1/3 for Gaussian turbulence). The constant α comes from assuming a quasi-Gaussian form for $\overline{w^2}\partial\overline{w^2}/\partial z$. Other terms have their standard connotations. The sign of $\overline{w^3}$ (or Sk_w) is determined by the relative importance and sign of the buoyancy production term and the mechanical transport term.

a. Buoyancy term. The moment $\overline{w^2\theta}$ [considered as $\overline{w(w\theta)}$] is the transport term in the turbulent heat flux budget equation for $\partial\theta/\partial t$ or [considered as $\overline{w^2}\,(g\theta/\Theta_o)$] as the buoyancy contribution to $\overline{w^3}$. In the convective surface layer $\overline{w^2\theta} > 0$ (Antonia et al., 1982), and it is observed to be < 0 in stable conditions. Over a model canopy in the wind tunnel, Raupach *et al.* (1987) found $\overline{w^2\theta} < 0$ in a narrow band near a concentrated heat source at canopy top, though they assert that temperature fluctuations in this experiment behaved as a passive scalar. We find $\overline{w^2\theta} < 0$ during the daytime with $\overline{w^2\theta} \rightarrow 0$ at night over the Amazon forest at Ducke (Fig 5).

b. Variance transport term. Although the mechanical transport term is only approximate, one gets insight about the sign of the contribution of this term by considering the vertical profile of $\overline{w^2}$, itself of sufficient interest to warrant some discussion. A conceptual model of this profile, based on current knowledge of the CBL turbulence for daytime and nighttime conditions is presented in Fig. 6. It is convenient to view $\overline{w^2}$ above the canopy as a linear combination of mechanical and convective turbulent effects (Hunt, 1984; Hunt *et al.* , 1988), $\overline{w^2} = a\,u_*^2 + b\,w_*^2$, where u_*^2 (= $-\overline{uw}$) is the local friction velocity at a given height and w_* is the convective mixed layer velocity scale ($[(g/\Theta_o)\,\overline{w\theta}\,z_i]^{1/3}$). If we assume that the CBL is well mixed in horizontal wind speed and use the mixed layer form for $w_*^2(z)$, the vertical profile of $\overline{w^2}$ in the lower part of the mixed layer ($z < 0.1z_i$) is approximately:

$$\overline{w^2} = u_{*o}^2\,(1 - z/z_i) + w_*\,(2\,z/z_i)^{2/3} \quad , \qquad (2)$$

where u_{*o} is the friction in the constant flux layer above the canopy. As expected, the shear contribution becomes less important as one leaves the surface. The level at which the two effects are equal contributors occurs at the solution of $[2\,w_*^2/\,u_{*o}^2]\,(z/z_i)^{2/3} + z/z_i - 1 = 0$, whose convective limit ($w_*^2 >> u_{*o}^2$) is approximately $z/z_i \approx 1/8$ Since -L was observed to be from 50 to 150 m on many days during ABLE-2b, $-L/z_i \approx 0.15$, and the crossover point is broadly in agreement with the $z/z_i \approx 0.1$ lower limit commonly put on the validity of convective mixed layer scaling. The importance for determining the sign of the vertical velocity skewness is that $\partial\overline{w^2}/\partial z > 0$ during CBL conditions, leading to a negative tendency for Sk_w. During the night, there is only mechanical coupling and $\partial\overline{w^2}/\partial z < 0$, this contributing a positive Sk_w tendency. A summary of the observed signs of terms in (2) for plane surface and canopy layers is shown in Table 2. In wind tunnel tests (Raupach *et al.* ,1986) and in observations over crops (Maitani, 1978), $\overline{w^3}$ becomes positive at 1 - 4 canopy heights, and we argue that this simply reflects the level

at which $\partial\overline{w^2}/\partial z$ changes sign. In the stable boundary layer, one expects $\partial\overline{w^2}/\partial z < 0$ just above the canopy, with $\overline{w^2}$ approaching zero at the top of the stable boundary layer (Nieuwstadt, 1984). Deep in the canopy, $\partial\overline{w^2}/\partial z > 0$ at all times, and we expect, in the average, to find negative skewness there at night as well, though statistics at night may present an incomplete picture of the phenomena. We address these questions in a companion paper (Fitzjarrald and Moore, 1989).

The present observations support the prediction that vertical velocity skewness changes sign from day to night (Fig. 5), and we can see positive Sk_w only a few meters above the canopy, in contrast to the neutral wind tunnel results. Note that Sk_w becomes more negative as one enters the canopy and that $\overline{w^2\theta}$ is most negative at level 2, approximately 4 m above canopy top ($\approx$ 35 m), while it is already approaching zero at 45 m and is highly damped at 15 m below the crown. It appears that the level at which Sk_w becomes positive is not far above the canopy. During the Electra flux flight on 4 May, Ritter (personal communication) reports that $Sk_w \approx 0.6$ and $\overline{w^2\theta} \approx 0.1$ at 150 m. These are in the range of observations seen elsewhere in the CBL. Hunt notes that $Sk_w \approx$ 0.4 in the lower part of the CBL. A linear interpolation of the skewnesses would put the Sk_w point of crossover from positive to negative at approximately 40 m above the canopy, approximately 2 canopy heights above the surface. This height is small relative to z_i. However, if one takes this to be the level at which one can reasonably expect to see fluxes and gradients related as they are in smoother convective plane surface layers, it is probably prohibitively high for one to consider locating a tower in the Amazon.

What are the length and time scales characteristic of turbulence inside and just above the rain forest canopy? Fitzjarrald *et al.* (1988) noted that the dissipation length scale measured just above the canopy did not show the linear increase with height that occurs in plane surface layers. That is, the displacement height analogy, where $\lambda \sim z - d$, is not appropriate for predicting this scale. It appears that a much longer length scale, from 20 to 100 m, is important for dissipation even a few meters above the average canopy top. Within the canopy, the presence of the stable layer and vegetation makes the choice of scales difficult. Inside canopy, one must question even the use of Taylor's hypothesis for obtaining length from time scales.

The scale of eddies that carry heat flux in the canopy layer can be deduced by reference to the average $\overline{w\theta}$ cospectrum (Fig. 7) to be approximately at a time scale of 30-40s, and corresponding to an approximate length scale of approximately 100 m with the observed 3.1 m/s horizontal wind speed. The time scale appropriate to the main flux-carrying eddies corresponds to an integral scale of the flux product $\overline{w\theta}$ of only 3-4 s. The cospectrum for wq is similar. Thus, it appears that one can "capture" the bulk of the heat and moisture fluxes, and, by inference, fluxes of other substances that are emitted at similar levels in the canopy, with instrumentation with response frequencies no higher than from 0.5 to 1 Hz.

Several candidate length and time scales observed just above and within the rain forest canopy are presented in Table 3. These include the dissipation length scale $\ell_\epsilon = u_*^3/\kappa\epsilon^3$ above the canopy and $\ell'_\epsilon = \sigma_w^3/\kappa\epsilon^3$ inside the canopy (with σ_w taking the place of u_* because we have no

direct momentum flux measurement), the local Monin-Obukhov length, -L, the integral length and time scales of vertical velocity fluctuations at three levels, T_w, and the buoyancy oscillation period $1/N_B$, where N_B is the Brunt-Väisälä frequency of the stable layer just below canopy top. We also include estimates of z_i, the convective boundary layer thickness, obtained from the tethered balloon profiles where possible.

Panofsky and Dutton (1984, p. 176), in cautioning against the use of the integral scale in atmospheric work, noted that there has been considerable variability in reported results. They cited the considerable scatter in estimates that results from using data for which trends have been inadequately removed. They recommended using $T_p \sim 1/f_{max}$, the frequency of the maximum fS(f), typically 4 to 6 times the integral scale. However, Lenschow and Stankov (1986) presented consistent estimates of the integral scale in the CBL, and we have followed their practical definition of T_w here. Baldocchi and Meyers (1988) found the scale obtained from the spectral maximum to be approximately 10 times the integral scale, and we find similar results for above-canopy data. There are additional reservations about the use of integral scales in forest canopies which we point out in the next section.

In Table 3, one sees that the integral time scales vary little with time of day or among days. No significant difference exists between σ_1 and σ_2, the vertical velocity variance at the two levels above the canopy, and these are about twice that seen below the crown. There is an apparent difference between ℓ_ϵ at the two levels above the canopy, in contrast to our earlier (Fitzjarrald *et al.*, 1988) assertion, but each was calculated using u* observed at the upper level. One expects u* to be decreasing rapidly with height in this layer (Shaw *et al.*, 1988), and this difference may be spurious. It is interesting to note that the buoyancy period in the stable layer in the upper canopy is approximately 130 s, about four times as long as the period of the dominant flux-carrying eddies but comparable to the buoyancy period in the very stable layer near the forest floor. It is interesting to speculate whether or not CBL eddies might, in some circumstances, provoke sympathetic oscillations deep in the canopy. It is clear that future studies should include sensitive pressure measuring devices in the forest, such as been done by Sigmon *et al* (1983).

Forest top is a porous boundary, and integral scales do not vary linearly with height. On May 8, three levels, two above and one below the canopy top were operating, and these data can be used to demonstrate that the integral time scale of vertical velocity fluctuations does not change with height just above the canopy. Fig. 8 shows the autocorrelation coefficient at the three levels and their respective integrals with time lag. There is little difference between T_1 obtained at 45 m, approximately 10 m above the canopy top, and T_2, obtained at 39 m, 4 m above canopy top for this case or the additional ones listed in Table 3. However, the integral time scale T_3, at 30 m within the canopy is longer. The curious result is that one finds the characteristic time scale getting longer just as one approaches the ground, and this is in agreement with what Baldocchi and Meyers (1988) found in a Tennessee deciduous forest. Table 3 indicates that our estimates for T_w in the canopy are approximately twice those seen in Tennesee. An explanation for the larger T_w inside canopy is that

the forest itself is only allowing eddies with longer time or length scales to penetrate. These time scales correspond more closely to those derived from peaks in the spectra. These larger eddies are present in the environment above the canopy surface layer. To assess this hypothesis we must consider mechanisms of vertical exchange seen during the convective portions of the day. First, we concentrate on the turbulent statistics for convective periods in relatively stationary turbulence (Section 4) and then present cases of extreme events that occur during storm outflows (Section 5).

4. Vertical exchange within the canopy

Vertical motions within the canopy reflect activity above the canopy in the daytime. The average diurnal course of the vertical velocity correlation coefficient above canopy and below crown (Fig.9a) shows a midday maximum near 0.45, as high a correlation coefficient as one finds between w and T or between T and q above the canopy, or indeed as high a correlation coefficent seen between turbulent variables in the plane surface layer. Vertical coupling is supressed during stable periods at night, and the correlation coefficient approaches 0.15. Time series of the correlation coefficient r_{wt} above and below the canopy (Fig. 9b) show that there is weak negative flux below the crown until approximately 1100. At this point the in-canopy r_{wt} rises abruptly at approximately the same time that σ_u and U (Fig. 3) are decreasing, reflecting the average change in sign of $\partial\Theta/\partial z$.

Inspection of typical wind signals above and below the canopy (Fig. 10) confirms that the correlation occurs because lower frequency fluctuations are passed preferentially into the canopy. In other words, the upper canopy serves as a low-pass filter, as hypothesized in modelling work by Wilson (1988) and Shaw and Seginer (1985). The frequency dependence of the "forest filter" effect is shown in Fig. 11, a comparison of w power spectra above and below the crown with the corresponding vertical cospectrum. Frequencies above 0.03 Hz are reduced by a factor of 100 while 30% of the variance in the energy-containing range near 0.01 Hz above the canopy is passed. In contrast to Baldocchi and Hutchison (1988), we find the -2/3 inertial subrange form both above and within the canopy, though the onset of the inertial subrange in the canopy occurs at a higher frequency because of the filtering effect. Filter characteristics presumably depend on the biomass density in the upper canopy. The observed median phase angle between vertical motions above and inside the canopy are small in the frequencies where most of the covariance occurs, ranging between 5 and 20 degrees.

The fact that the vertical velocity integral scale is larger within the canopy than above can be a simple consequence of high-frequency filtering changing spectral shapes. In theory, the integral scale is defined by the integral of the autocorrelation coefficient over all possible time lags and the autocorrelation coefficient is the Fourier transform of the power spectrum (Tennekes and Lumley, 1972). The filtering effect of the upper canopy selectively removes high-frequency variance, and this means that one should not necessarily conclude that the characteristic scale of the large eddies is different above and below the crown. It is clear from Fig. 11 that a significant difference between

the spectrum below the canopy and that above occurs at a particular filter cutoff frequency. If one idealizes this cutoff to be total, allowing no variance above the cutoff frequency, the relationship between cutoff frequency and consequent integral scale displayed in Fig. 12 results. At approximately 0.05 Hz, the integral scale for vertical velocity variance inferred from filtering the w_2 signal, is close to that observed as the integral scale of the w_3. This result is an unavoidable consequence of the combining the forest filtering effect with the definition of the integral scale and represents another way to view the action of the filter. The integral scale estimated within the canopy differs from that above in a manner determined by the forest filter cutoff frequency. One should be rather cautious when ascribing comparable physical meaning to each integral scale.

Although vertical motions are observed within the canopy, these do not normally lead to significant heat or moisture fluxes there. For example, Θ gradients can be typically stable or near neutral in the upper canopy (Fig. 1), but these conditions need not obtain for trace gas constituents. Though the sensible heat flux is small in the canopy, its sign reflects the change in gradient that occurs as mixing penetrates the canopy in the afternoon. The average daily time series of r_{wT}, the correlation coefficient between w and T, illustrates the difference between the morning and afternoon regimes (Fig. 9b). As the upper canopy heats during the morning there is downward heat flux below the crown. The bottom level shows positive heat flux only after mixing has reversed the Θ gradient, seen in the sample profiles in Fig. 1 only at 1000 LST.

5. Transient phenomena and transports.

Atmosphere-canopy interaction during the rainy season is modulated by the effects of rain and convective clouds. Unfortunately, it is precisely during rainy periods that micrometeorological instruments often do not work properly and, indeed, one of the statistical foundations of the time series analysis of turbulent measurements, stationarity, is not really satisfied when raining clouds are common. Cloud downdrafts flood the surface layer with low-Θ_e air. As the downdraft arrives, there is usually a gust. The net effect is to remove the stability at all levels within the forest while temporarily increasing stability above. Although such events may be important to heat and moisture budgets, they are potentially more important to transport of substances, such as nitrogen oxides, that are produced near the forest floor and might be trapped by the persistent stable layer there (Bakwin *et al.*, 1989). The events can be easily identified in time series plots of temperature and wind speed seen at the top of the forest. If the event happens during the middle of the day, the normal stability regime (Fig. 1) returns after a time. Cloud downdraft events occur only a few times each day, and here three examples are presented. Observed response of the canopy to the downdrafts is presented and then we relate the outflows to clouds seen on the radar.

Large changes in mean Θ, wind speed, and turbulent fluxes occur during outflow episodes. To assess the effect of these events on turbulent fluxes, we shorten the averaging interval for their calculation to 6.8 minutes, accepting the compromise that this increases the theoretical uncertainty in their values. Wyngaard (1983) showed that the relation among averaging time T_{ave}, required to

obtain "accuracy" a, the ratio of the standard deviation of an estimate from its ensemble mean value divided by its observed mean value, in estimating the turbulent flux wx, with integral scale T_{wx} is:

$$a \approx 1.4\,[\sigma_{wx}/\overline{wx}]\,[T_{wx}/T_{ave}]^{0.5}.$$

where σ^2_{wx} is the standard deviation of the sample. Observed daytime values of $T_{w\theta}$ for the heat flux product $w\theta$, for example, are typically 3 s, $\sigma_{w\theta} \approx 0.25$ ms^{-1}K, $\overline{w\theta} \approx 0.16$ ms^{-1}K and with T_{ave} = 6.8 minutes, this leads to $a \approx 0.2$. We can hope to approach within 20% of the ensemble mean during this averaging period. The value of $T_{w\theta}$ is approximately a tenth of the period of the main flux-carrying eddies seen just above the canopy, as deduced from the $w\theta$ cospectrum (Fig.7).

Case 1, May 5, 1987. There were scattered showers on this day. Gusts from storm outflows disrupted the stability in the canopy on four marked events, approximately at 1115, at 1300, at 1330, and just after 1600. Changes in the canopy associated with the events are seen in the Θ_v and U time-height sections (Fig.13). It is also apparent that only a few gusts manage to affect the canopy below 25 m altitude. The turbulent signature of one of the gusts is shown in the 1-s averaged time series above and below the canopy top (Fig. 14). During the afternoon, the radar was operating, and we can clearly identify the echoes that produced the outflow gusts (Fig.15). It appears that the echo must pass rather close to the tower for the cloud's wake effects to be felt. The cloud that produced the gust in Fig. 14 passed within 2 km of the Ducke tower (Fig. 15). Approximately neutral stability in the canopy layer appears in Fig. 13 as vertical Θ_v contour lines, and the duration of the vertical contours is a measure of how long it takes the canopy to reestablish the convective canopy surface layer with its attendant stable layer below the crown. In the case of the 1330 gust, the recovery period is approximately 30 minutes, though this time depends on how long direct solar radiation is shielded by the remnant cloud. On 5 May, the cloud was isolated, and solar heating began just after the echo passed. Turbulent heat and moisture fluxes on this day (Fig. 16) show that one effect of the clouds is to cause a peak in $\overline{w\theta}$ and $\overline{wq}$, followed by a period of very small, even negative $\overline{w\theta}$, as the outflow stabilizes the canopy surface layer. The fourth event occurred just after 1600, late enough in the day that the transient stabilization from the outflow hastened the onset of the early evening stable transition. We observed this cloud to pass directly over the tower, and rain was observed there. The echo was similar in size to the 1330 cloud, and the echo travelled at a similar speed. The gust was felt deep into the canopy and the strong Θ_v inversion moved from forest floor to forest top during the event (Fig.13).

Case 2, April 29, 1987. Time-height sections for Θ_v and wind speed for this day are shown in Fig. 17. It is clear that, apart from the large event at approximately 1620, transient mixing episodes are weaker than during Case 1. Because of signal attenuation caused by cells between the radar and Ducke, we have radar data at the tower site only after 1300. A weak cell (14 Dbz) passed over Ducke at between 1310 and 1320, and the gust penetrated only to the 30 m level in the canopy (Fig. 17). The gust just after 1400 was apparently produced by somewhat stronger cell (27 Dbz). The main feature of the day is the squall line passage at approximately 1620. This line encompassed the entire MCC triangle, with an echo maximum exceeding 30 Dbz passing over the tower (Fig.18).

The effect on the canopy was pronounced, with mixing extending through the entire canopy layer. The abrupt establishment of static stability at canopy top after the line passed is similar to that observed on May 5. During the gust, vertical motions exceeding 1.0 m/s were seen above the canopy and up to 0.8 m/s within the canopy.

Case 3, May 8, 1987. Effects of cloud downdrafts are only seen during the afternoon (Fig. 19). The time series of $w\theta$ (Fig. 20), shows relatively smooth increases up until approximately 1300. Two large outflows, at approximately 1300 and again at approximately 1400 neutralized the forest canopy. Figure 21 illustrates the cloud echo trajectory on May 8 around 1409 LST. From 1300 until approximately 1430, the canopy remained well mixed. Remarkable evidence demonstrating that deep canopy exchange occurred during these events is presented in Fig. 20, where we include a short section CO_2 flux observations from the Harvard group (Fan *et al.*, 1989). The two flux signals are anticorrelated, as expected during the day when there is CO_2 uptake by the leaves. However, there is a brief period of $\overline{wCO_2} > 0$ coincident with $w\theta < 0$ after the second gust. It appears that the second gust, by mixing the entire canopy layer, was able to vent CO_2 accumulating at the forest floor into the atmosphere.

Occurrence of only a few mixing events can probably prevent accumulation of trace gases in the rain forest canopy. What is not yet clear is how to quantify what fraction of the total transport of a substance during a day can plausibly be associated with such convective mixing events. An upper limit to this transport can be estimated as follows: If we consider a hypothetical trace gas s with a source at the forest floor, and assume that, during a deep mixing event, a mass of the gas equal to the difference between its average canopy value $s_c = (1/H)\int s\, dz$ and its above-canopy average s_a enters the atmosphere. Noting the number of such events that occur each day, one can then augment estimates of the normal turbulent flux by the appropriate amount. The mixing events are usually sufficiently infrequent that there is sufficient time for surface emissions of a substance to "recharge" the canopy layer.

These examples should be sufficient to caution one from basing trace gas transport on simple analogy with heat or moisture transport. As cases 1 and 3 illustrate, even relatively small, isolated raining clouds are sufficient to lead to transient periods of deep mixing and nearly neutral conditions. It is also important to observe and take into account the source and sink levels for the quantity considered. Perhaps these data may indicate first steps toward developing a model for forest-atmosphere interaction that takes into account the importance of isolated extreme events.

6. Empirical relationships

To quantify horizontal gradients of flux and turbulent quantities over the Amazon, there will be a continuing need for long time series of observations at a large number of sites. However, very few towers such as that used in this work are available, and it is a continual battle to keep sophisticated instrumentation operating in the rain forest. One would like to extend the applicability of the measurements made during the short field experiment reported on here to apply to a wider

area and over a longer time period. There is also continual interest among modellers in simple surface parameterizations of heat and momentum fluxes. These two interests are similar, but not identical. In the former situation, one seeks *surrogate measurements*, made with robust, inexpensive instruments that can operate with minimal oversight for extended periods. These measurements, such as the horizontal wind speed and its variance and solar radiation, are frequently available at climatological stations. Most large-scale models, however, do not compute variances. For such models, one seeks flux-gradient relationships to connect mean fields with the bottom boundary condition. It is clear from Fig.2 that the diurnal pulses seen most clearly in σ_u and S, but also apparent in the mean wind U, should lead to some kinds of proportional relationships with sensible heat or momentum fluxes, which also vary in like manner. If they are sufficently strong, such relationships are the empirical parameterizations we seek.

In the following, data for the entire experiment are averaged by hour of the day before linear regressions are calculated. Tests show this changes the result very little. Momentum flux, as u_*^2, is not only adequately represented by measurements of σ_u^2 (Fig. 22), but the empirical relationship follows the Panofsky *et al.* (1977) formula, assuming a plausible value of $-z_i/L \approx 6$. This relationship was used to estimate u_*^2 from σ_u^2 to scale horizontal wind speed spectra earlier (Fig.4). A simple linear fit does a good job of predicting $w\theta$ from σ_u^2 (Fig.23), and this is probably a good surrogate measurement for heat flux, assuming that there is sufficient solar radiation. (In a plane surface layer, $\sigma_u^2 \approx \sigma_w^2 \rightarrow [w\theta]^{2/3}$, in the free convection limit.) Although the diurnal signal in U is not as pronounced as that of σ_u (Fig. 2), it also exhibits a reasonable linear fit with the heat flux, if one includes only periods with $w\theta > 0$ and rejects periods with very small flux (Fig.24). A linear U-$w\theta$ relationship is consistent with the commonly used bulk aerodynamic formula $w\theta \approx C_H U (\Theta_2 - \Theta_1)$, with C_H a transfer coefficient, U the mean horizontal wind speed, Θ_2 the temperature at the "surface", and Θ_1 the temperature at a reference level. At Ducke, $(\Theta_2 - \Theta_1)$ varies little during the convective portion of the day, with average values of the 39 to 45 m Θ difference being about 3 K. The regression line $\rho c_p w\theta$ [W/m^2] $\approx$ 95 U [m/s] - 99. for U > 1 m/s, with a temperature difference of 3 K leads to an estimate of $C_H \approx 3 \times 10^{-3}$, a commonly observed value, though in normal usage one does not include an offset term. A similar regression line was found for the latent heat flux: Lwq[W/m^2] $\approx$ 207 U -244.

We do not suggest that the formulas presented here have universal validity, but they may be extremely useful when applied to extending the limited measurements available for the Amazon rain forest. They contain implicitly the physical correlations between elements of the heat balance at canopy top and the control that static stability exerts on turbulent fluxes, and the net effect of dry and moist convective motions on the boundary layer. We tested other empirical forms, among them the proposed relationship between temperature skewness and $\overline{w\theta}$ of Tillman (1972), but no clear relationships were found. A linear relationship between incoming solar radiation and σ_u^2, similar to that between u_*^2 and σ_u^2 was also found, reflecting the average diurnal behavior of these quantities.

The empirical relations presented above do not directly assist the researcher who wishes to estimate the flux of a trace gas from the canopy, knowing only the gradient of the quantity of interest. It is clear from the previous sections that most fluxes are likely to occur during the daytime, and that there will be a significant diurnal signal. Further, transient events modulate any signal seen during the rainy season, and the best one can hope for are fluxes obtained from gradients averaged over a large number of relatively fair days. Because there is great interest in obtaining fluxes of many important trace gas species in spite of large potential uncertainties, we offer the following procedure to make the flux estimates.Because of its monotonic gradient in the canopy (Fig. 1) q is the best physical candidate for a flux-gradient relation standard, and we wish to estimate the average diurnal behavior of the transport velocity $\overline{wq}/\Delta q$. It is clear from Fig. 1 and data from other similar days that the wind-induced mixing does not frequently influence the layer below 20 m, though large gradients in q, for example, are present in the very stable layer near the forest floor. Thus, we take Δq to be the difference between the concentration from 20 to 30 m height within the canopy and the average q value above the canopy. The observed mean value of Δq reaches a maximum at 1100, typically the hour when clouds build up and reduce incoming solar radiation. The average by hour of this quantity (Fig. 25) contains implicitly the relationships in Figs. 22-24, the diurnal change in turbulent mixing efficiency. It appears that the characteristic transport velocity is approximately constant at 0.15 m/s during the middle of the day, but there is a significant drop shortly after noon. One should use this relation to estimate trace gas fluxes judiciously, bearing in mind the importance of individual events to effect large transient transports sporadically (Section 5).

7. Conclusions and recommendations

We offer the following conclusions:

1. Filter characteristics of turbulent transfer into the Amazon rain forest canopy have been quanitified, and it is clear the eddies on the scale of 50-200 m are important below the crown as well as just above canopy top.

2. Convective processes during the rainy season can alter the diurnal course of turbulent fluxes. In wake of giant coastal systems, no significant wind speed variations, and by inference, no significant heat or moisture fluxes occur for up to a day after the event.

3. The frequency distribution of horizontal wind speed variance, on average, is well described by dry CBL similarity hypotheses, in spite of ubiquitous presence of clouds during the rainy season. The turbulent environment of the upper canopy is strongly linked to processes occurring in the entire CBL. One cannot describe the daytime canopy-atmosphere interaction without reference to the prevailing boundary layer state.

4. Observed large changes in the integral scale for vertical velocity fluctuations inside the canopy can be described as another aspect of the filtering effect of foliage in the upper canopy, where high frequency turbulence is selectively produced and dissipated.

5. Diurnal changes in the sign of the vertical velocity skewness observed above and inside the canopy can plausibly be explained by differences in the relative sizes of elements of the skewness budget.

6. Even small raining clouds can evacuate the canopy, and recovery can take up to one hour, even during mid-day, but if storm passage occurs late in the day, a period of canopy layer static stability caused by the outflow persists into the evening transition, producing an effective "early nightfall". Deep mixing events in the Amazon appear always to be related to storm outflows. Although they are infrequent (one to four times per day), they are potentially capable of removing gases that accumulate at the forest floor.

7. To understand details of turbulent processes in the Amazon forest canopy, it is absolutely necessary to consider stability within the canopy. On undisturbed days, repeatable sequences of environments occur, and perhaps it is more instructive to look at temporal sequences of structure, to understand processes, than to categorize turbulent fluxes using stability indices.

8. Simple empirical relations for surrogate flux measurements open the possibility of operating larger networks of surface sites for long periods of time in the Amazon. Standard deviation of the horizontal wind, when averaged over long periods of time, correlates well with turbulent heat flux $w\theta$. Estimates of mean exchange velocities for substances whose gradients are known in the upper canopy and just above permit rough estimates of fluxes of these quantities. However, case studies show that, if a substance accumulates at the forest floor, this parameterization may by mechanistically flawed.

Recommendations. Larger networks of surface stations are needed if regional differences in heat and moisture fluxes are to be monitored in the Amazon rain forest. In particular, growing concern over deforestation and subsequent regrowth emphasizes the importance of quantifying the physical and chemical differences that are already occuring as the surface changes. It remains the case that the only detailed micrometeorological experiments in the Brazilian Amazon have come from the tower at Ducke.

More generally, the results presented here suggest to us that expanding the concept of the "forest filter" to include quantitatively the relation between the biomass density profile and the filter transfer function would be a fruitful area of continuing research. There is a need to relate vertical velocity skewness values and gradients to the height at which the forest appears to the atmosphere above as identical to the familiar plane convective surface layer. This may be an area in which careful modelling efforts would be useful. The difficulties we found in relating the integral scales to the scales of the predominant eddies just above the canopy point out the limitations of traditional spectral analysis. Recently, Mahrt (1989) presented idealized time series to illustrate his contention that, in prototypically convective conditions, edges between larger structures can contribute to high-frequency variance in a manner that has little to do with the traditional inertial subrange energy cascade. In future work, it would be prudent to consider Mahrt's suggestions on the use of different structure functions in place of exclusive reliance on spectra.

8. Acknowledgements

This work, part of the GTE ABLE-2b field mission, was supported by NASA Grant NAG-1-692 to the Atmospheric Sciences Research Center (ASRC) at the State University of New York at Albany and by INPE, the Brazilian Space Institute. G. G. Lala of ASRC helped with experiment planning and wrote the Datalogger acquisition program in the field. Amauri P. de Oliveira assisted with operations in the field and offered advice at ASRC. We are grateful to J. W. Sicker at ASRC for technical support before and after the experiment. In Manaus, researchers from the Instituto Nacional de Pesquisas da Amazônia (INPA) and from INPE were very helpful. Special thanks go to S. Wofsy, P. Bakwin, and S-M Fan, all of Harvard University, who took went to extra trouble to help record the large amounts of raw data obtained during this experiment. M. Garstang, C. Martin, S. Greco and colleagues at the University of Virginia and at Simpson Weather Associates operated the radar and PAM systems in the field and graciously provided access to radar and PAM data sets. Operating our instruments and acquiring the data presented in this paper depended in large part on the cheerful cooperation of other research teams from both Brazil and the United States that were in the field during ABLE-2b.

9. References

Antonia, R. A., A. J. Chambers, and E. F. Bradley, Third- and fourth-order mixed moments of turbulent velocity and temperature fluctuations in the atmospheric surface layer, *Boundary-Layer Meteorol., 22,* 421-430, 1982.

Baldocchi, D.D. and T. P. Meyers, A spectral and lag-correlation analysis of turbulence in a deciduous forest canopy, *Boundary-Layer Meteorol.*, submitted, 1988.

Baldocchi, D. D. and B. A. Hutchison, Turbulence in an almond orchard: spatial variations in spectra and coherence, *Boundary-Layer Meteorol., 42,* 293-311, 1988.

Bakwin, P. S., S. C. Wofsy, Song-Miao Fan, M. Keller, S. Trumbore, and J. Maria da Costa, Emission of Nitric Oxide (NO) from tropical forest soils and exchange of NO between the forest canopy and atmospheric boundary layers, *J. Geophys. Res.*, (submitted), 1989.

Chiba, O., Stability dependence of the vertical velocity skewness in the atmospheric surface layer, *J. Meteorol. Soc. Jpn., 56,* 140-142, 1978.

Fan, S.-M., P. S. Bakwin, S. C. Wofsy, D. R. Fitzjarrald, and O. M. R. Cabral, Eddy correlation measurements of the exchange of CO_2 and O_3 between the Amazon forest and the atmosphere, *J. Geophys. Res.*, (submitted), 1989.

Fitzjarrald, D. R. and M. Garstang, Vertical structure of the tropical boundary layer, *Mon. Weather Rev, 109,* 1512-1526, 1981.

Fitzjarrald, D. R., B. L. Stormwind, G. Fisch, and O. M. R. Cabral, Turbulent transport just above the Amazon forest, *J. Geophys. Res., Vol. 93,* No. D2, 1551-1563, 1988.

Fitzjarrald, D. R. and K. E. Moore, Nocturnal exchange between rain forest and atmosphere, *J. Geophys. Res.*, this issue

Garstang et al., The Amazon Boundary Layer Experiment (ABLE-2B): A meteorological perspective, *Bull. Am. Meteor. Soc.* (submitted), 1989.

Greco, S. ,S. Ulanski, R. Swap, M. Garstang, M. Shipham, M. O. Andreae, R. C. Harriss, R. Talbot, and P. Artaxo, Rainfall and surface kinematic conditions over central Amazonia during

ABLE 2B, *J. Geophys. Res.* (submitted),1989. et al.

Højstrup, J., Velocity spectra in the unstable planetary boundary layer, *J. Atmos. Sci., 39,* 2239-2249, 1982.

Hunt, J.C.R., J.C. Kaimal, J.E. Gaynor, Eddy structure in the convective boundary layer-new measurements and new concepts, *Q J. R Meteorol. Soc. 114* (482):827-858, 1988.

Hunt, J.C. R.1984.Turbulence structure in thermal convection and shear-free boundary layers. J. Fluid Mech. 138: 161-184.

Hutchison, B. A. and B. B. Hicks, eds., *The Forest-Atmosphere Interaction,* D. Reidel, 1985.

Kaimal, J. C., Horizontal velocity spectra in an unstable surface layer, *J. Atmos. Sci. 35,* 18-24, 1978.

Lenschow, D. H. and B. B. Stankov, Length scales in the convective boundary layer, *J. Atmos. Sci. 12,* 1198-1209, 1986.

Mahrt, L., Intermittency of atmospheric turbulence, *J. Atmos. Sci. 46,* 79-95, 1989.

Maitani, T., On the downward trasport of turbulent kinetic energy in the surface layer over plant canopies, *Boundary-Layer Meteor. 14,* 571-584, 1978.

Martin, C. L., D. R. Fitzjarrald, M. Garstang, A. P. Oliveira, S. Greco, and E. Browell, Structure and growth of the mixing layer over the Amazonian rain forest . *J. Geophys. Res., Vol. 93,* No. D2, 1361-1375, 1988.

Menzel, W. P., T. J. Schmit, B. M. Goodman, D. P. Wylie, and E. C. Cutrim, Diurnal characteristics of cloud cover over Amazonia derived from multispectral VAS observations, *J. Geophys. Res.* (submitted), 1989.

Nieuwstadt,F. T, M., The turbulent structure of the stable, nocturnal boundary layer, *J. Atmos. Sci., 41,* 2202-2216,1984.

Panofsky, H. A., H. Tennekes, D. H. Lenschow and J. C. Wyngaard. The characteristics of turbulent velocity components in the surface layer under convective conditions. *Boundary Layer Meteorol.* **11,** 355-361, 1977.

Panofsky, H. A. and J. A. Dutton . *Atmospheric Turbulence*, John Wiley, N. Y., 1984.

Raupach, M. R., A Lagrangian analysis of scalar transfer in vegetation canopies, *Q. J. R. Meteorol. Soc., 113,* 107-120, 1987.

Raupach, M. R., P. A. Coppin, and B. J. Legg, Experiments on scalar dispersion within a model plant canopy, Part I: The turbulence structure, *Boundary-Layer Meteorol., 35,* 21-52, 1986.

Raupach, M. R., A. S. Thom, I. Edwards, A wind-tunnel study of turbulent flow close to regularly arrayed rough surfaces, *Boundary-Layer Meteorol., 18,* 373-397, 1980.

Roberts, J., O. M. R. Cabral, and L. F. De Aguiar, Stomatal and boundary layer conductances measured in a Terra Firme rain forest, Manaus, Amazonas, Brazil, *J. Appl. Ecol.,* in press.

Sá, L. D. A., Y. Viswandadham, A. O. Manzi, Energy receipt partitioning over the Amazon forest. Publication INPE-3980-PRE/990. Available from Instituto de Pesquisas Espaciais, 12201 São José dos Campos, SP, Brazil.

Shaw, R. H. and I. Seginer The dissipation of turbulence in plant canopies. 7th Symposium on Turbulence and Diffusion. Am. Met. Soc. Boston, pp.200-203, 1985.

Shaw, R. H., G. den Hartog, and H. H. Neumann, Influence of foliar density and thermal stablitiy on profiles of Reynolds stress and turbulence intensity in a deciduous forest, *Boundary-Layer Meterol.., 45,* 391-409,1988.

Shuttleworth, W. J., et al., Eddy correlation measurements of energy partition for Amazonian forest, *Q. J. R. Meteorol. Soc., 110,* 1143-1162, 1984a.

Shuttleworth, W. J., Observations of radiation exchange above and below Amazonian forest, *Q. J. R. Meterol. Soc. 110,* 1163-1169, 1984b.

Shuttleworth, W. J.,et al., Daily variations of temperature and humidity within and above Amazonian forest. *Weather 40*(4), 102-108, 1985.

Sigmon, J. T., K. R. Knoerr, E. J. Shaughnessy, Microscale pressure fluctuations in a mature deciduous forest, *Boundary-Layer Meteorol. 27,* 345-358, 1983.

Stull, R. B., *An Introduction to Boundary Layer Meterology*. Kluwer Academic, Boston, 1988.

Tennekes, H. and J. L. Lumley, *A First Course in Turbulence,* MIT Press, Cambridge, Ma., 1972.

Tillman, J. E., The indirect determination of stability, heat and momentum fluxes in the atmopsheric boundary layer from simple scalar variables during dry unstable conditions, *J. Appl. Met. 11,* 783-792, 1972.

Wilson, J. D., A second-order closure model for flow through vegetation. *Boundary-Layer Meteorol. ,42,* 371-392, 1988.

Wyngaard, J. C., Lectures on the planetary boundary layer, in *Mesoscale Meteorology--Theories, Observations and Models,* D. K. Lilly and T. Gal-Chen (eds.), D. Reidel, Dordrecht, the Netherlands, 1983.

10. Tables

11. Figure Captions

Fig. 1 Mean profiles of Θ, q, and wind speed within the canopy.
Fig. 2a Time series of U (m/s).
Fig. 2b Time series of σ_u (m/s).
Fig. 2c Time series of incident solar radiation (W/m^2).
Fig. 3a Average diurnal wind speed for Julian days 108-129 (April 19-May9).
Fig. 3b Average diunal σ_u for days 108-129.
Fig.4 Power spectrum of the horizontal wind at 45 m.
Fig.5 Time series of Sk_w and $\overline{w^2\theta}$ during May 8. The median and range of 50% of the values for other days in early morning, daytime, and evening hours are plotted as additional points with vertical bars. The "x" symbols are for level 2, triangles are for level 3.
Fig. 6 Sketch of the components of w^2 in the convective boundary layer.
Fig. 7 Mean $\overline{w\theta}$ cospectrum for May 8 above the canopy (level 2).
Fig. 8a Autocorrelation coefficient at levels 1, 2, and 3 on May 8 for the time period 1010 to 1044.
Fig. 8b Estimate of the integral scale obtained by integrating the results of 3.6a. $T_w=\int R_w d\tau$.

Fig. 9a Correlation coefficient r_{w2w3}, between vertical velocity fluctuation above the canopy and those below the crown.
Fig. 9b Correlation coefficient r_{wT} above the canopy (solid)and those below the crown (dashed).

Fig. 10 Typical wind signals during the day. Top panel: Horizontal wind speed (solid) and direction (dotted) from the Gill anemometer. Middle panel: Vertical velocity deviation from the mean at level 2 (39 m). Bottom panel: Vertical velocity deviation from the mean at level 3 (30 m).

Fig. 11 Vertical velocity power spectra for w1 (45 m), w2 (39 m), above the canopy, and w3 (30 m), below the crown. Also shown is the w2-w3 cospectrum.

Fig. 12 Integral scale resulting when all the variance above a cutoff frequency is removed. The observed integral scales above and within the canopy are indicated by w2 and w3, respectively.

Fig. 13 Time-height section of horizontal wind speed (upper panel) and Θ_v (lower panel) on May 5. Windspeed contour interval is 0.5 m/s, Θ_v interval is 0.5 K.

Fig. 14 Sample plot of gust arrival at Ducke tower. Top panel: Horizontal wind speed (solid) and direction (dotted) from the Gill anemometer. Middle panel: Vertical velocity deviation from the mean at level 2 (39 m). Bottom panel: Vertical velocity deviation from the mean at level 3 (30 m).

Fig. 15 Radar echo field at 1333 LST (1733 GMT) on May 5. The center of mass of the echo near Ducke is shown at later times is indicated by the arrow. Symbols indicate cloud mass at 10 minutes intervals.

Fig. 16 Kinematic heat (Km/s) and moisture ($g/m^3 \cdot m/s$) fluxes observed during May 5. Solid line is above canopy, dashed is within canopy.

Fig. 17 Time-height section of horizontal wind speed (upper panel) and Θ_v (lower panel) on April 29.

Fig. 18 Radar echo field at 1618 LST (2018 GMT) on April 29 shows the squall line passing over Ducke tower.

Fig. 19 Time-height section of horizontal wind speed (upper panel) and Θ_v (lower panel) on May 8.

Fig. 20 Kinematic heat (solid line) and moisture (dashed) fluxes observed above the canopy during May 8 (upper panel). Lower panel shows CO_2 flux during this period.

Fig. 21 Radar echo field at 1409 LST (1809 GMT) on May 8 and the cloud mass trajectory. Symbols represent location of cloud mass at 10 minute intervals.

Fig. 22 Relation between σ_u^2 and u_*^2. Data were averaged by time of day for periods when both observations were available. The regression line is y=0.21x. R^2=0.98. The mass of points in the lower left corner represent night-time observations.

Fig. 23 Relation between σ_u (ms^{-1}) and heat flux (Wm^{-2}). Data were averaged by time of day for periods when both observations were available. The regression line is y=-38-39+1.477x. R^2=0.94.

Fig. 24 Relation between U (ms^{-1}), the horizontal wind speed at 45 m, and heat flux (Wm^{-2}). Data were averaged by time of day for periods when both observations were available. The

regression line is $y=-99.09+0.949x$. $R^2=0.92$.

Fig. 25 The ratio $\overrightarrow{wq}/\Delta q$, where Δq is the difference in specific humidity between the 20-30 m average in the canopy and all observed values above the canopy (up to 45 m), by time of day. This ratio is an estimate of the proportionality coefficient that would relate the flux of a trace gas s, $\overline{ws}$, to a gradient Δs observed in the same layer.

Table 1. Heights and types of measurements available on Ducke tower.

Height, m	INPE	SUNYA	Harvard[1]
1.45	q,q		
2.49	q,q		
13.5	u,q,q		
23.3	u,q,q	w',t',q' (level 3)	
30.5	u,q,q		
35.7	u,q,q		
37.5	u		
39.3	u,q,q	w',t',q' (level 2)	CO_2, O_3
41.0	u,q,q		
42.8	u		
44.7	u,q,q	Gill: u,ϕ; w',t',q' (level 1)	
48.7	u,q,q		

1 Harvard also measured mean CO_2, O_3 and NO concentrations at 0, 3, 6, 12, 19, 27, 36 and 41 m.

Table 3. Characteristic length and time scales in and above the canopy. Subscripts refer to levels.

	λ_1	λ_2	λ_3	T_1	T_2	T_3	σ_{w1}	σ_{w2}	σ_{w3}	1/N	L	z_i
	m			s			m/s			s	m	m
Date, hour of day												
April 29												
8-9								.39	.18	242	90	
9-10								.63	.27	236	150	
10-11		24	45		3.5	7.5		.63	.27	180	87	
11-12	9	27	68	5.3	4.9	11.2	.45	.62	.32	293	120	
12-13	41	32	65	5.3	5.5	8.1	.64	.60	.33	706	130	
13-14		38	71	4.8	6.0	8.4		.52	.26	382	150	
14-15		50	61	3.9	4.9	9.8	.42	.53	.25	379	-34	1120
15-16	9	19	56	5.0	6.0	8.9	.46	.47	.19	327	178	1200
16-17		16	41		8.0	14.0		.14	.11	167	285	
May 5												
8-9		19	47		5.8	9.4		.46	.21	250	306	400
9-10		19	28		5.6	8.8		.54	.26	259	185	525
10-11		39	86		5.2	7.8		.82	.45	228	162	
11-12		157	648		4.2	7.8		.54	.33	226	157	1120
12-13		24	72		5.7	7.8		.63	.29	n/a	127	
13-14		17	44		7.5	9.3		.46	.22	331	-206	
14-15		19	38		7.2	9.5		.45	.20	n/a	46	
15-16		10	61		8.3	12.7		.33	.14	459	276	
16-17								.32	.14	217	104	
May 8												
8-9	35	39	36	5.0	4.2	9.0	.57	.61	.29	243	70	
9-10	38	21	54	4.2	4.2	6.8	.71	.74	.33	233	123	560
10-11	58	25	57	5.0	4.5	8.0	.63	.65	.35	386	119	800
11-12	45	23	57	4.5	4.5	7.5	.68	.69	.36	275	135	
12-13	42	26	71	7.0	7.5	9.0	.56	.53	.32	312	302	
13-14	20	11	40	8.0	6.5	13.0	.53	.56	.25	186	-67	1200
14-15	17	9	75	5.0	5.0	24.0	.21	.24	.13	141	192	
15-16								.42	.10	146	103	
16-17							.30	.30	.10	197	-75	700

Table 2. Skewness tendency produced by terms in the schematic w^3 budget.

$$\overline{w^3}/T_L \approx \underset{B}{(g/\Theta_0)\,\overline{w^2\theta}} + \underset{T}{[-a\,\overline{w^2}\,d\overline{w^2}/dz]}$$

	Canopy		Surface Layer	
	day	night	day	night
Buoyancy (B)	-	≈0	+	-
Transport (T)	-	+	-	+
Skewness (Observed)	-	+	+	-

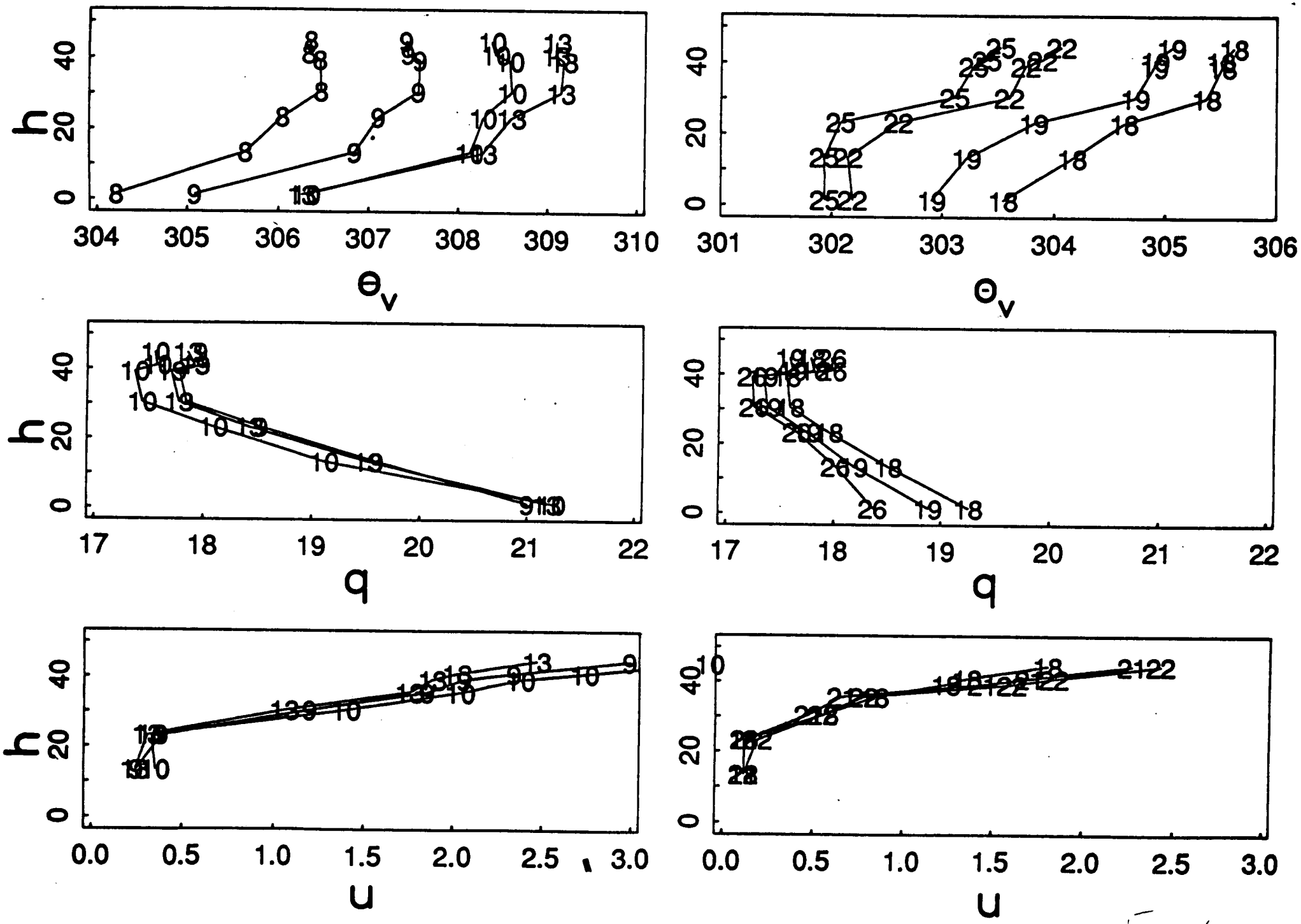
h
0
20
40
304
305
306
307
308
309
310
θ_v
301
302
303
304
305
306
θ_v
h
17
18
19
20
21
22
q
q
h
0.0
0.5
1.0
1.5
2.0
2.5
3.0
u
u

FIG. 1

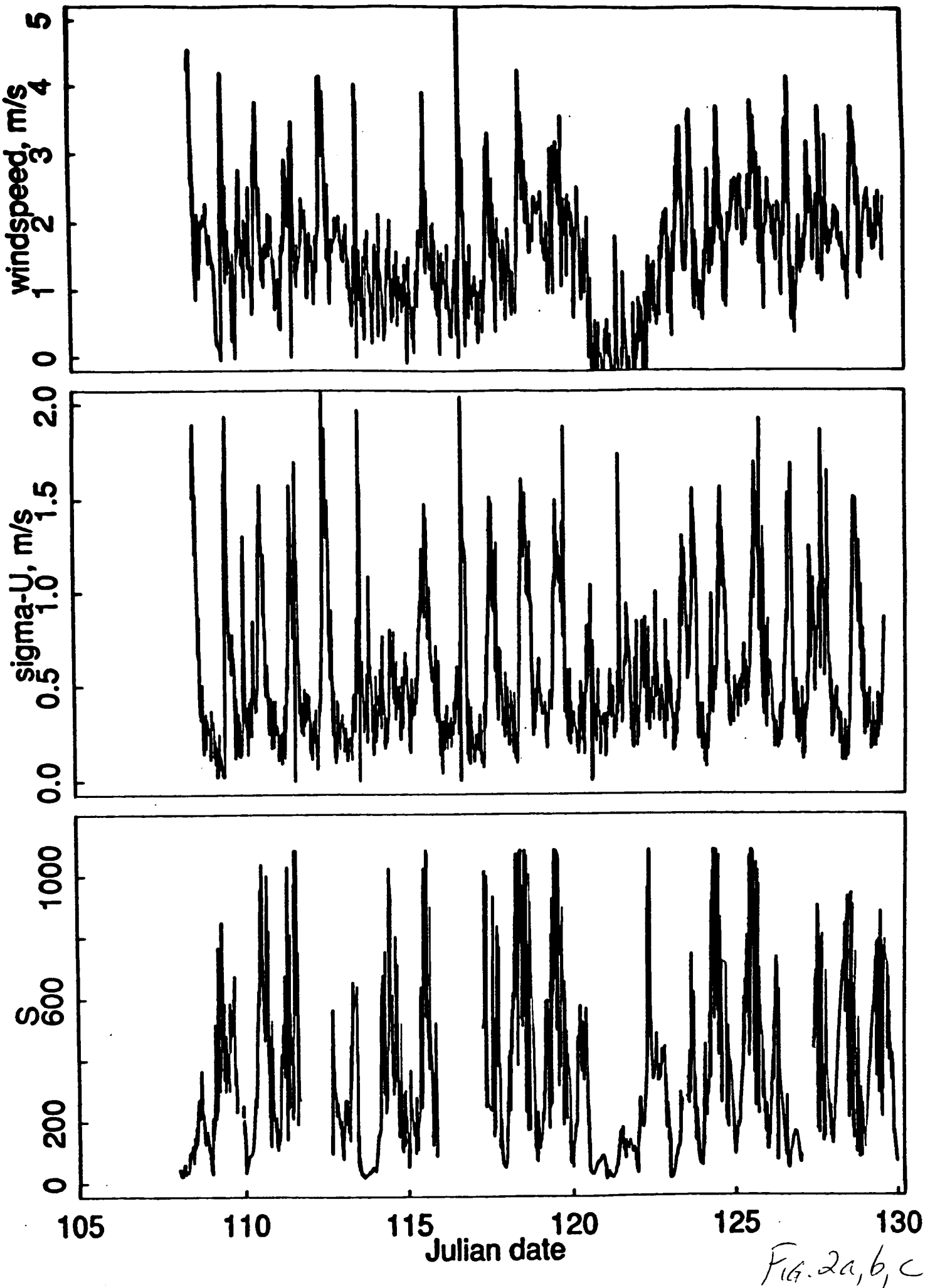
windspeed, m/s
0
1
2
3
4
5
sigma-U, m/s
0.0
0.5
1.0
1.5
2.0
S
0
200
600
1000
105
110
115
120
125
130
Julian date

FIG. 2a, b, c

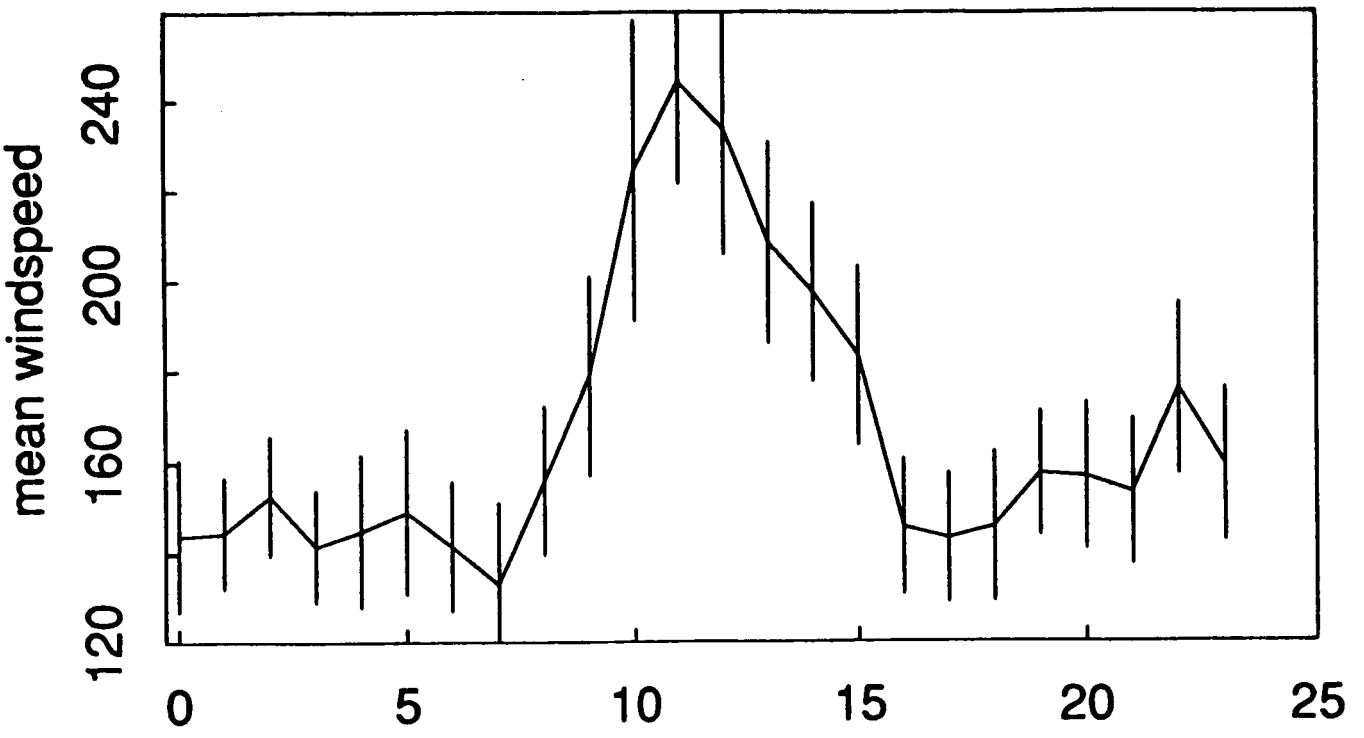
mean windspeed
120
160
200
240
0
5
10
15
20
25

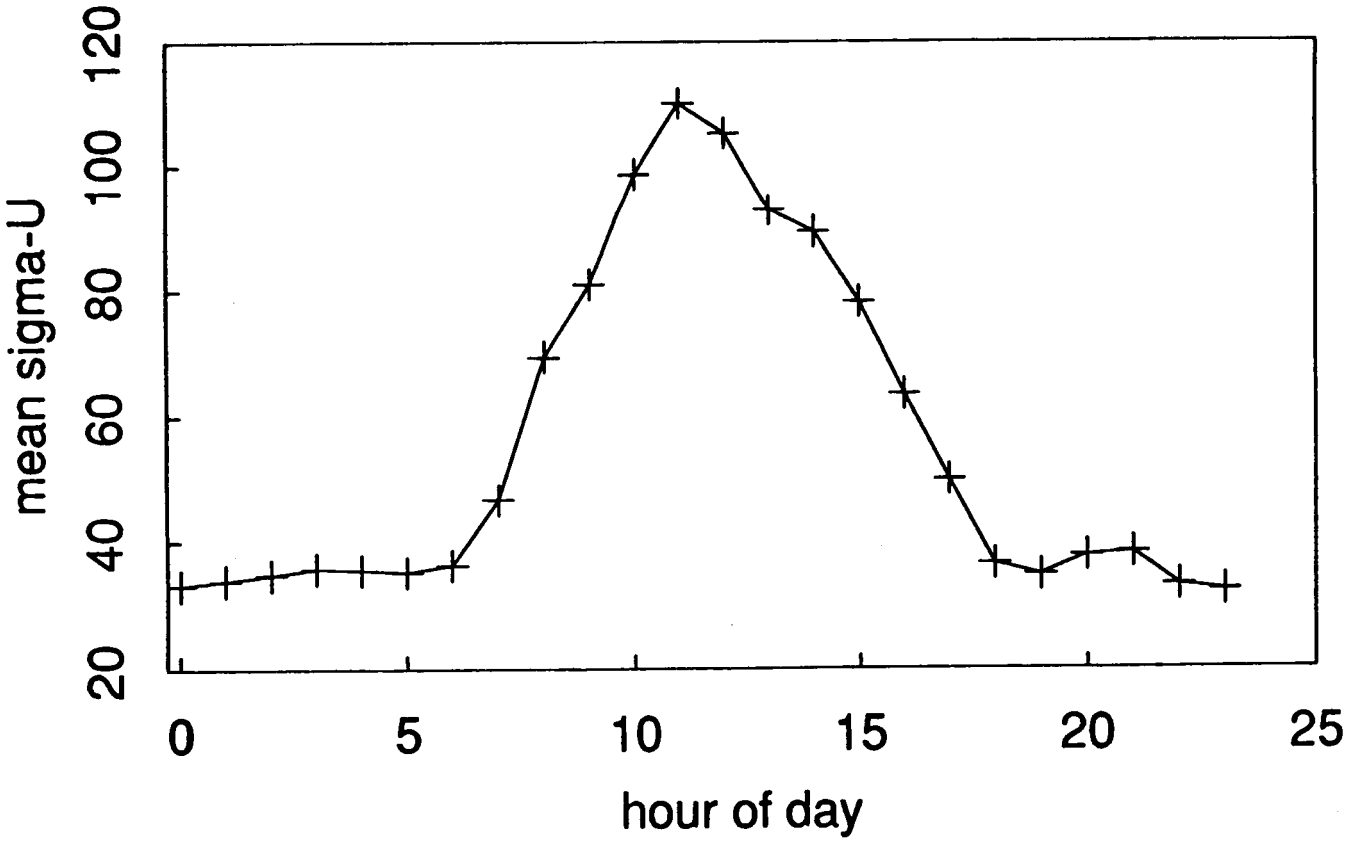
mean sigma-U
20
40
60
80
100
120
0
5
10
15
20
25
hour of day

FIG. 3a,b

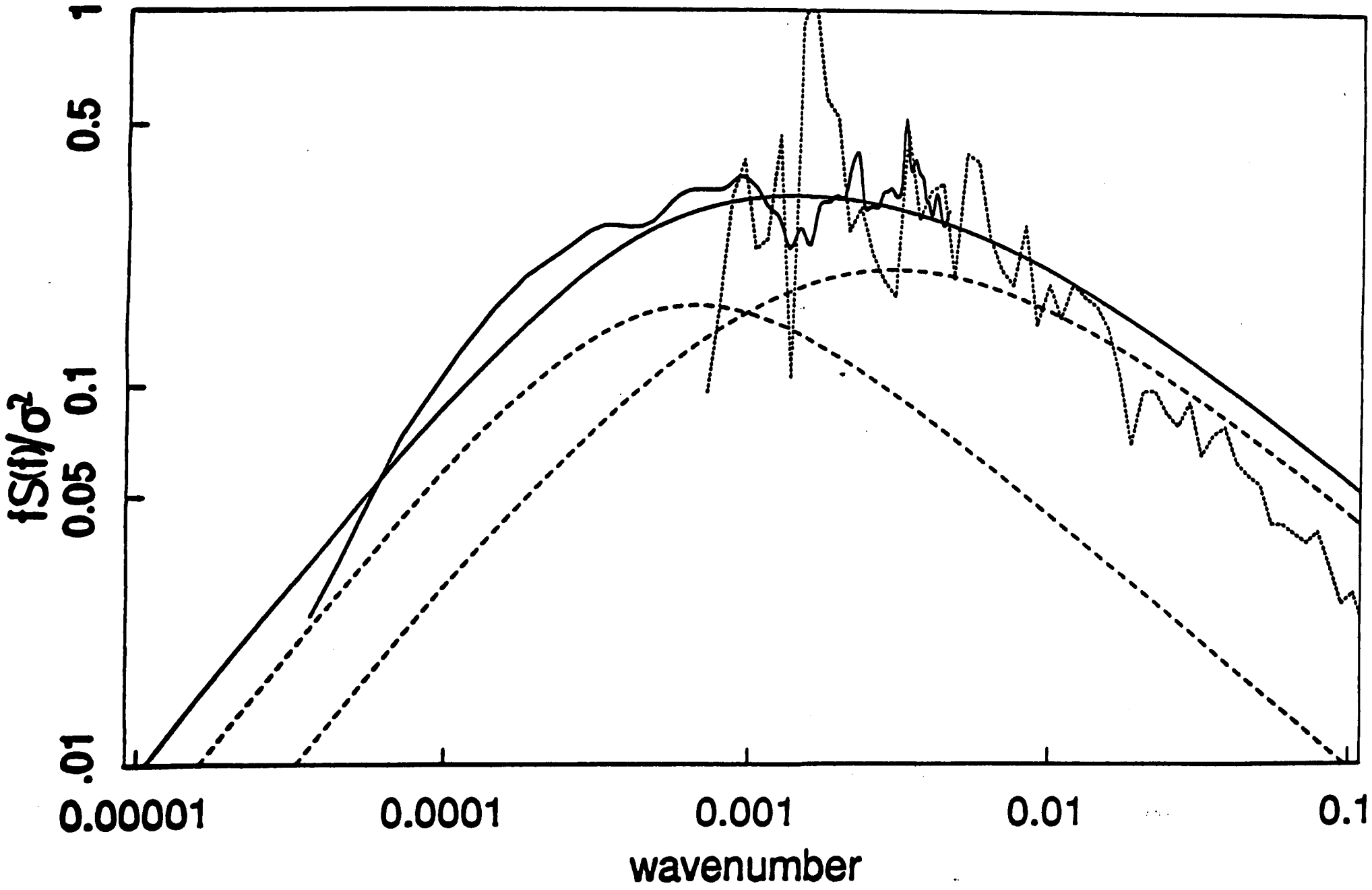

FIG. 4

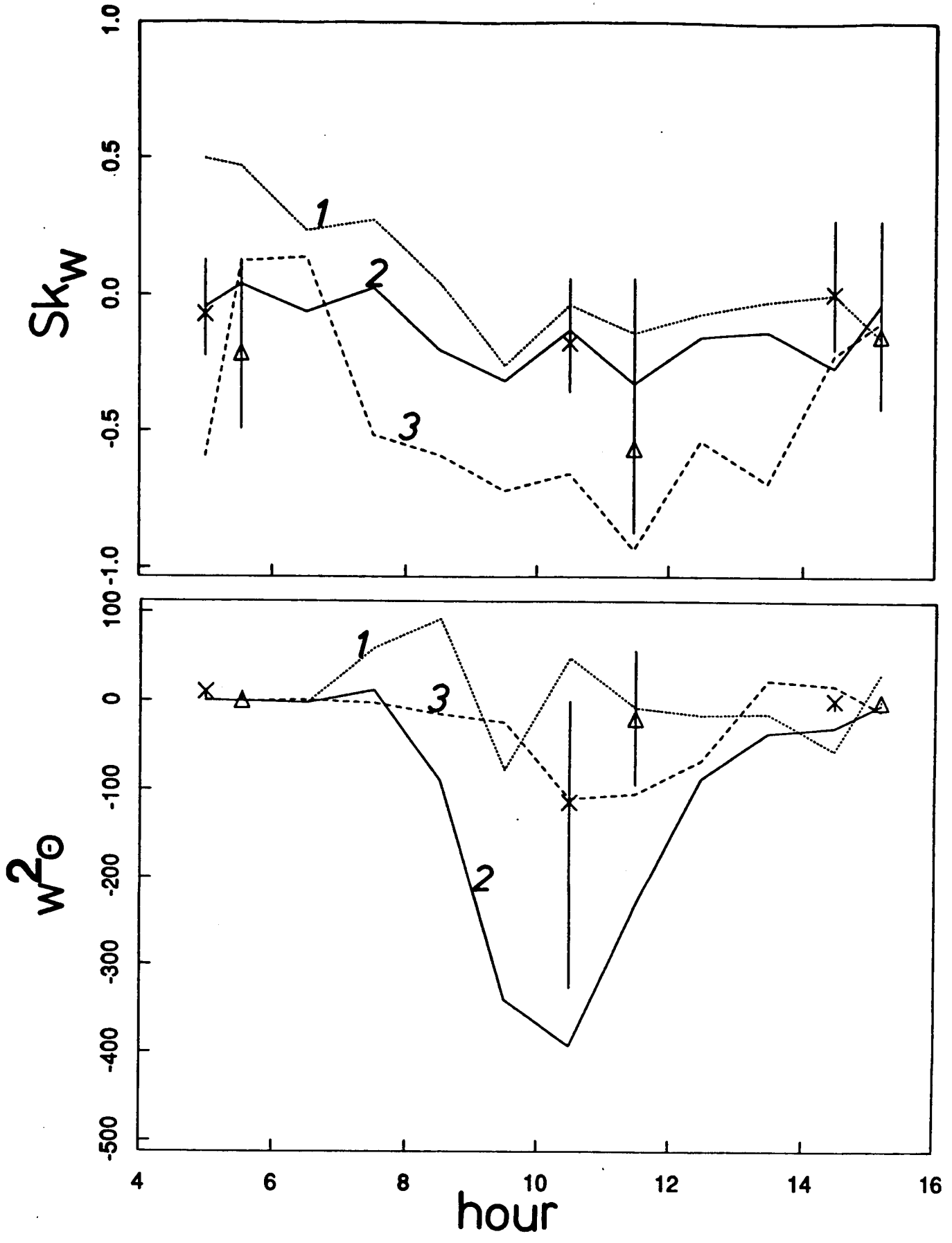
Sk_w
1.0
0.5
0.0
-0.5
-1.0
1
2
3
w²θ
100
0
-100
-200
-300
-400
-500
1
3
2
4
6
8
10
12
14
16
hour

FIG. 5

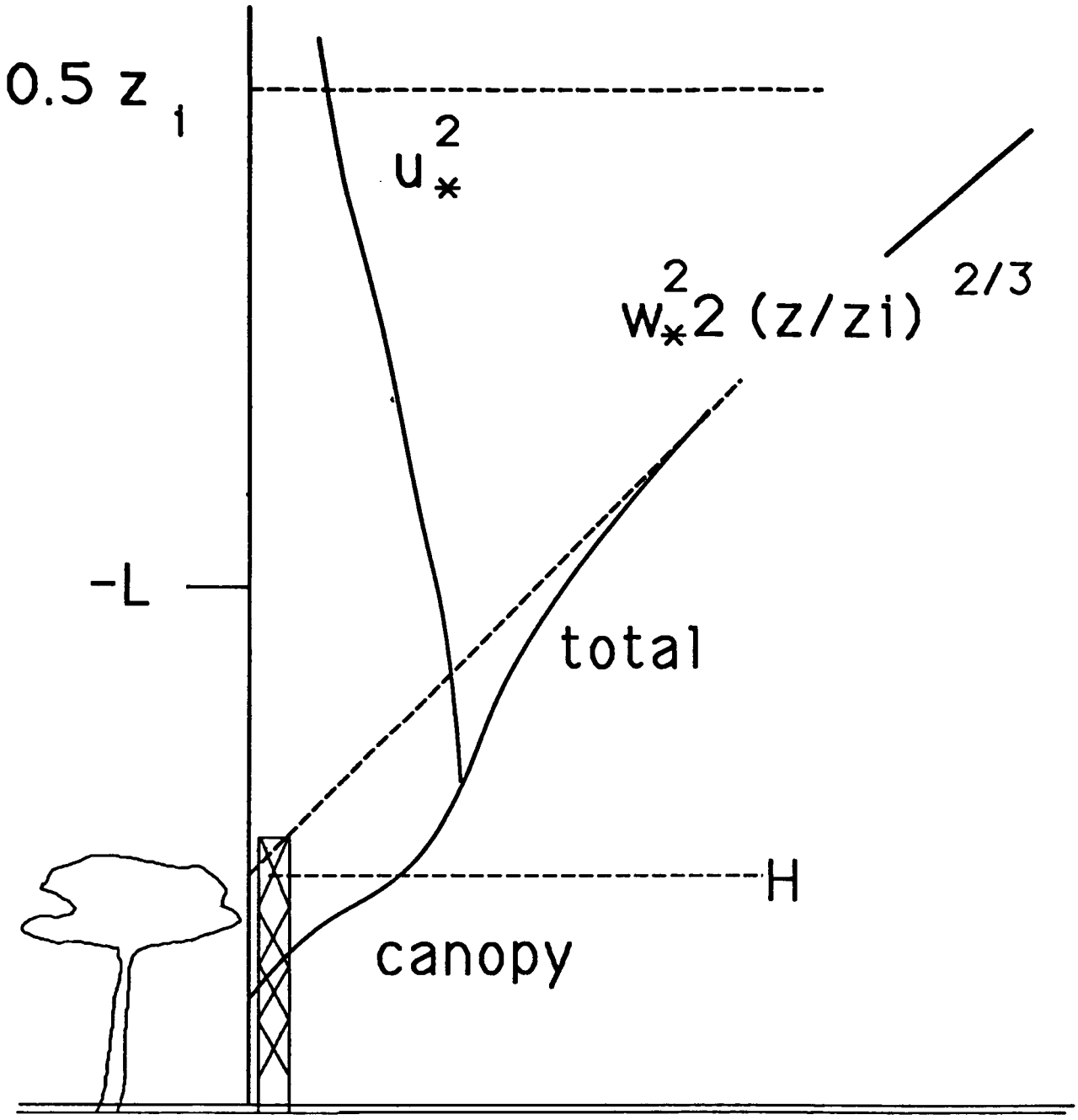

FIG. 6

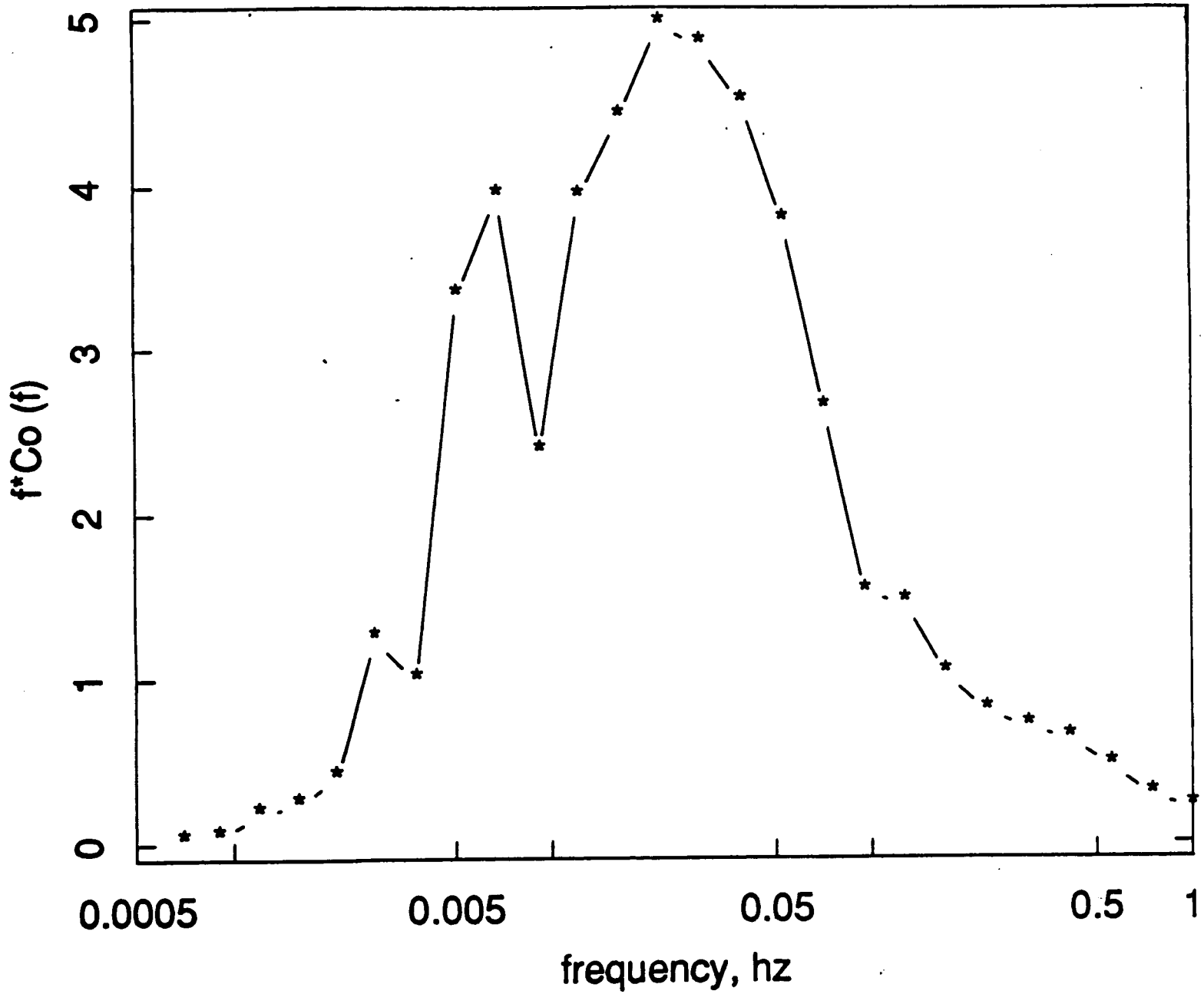

FIG. 7

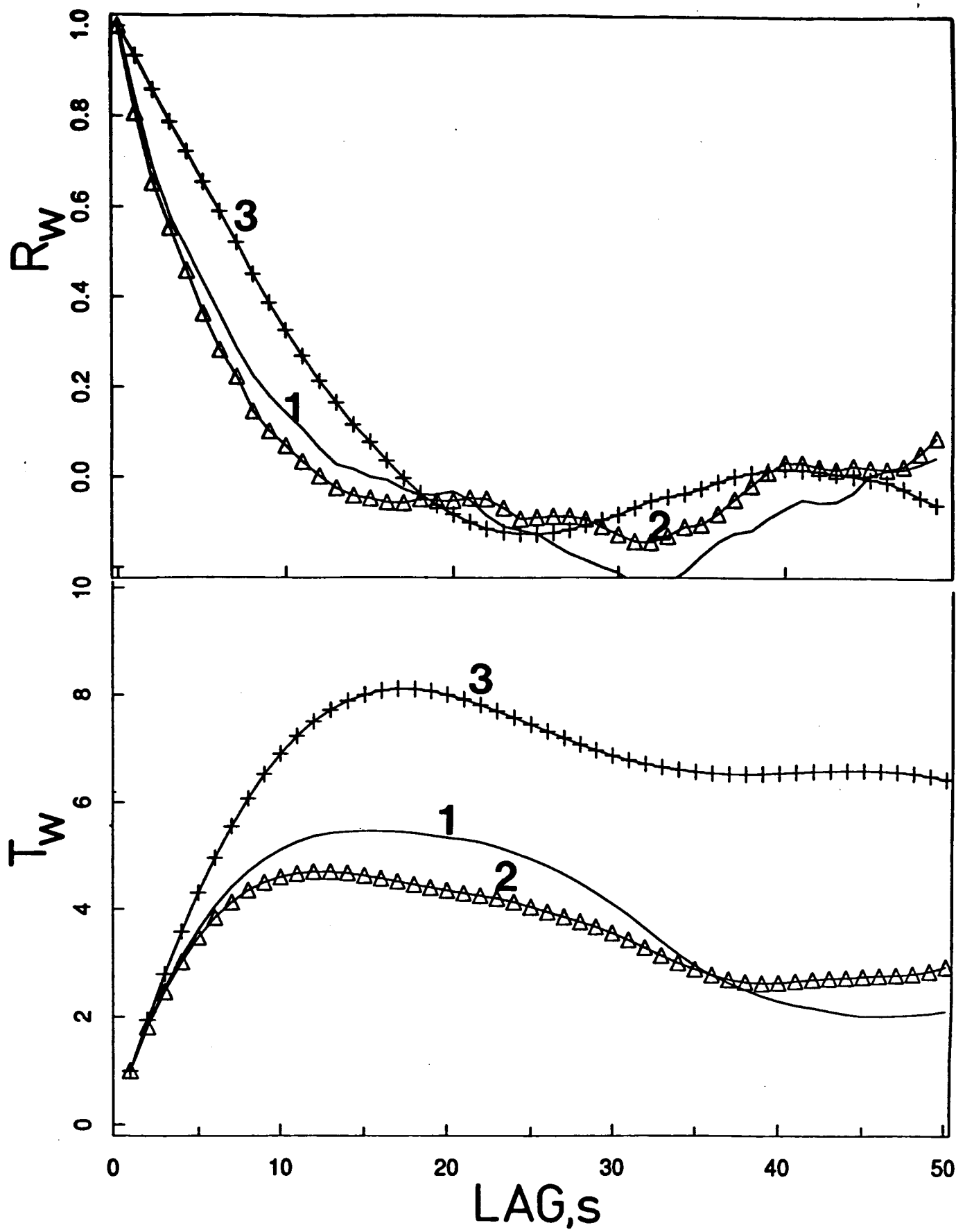

FIG. 8a,b

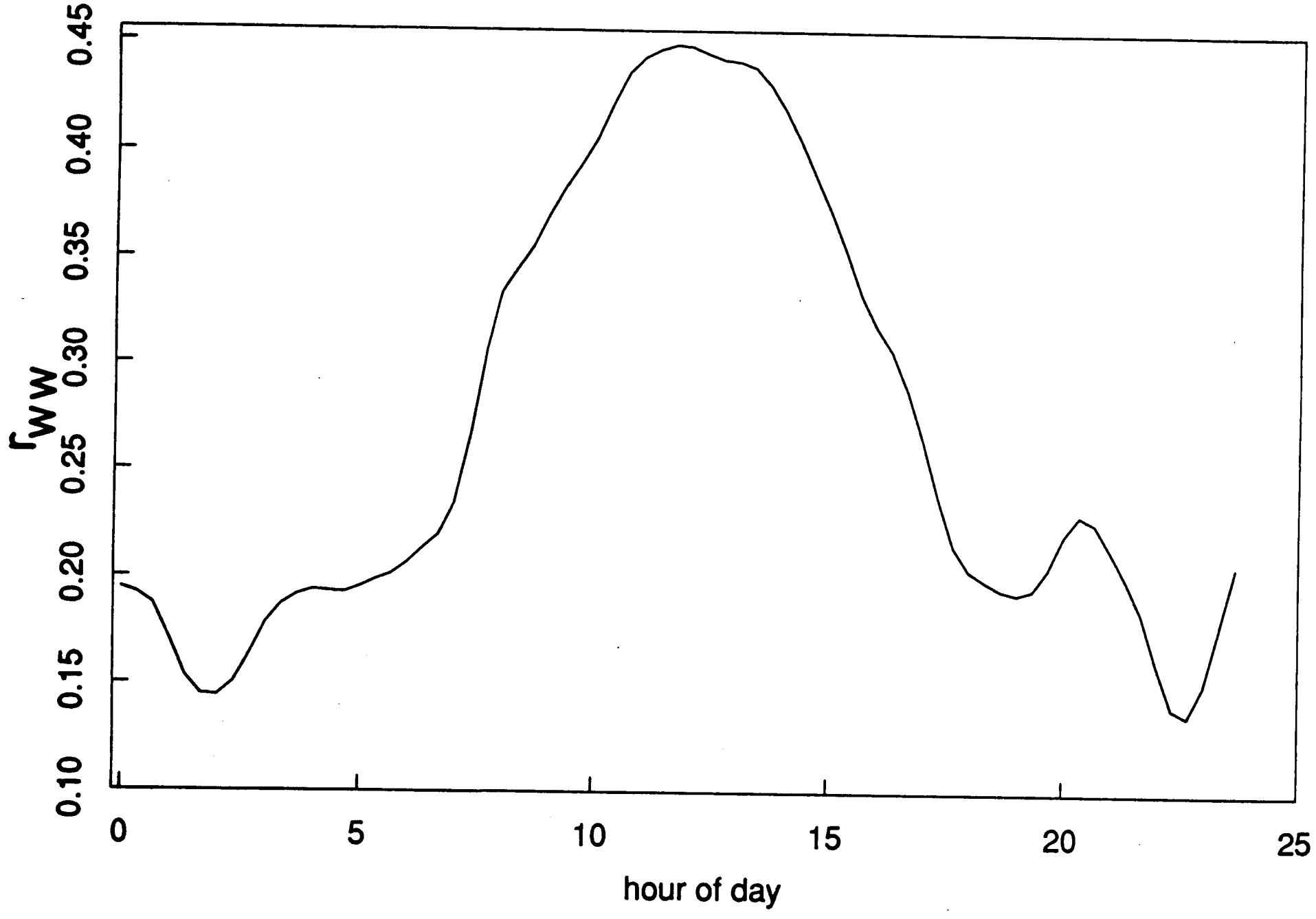

FIG. 9a

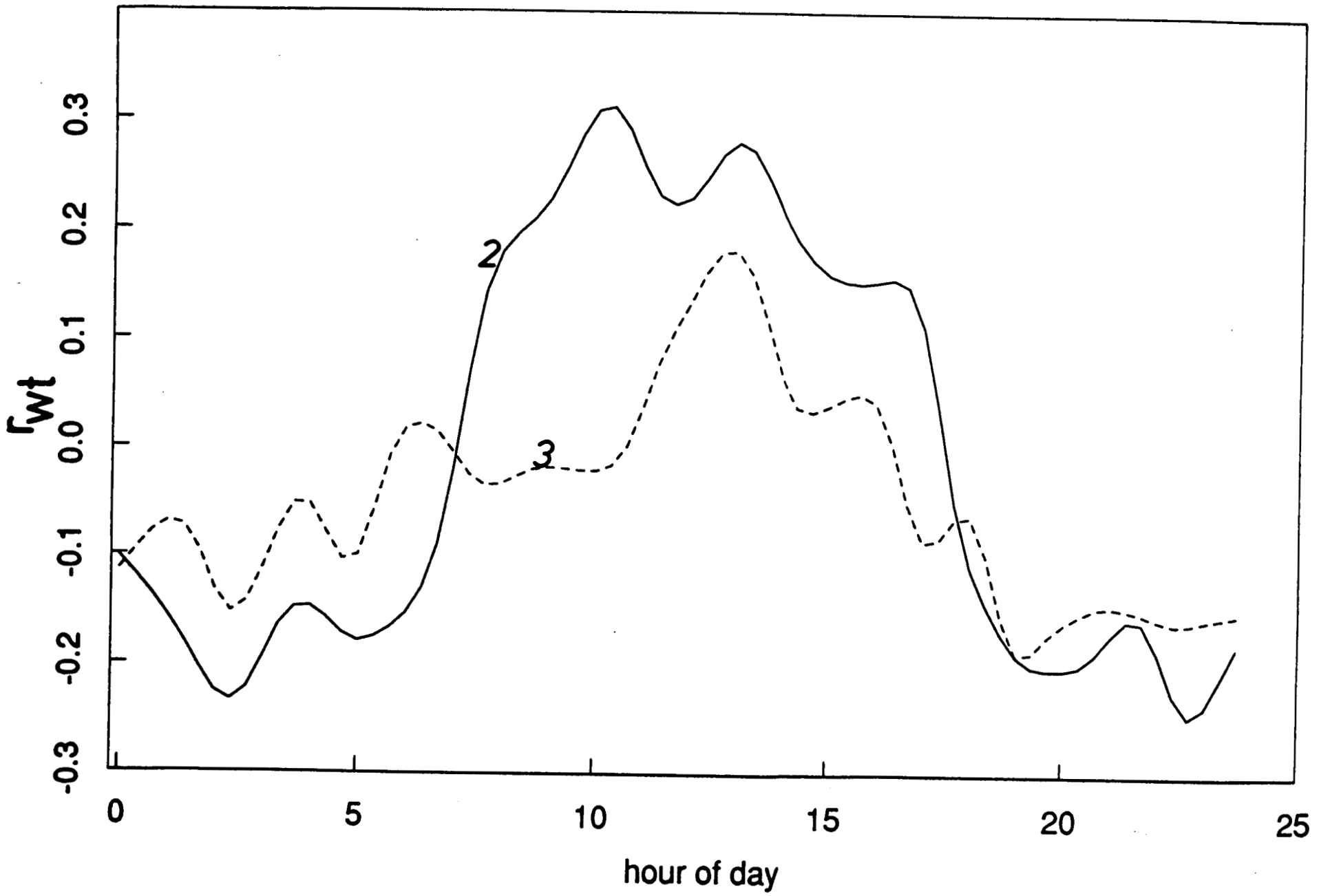

FIG. 9b

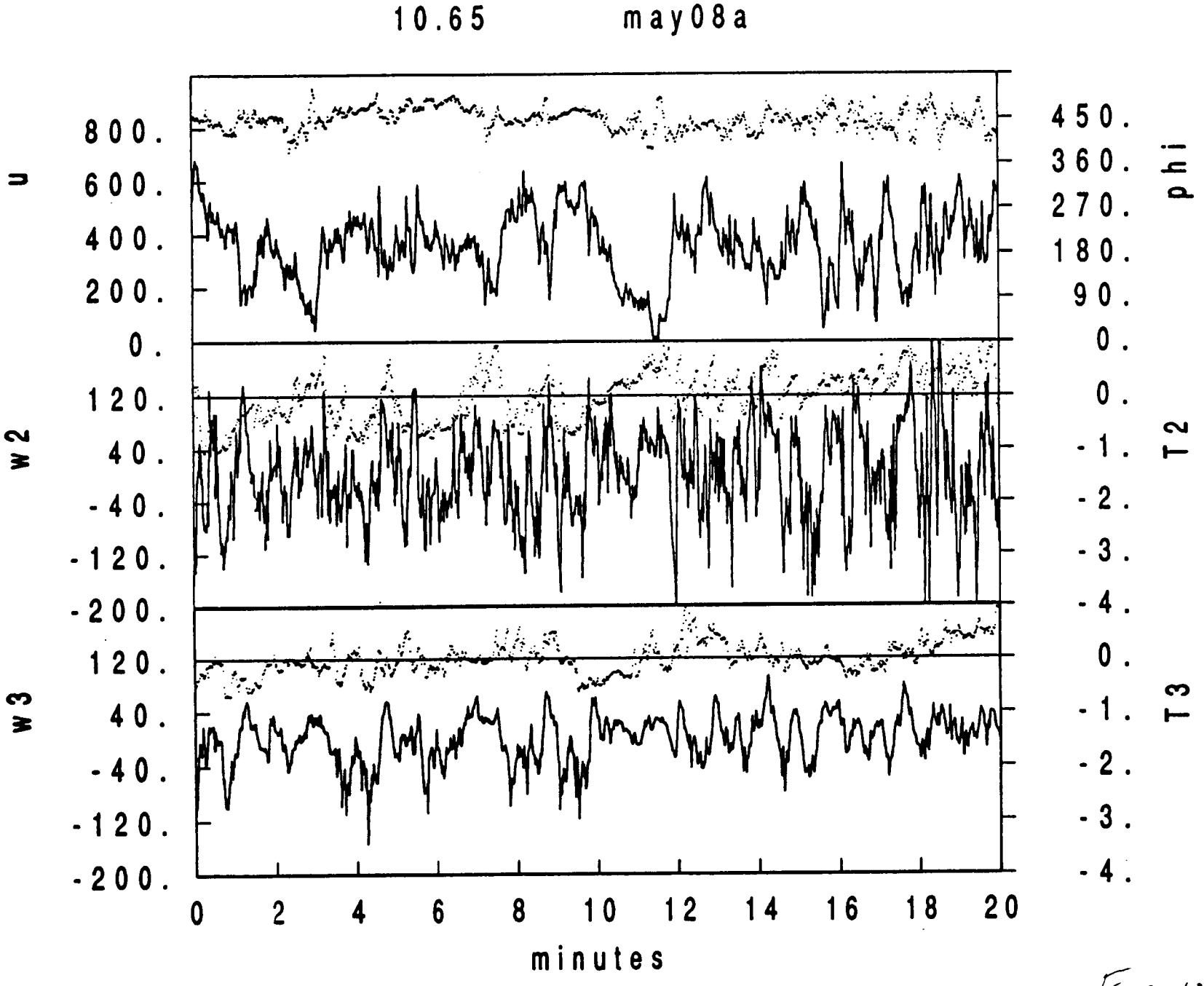
10.65
may08a
u
800.
600.
400.
200.
0.
phi
450.
360.
270.
180.
90.
0.
w2
120.
40.
-40.
-120.
-200.
T2
0.
-1.
-2.
-3.
-4.
w3
120.
40.
-40.
-120.
-200.
T3
0.
-1.
-2.
-3.
-4.
0
2
4
6
8
10
12
14
16
18
20
minutes

FIG. 10

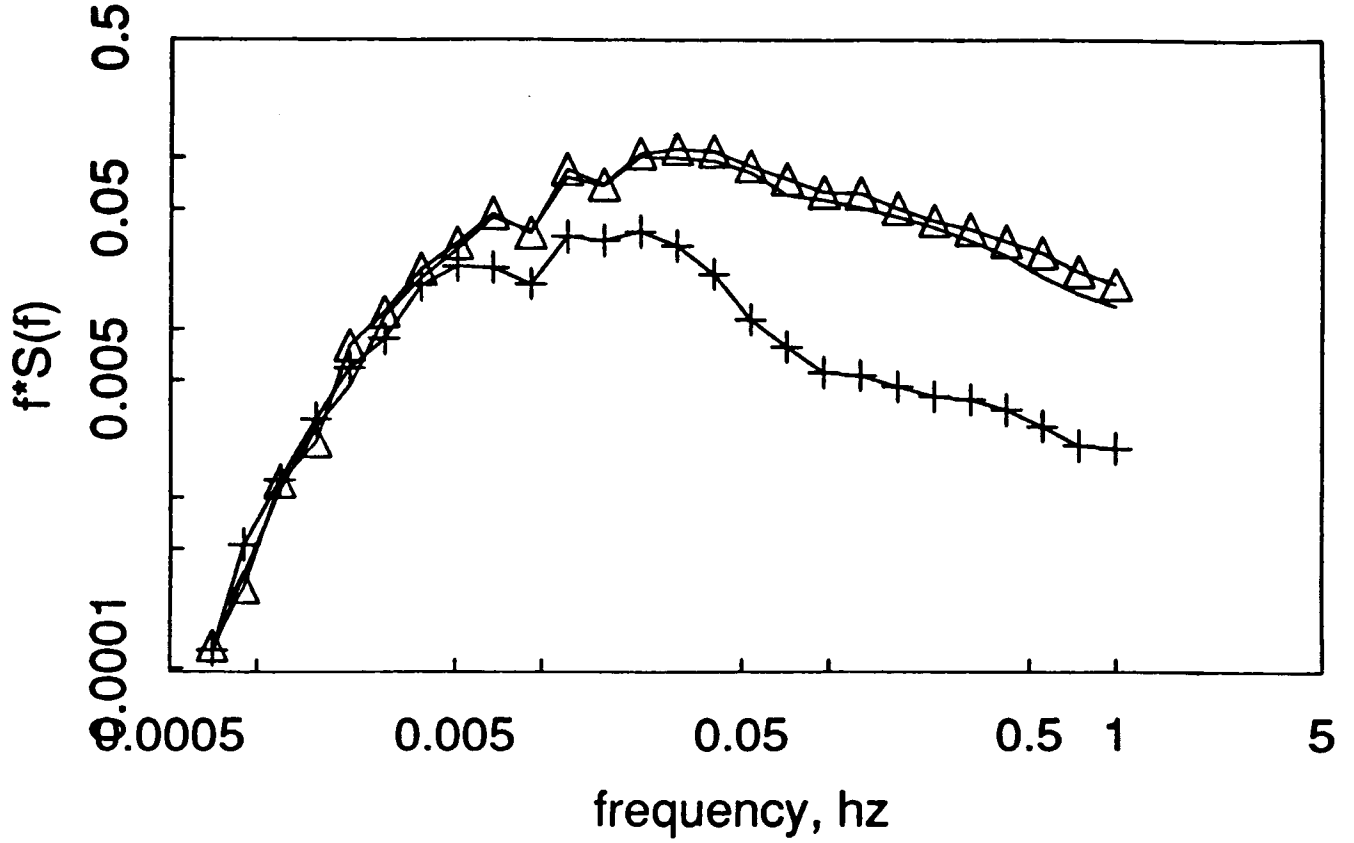
f*S(f)
0.5
0.05
0.005
0.0001
0.0005
0.005
0.05
0.5
1
5
frequency, hz

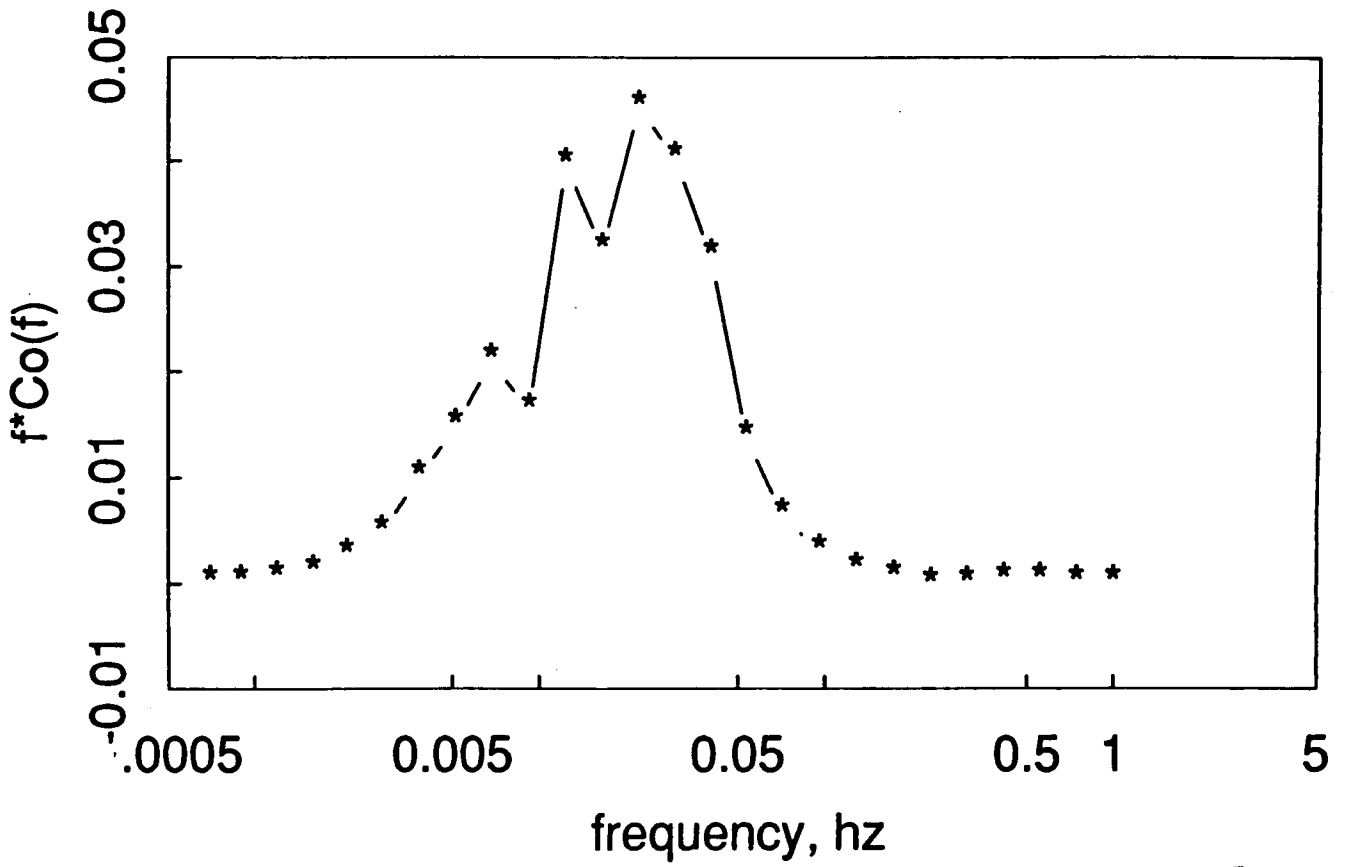
f*Co(f)
0.05
0.03
0.01
-0.01
.0005
0.005
0.05
0.5
1
5
frequency, hz

FIG. 11

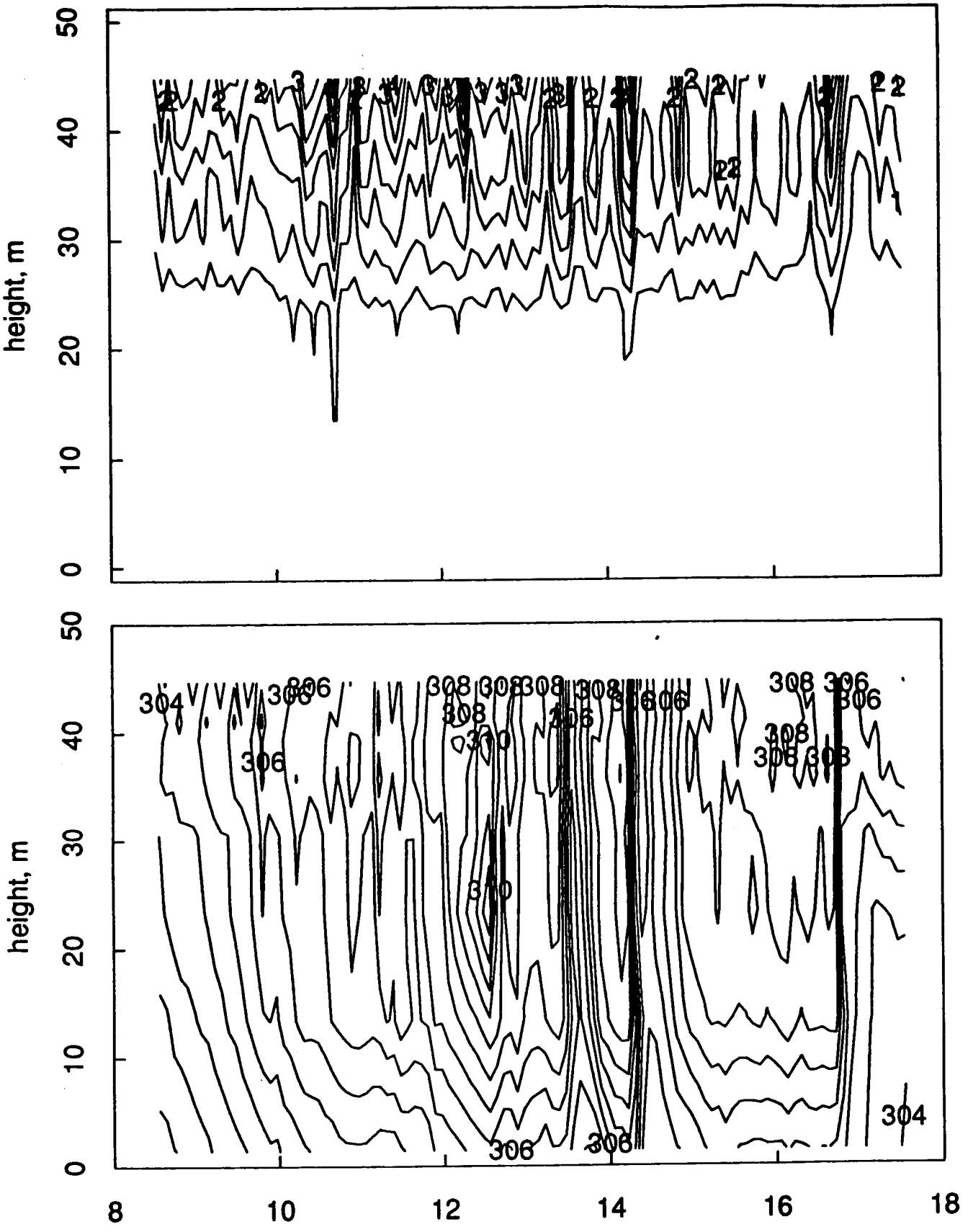
height, m
0
10
20
30
40
50
304
306
308
310
8
10
12
14
16
18
time on May 5

FIG. 13

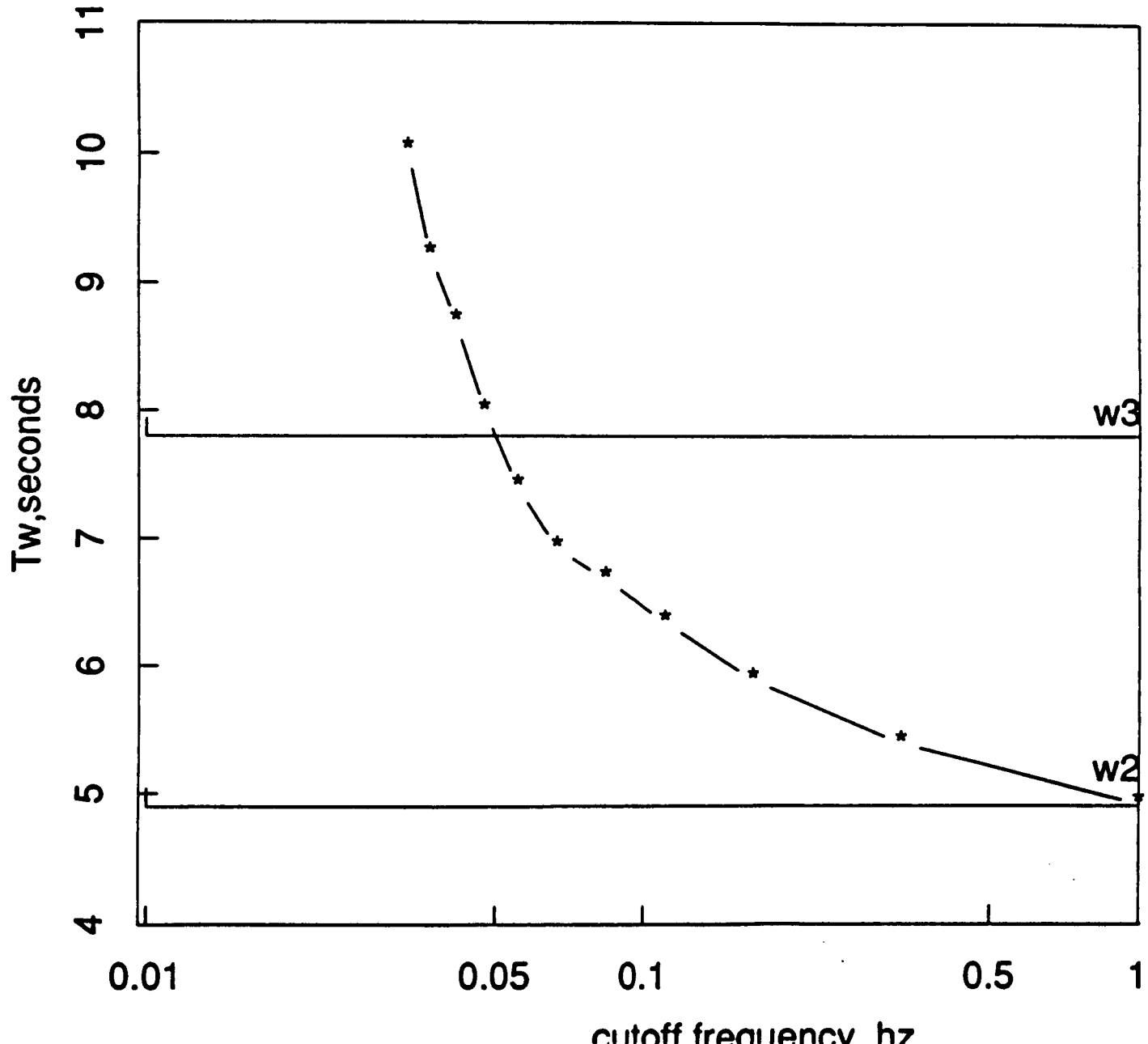
Tw,seconds
11
10
9
8
7
6
5
4
w3
w2
0.01
0.05
0.1
0.5
1
cutoff frequency, hz

FIG. 12

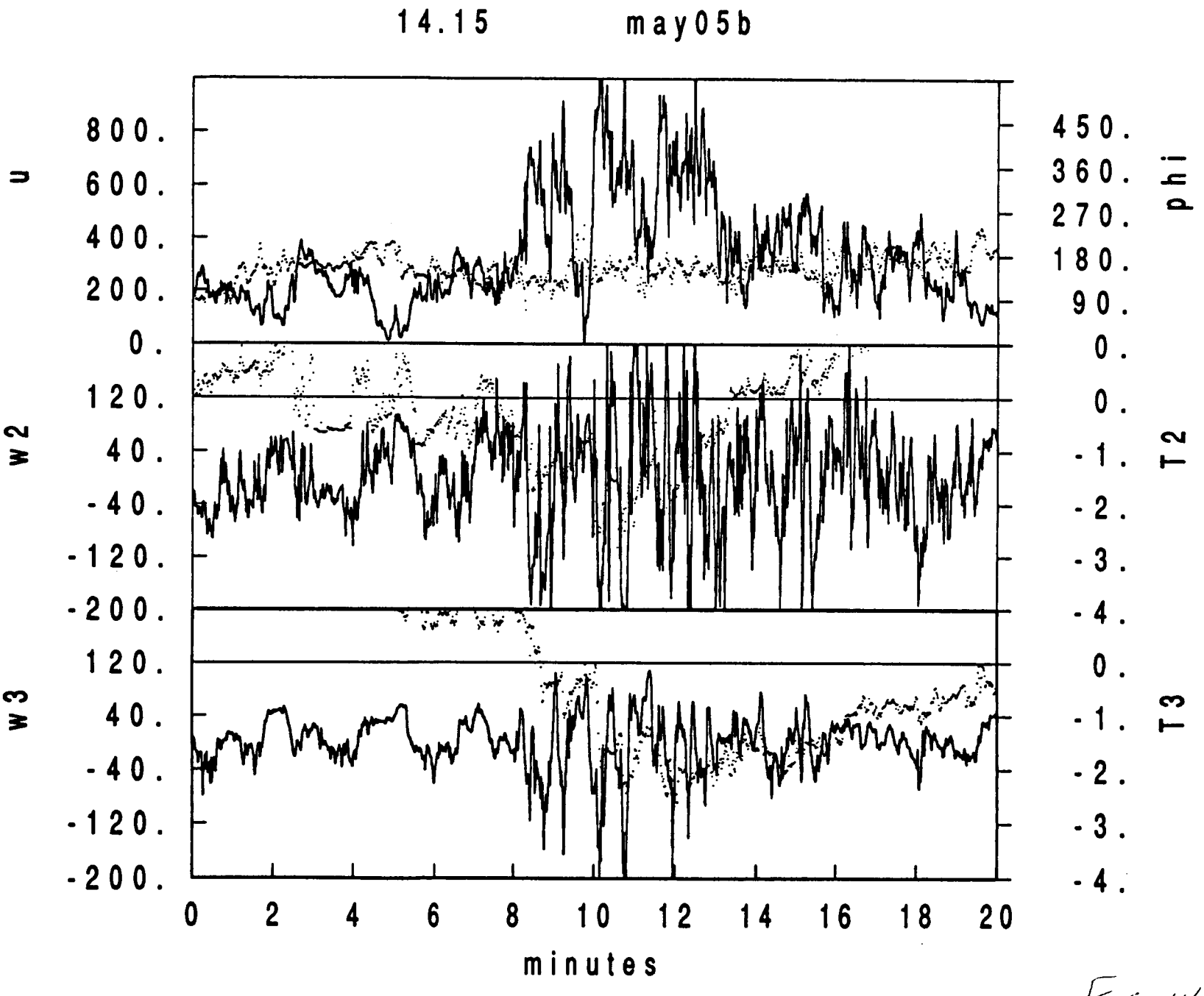
14.15
may05b
u
800.
600.
400.
200.
0.
phi
450.
360.
270.
180.
90.
0.
w2
120.
40.
-40.
-120.
-200.
T2
0.
-1.
-2.
-3.
-4.
w3
120.
40.
-40.
-120.
-200.
T3
0.
-1.
-2.
-3.
-4.
0
2
4
6
8
10
12
14
16
18
20
minutes

FIG. 14

05 MAY 1987 17 33 09 GMT

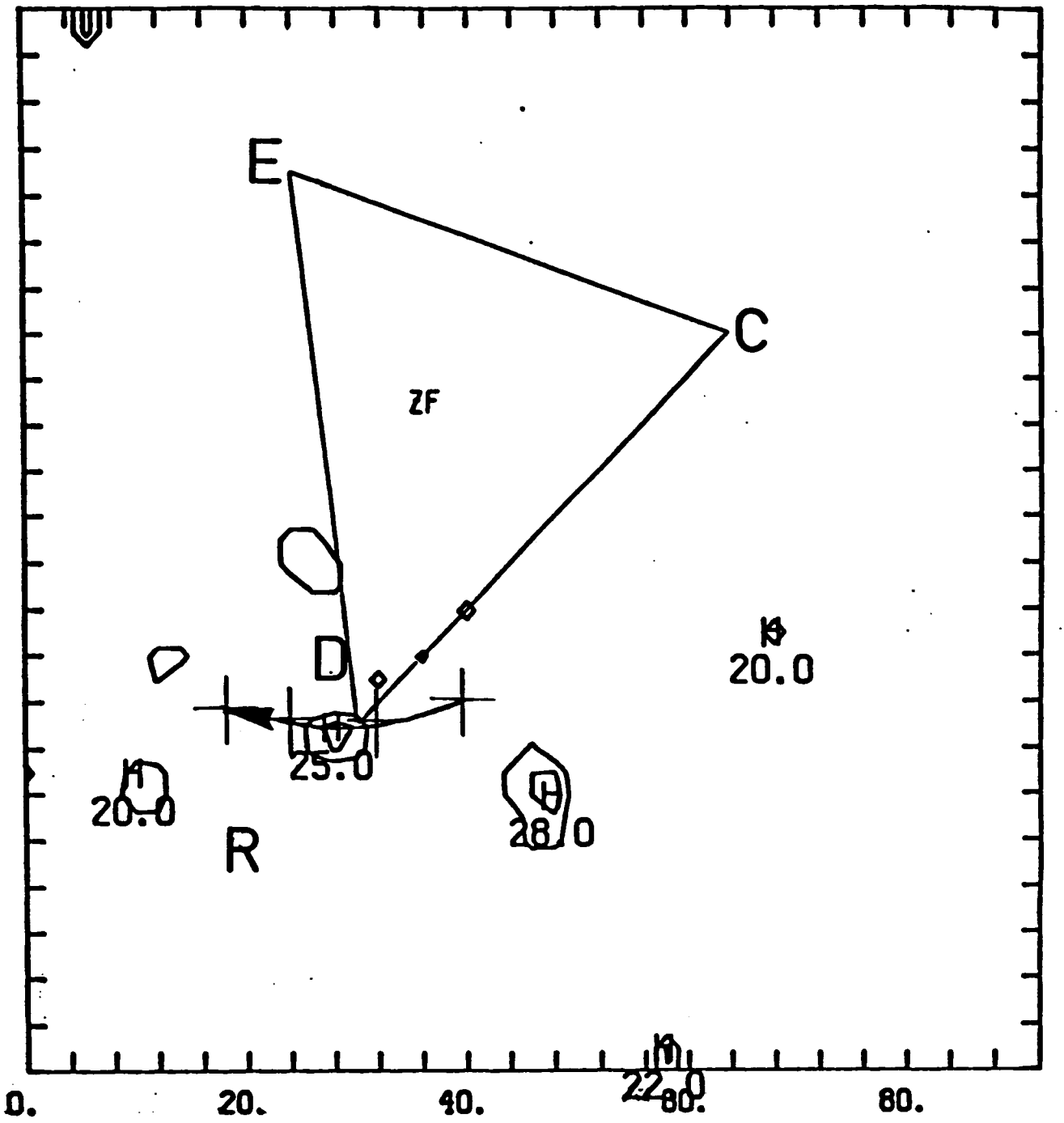

DISTANCE (KM)

FIG. 15

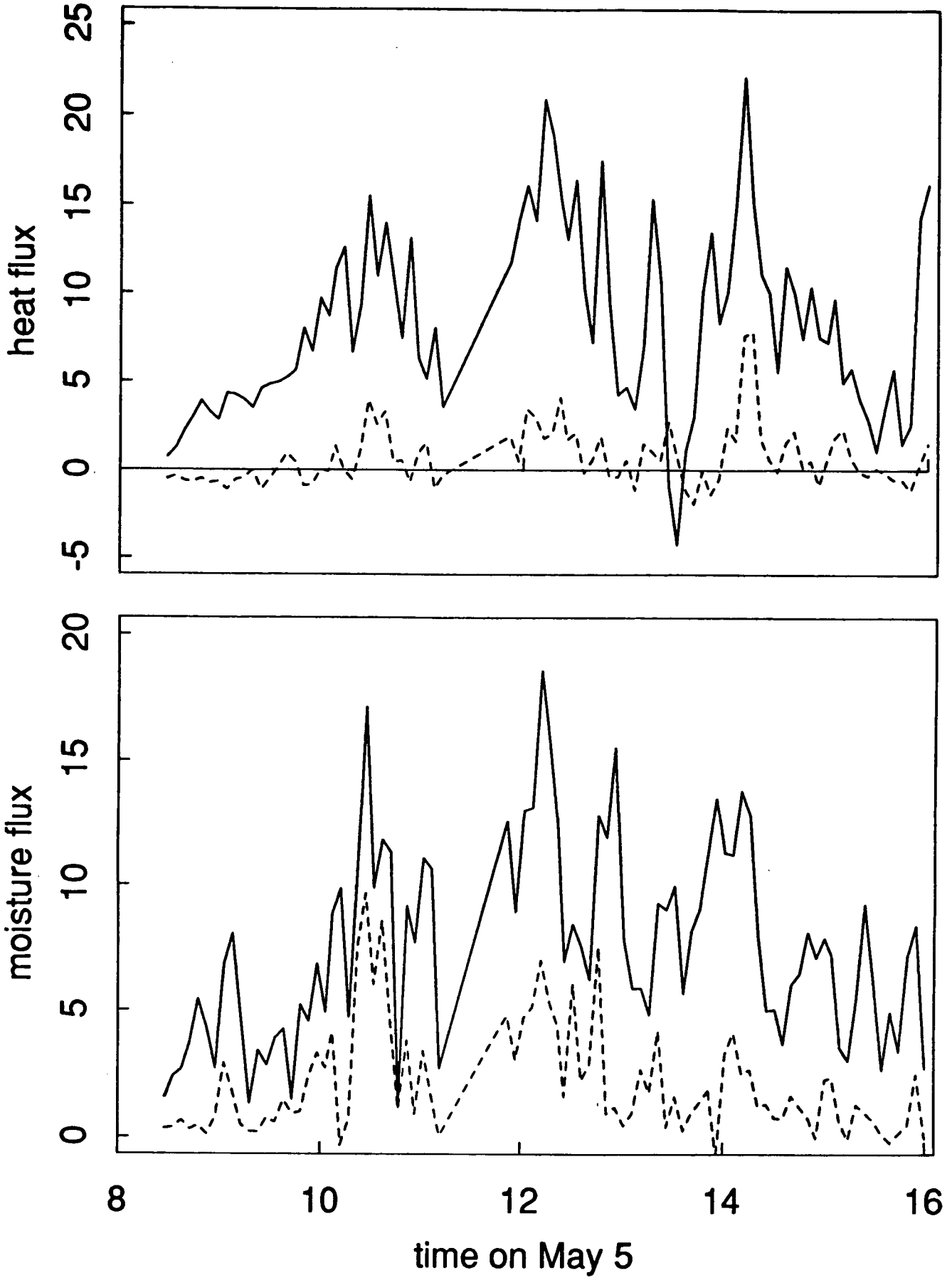
heat flux
25
20
15
10
5
0
-5
moisture flux
20
15
10
5
0
8
10
12
14
16
time on May 5

FIG. 16

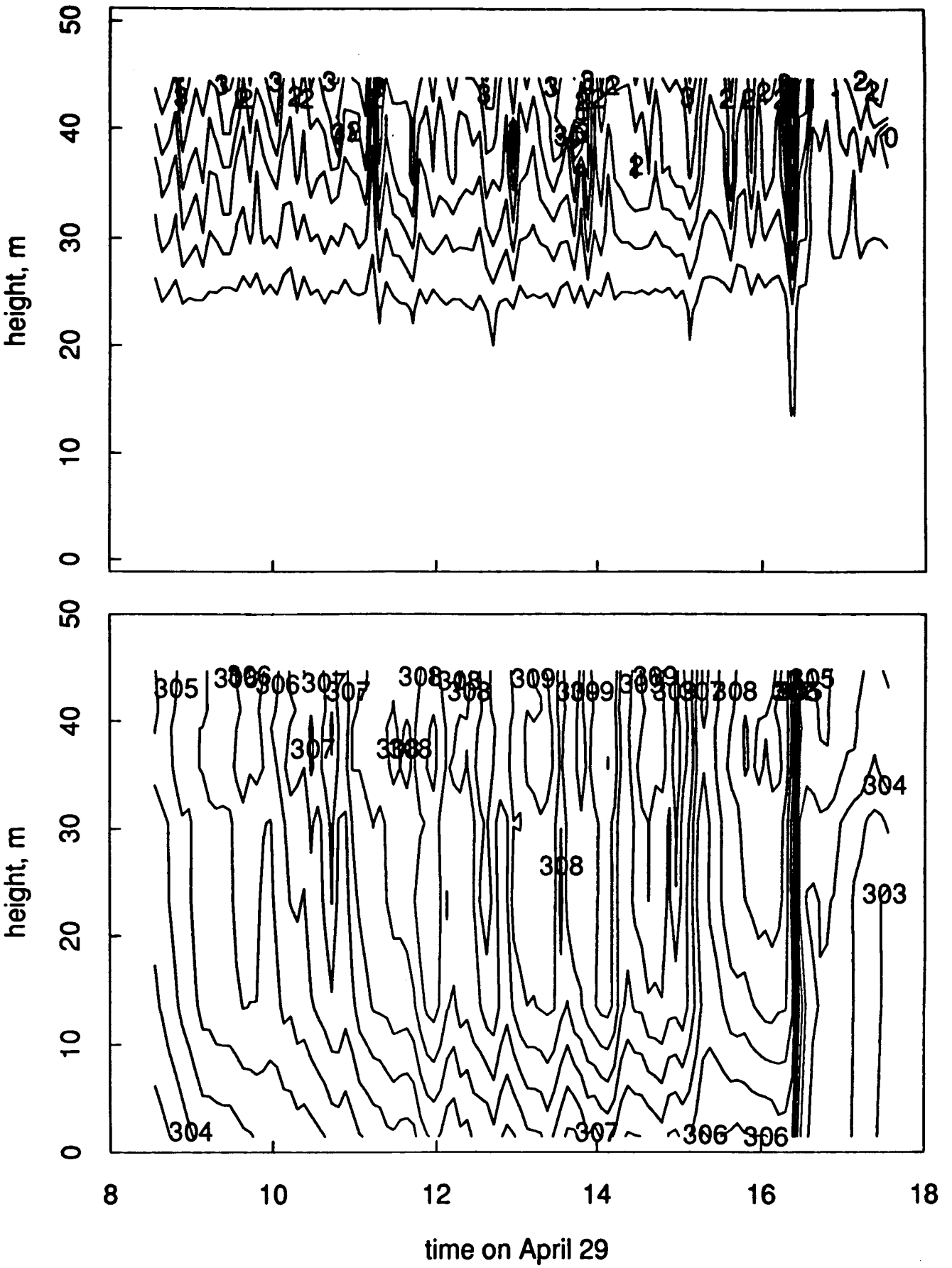
height, m
0
10
20
30
40
50
8
10
12
14
16
18
time on April 29
305
304
307
308
303
306

FIG. 17

APRIL 29 20 18 26 GMT

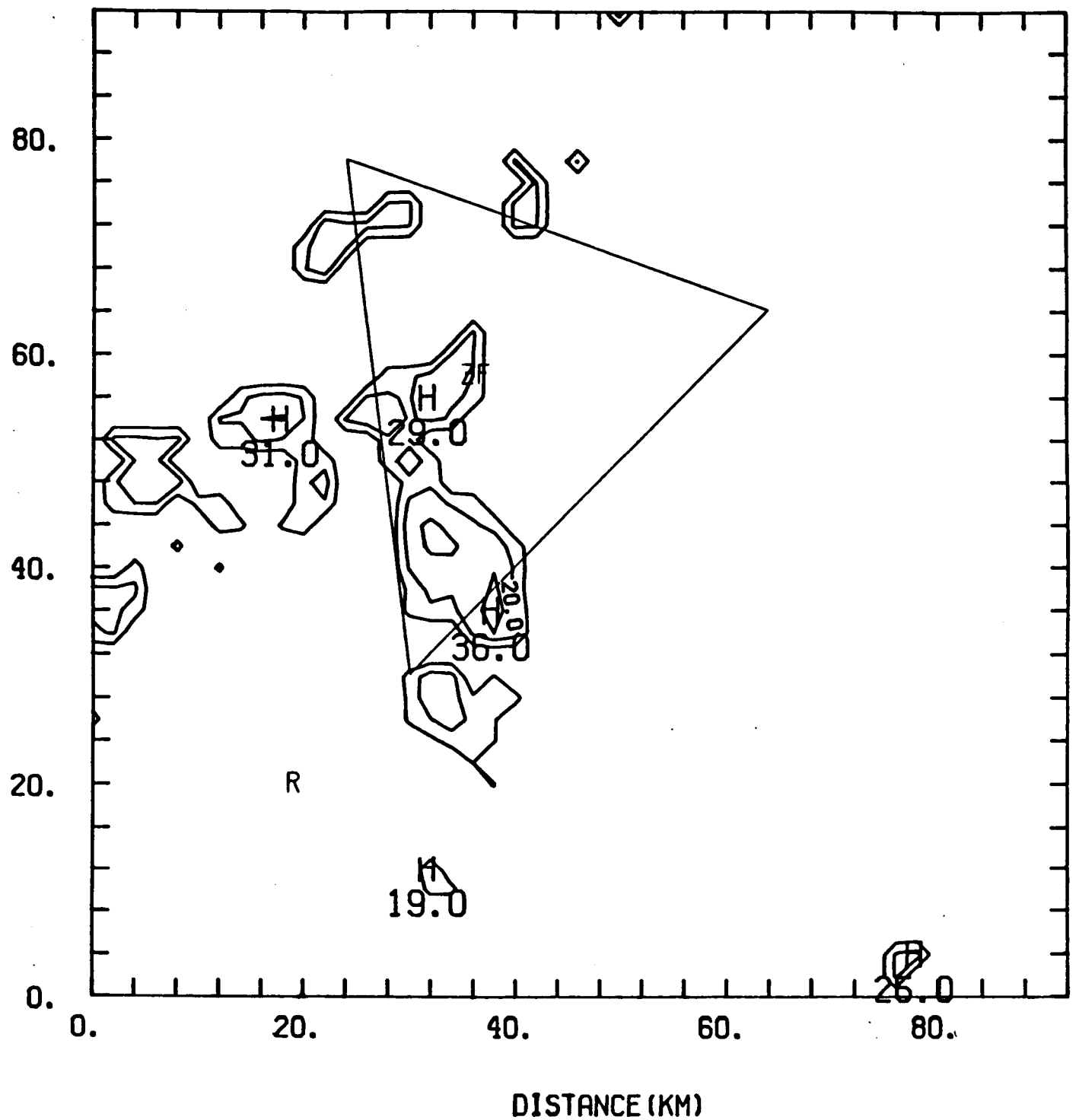

CONTOUR FROM 0. TO 40.000 CONTOUR INTERVAL OF 10.000 PT(3,3)= 0.

FIG. 18
Ex 5.7

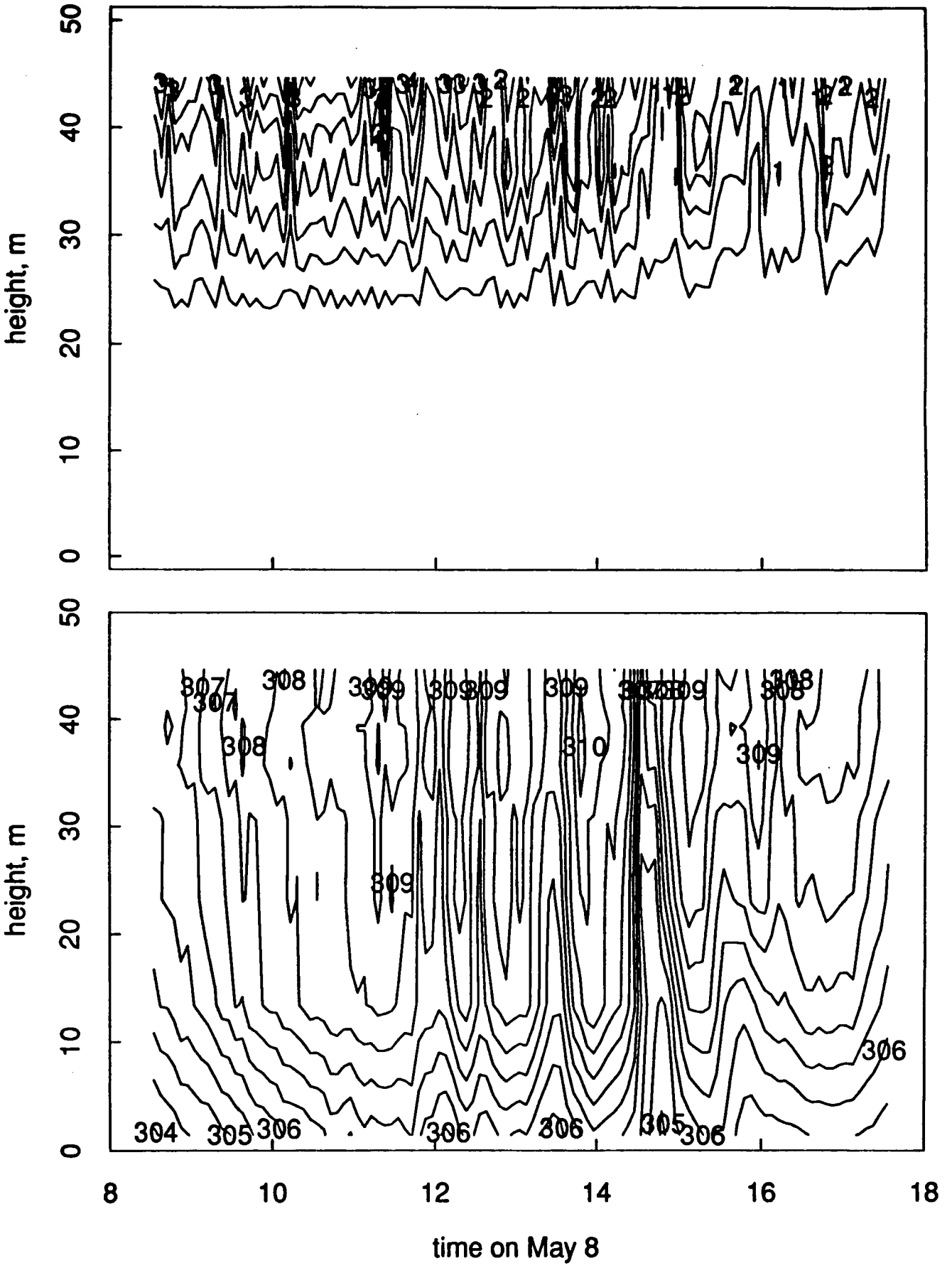
height, m
0
10
20
30
40
50
height, m
0
10
20
30
40
50
307
308
309
310
304
305
306
8
10
12
14
16
18
time on May 8

FIG. 19

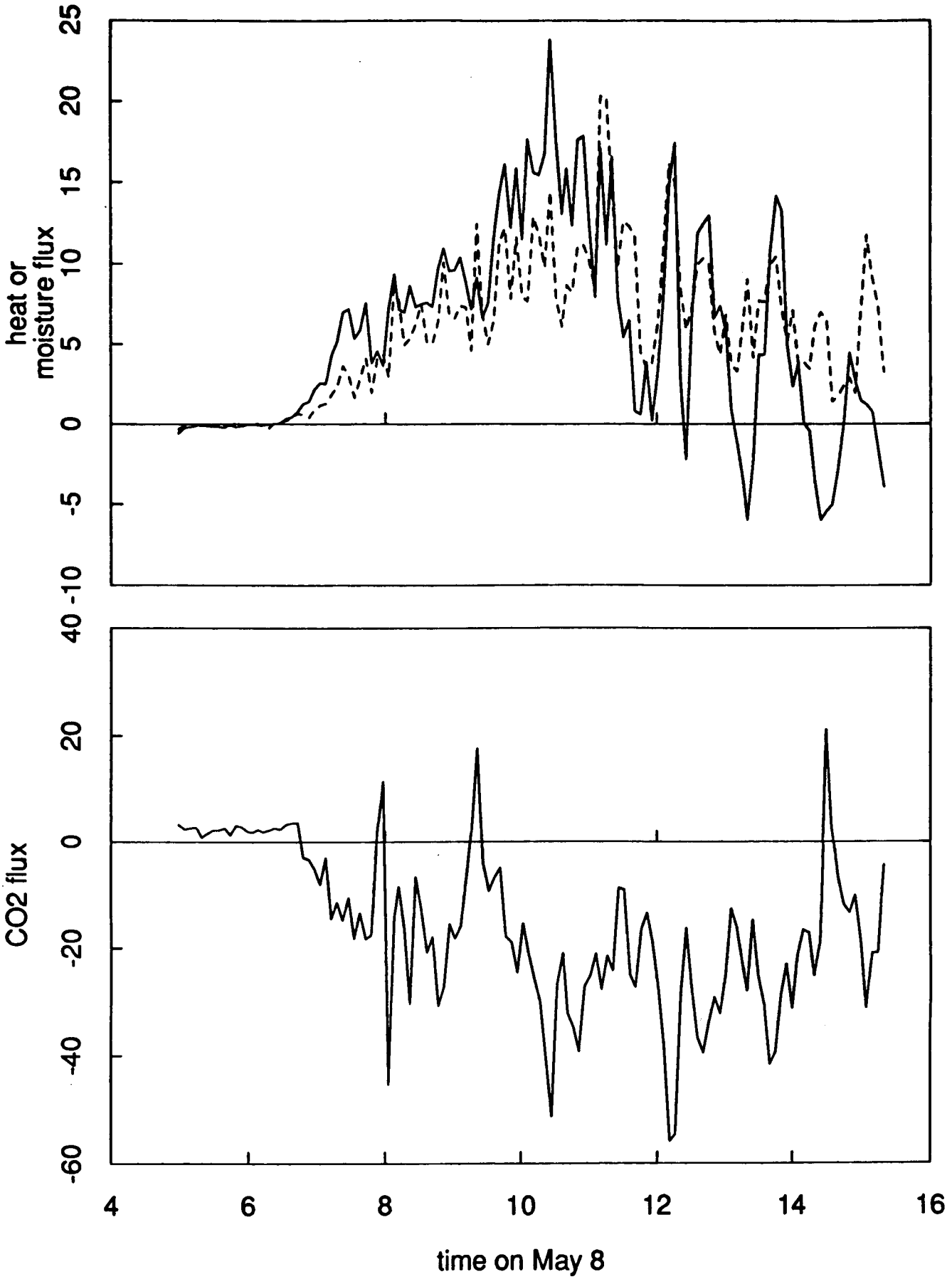
heat or
moisture flux
25
20
15
10
5
0
-5
-10
CO2 flux
40
20
0
-20
-40
-60
4
6
8
10
12
14
16
time on May 8

FIG. 20

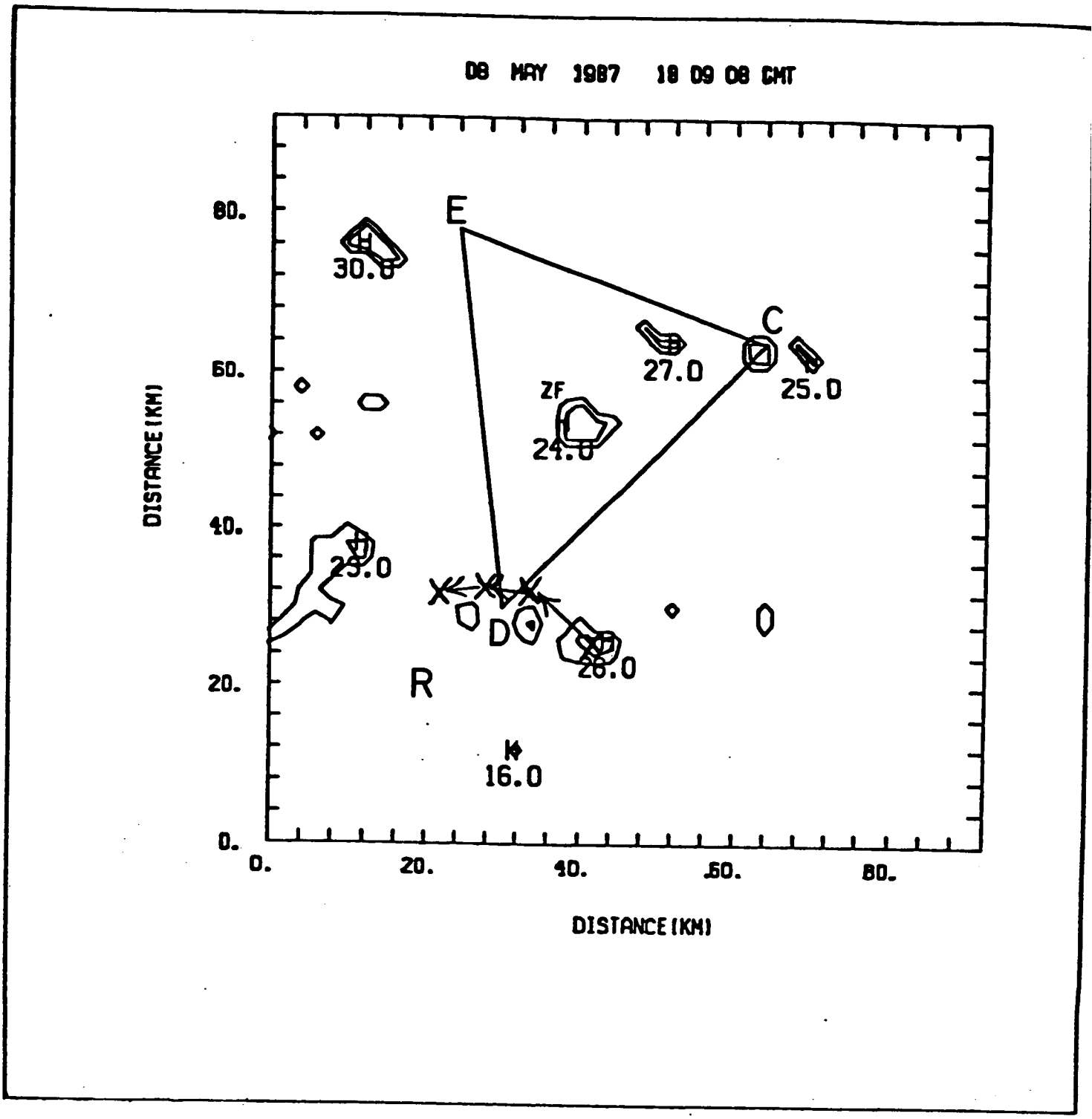
08 MAY 1987 18 09 08 GMT
80.
60.
40.
20.
0.
DISTANCE (KM)
E
C
ZF
D
R
30.8
27.0
25.0
24.0
29.0
28.0
16.0
0.
20.
40.
60.
80.
DISTANCE (KM)

FIG. 21

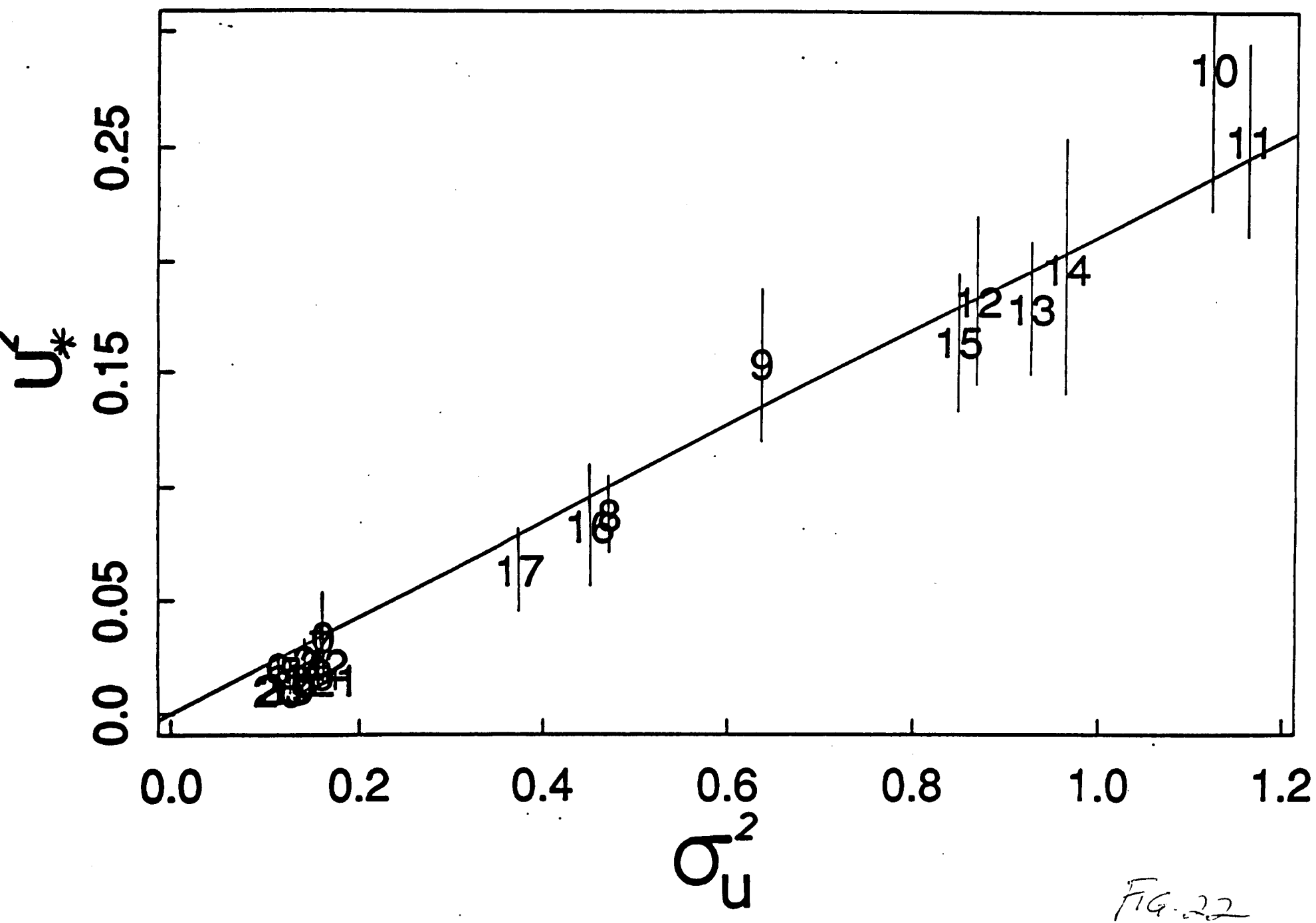
u_*^2
0.0
0.05
0.15
0.25
0.0
0.2
0.4
0.6
0.8
1.0
1.2
σ_u^2
10
11
14
12
13
15
9
16
8
17

FIG. 22

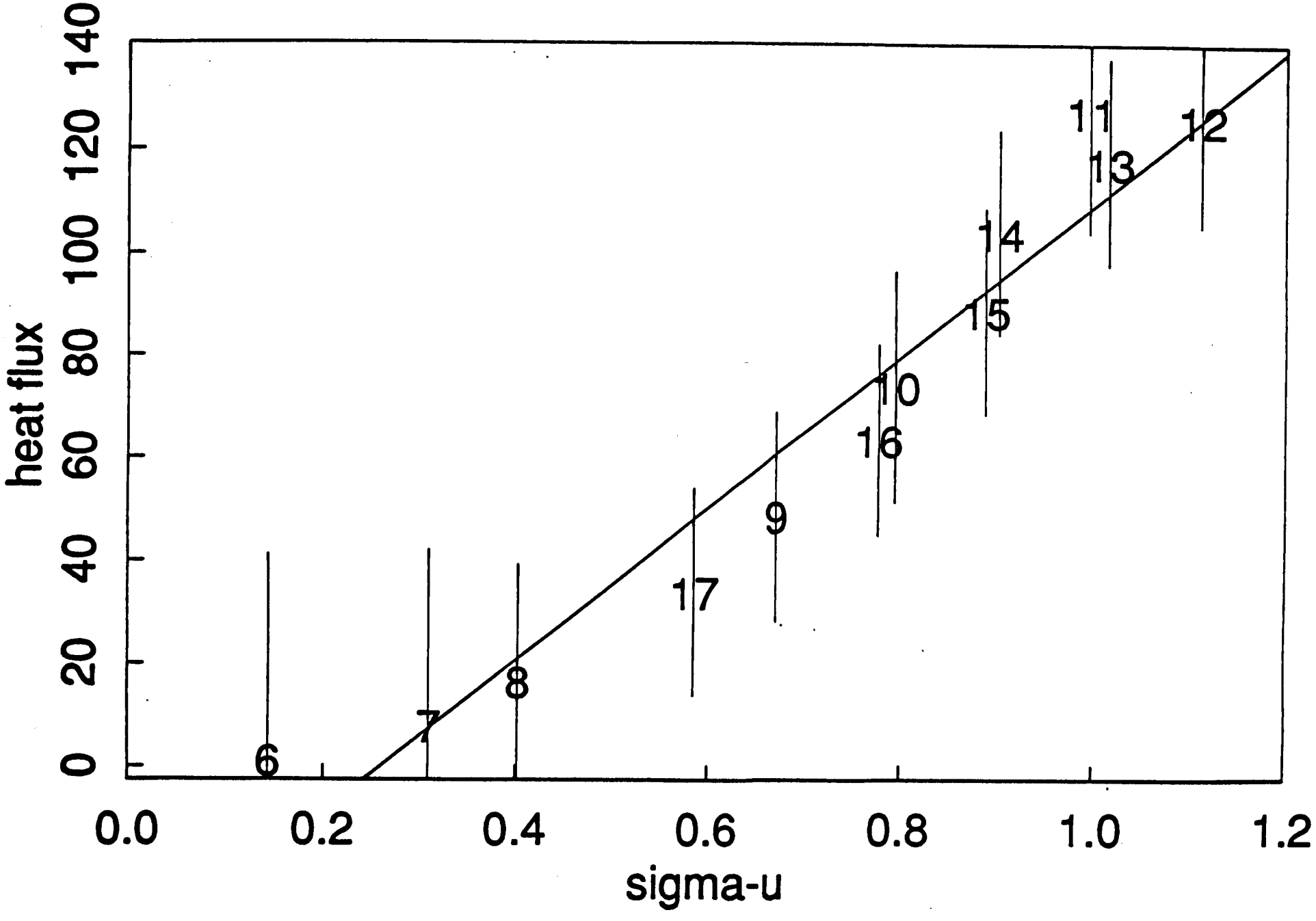
heat flux
0
20
40
60
80
100
120
140
0.0
0.2
0.4
0.6
0.8
1.0
1.2
sigma-u
6
7
8
17
9
16
10
15
14
11
13
12

FIG. 23

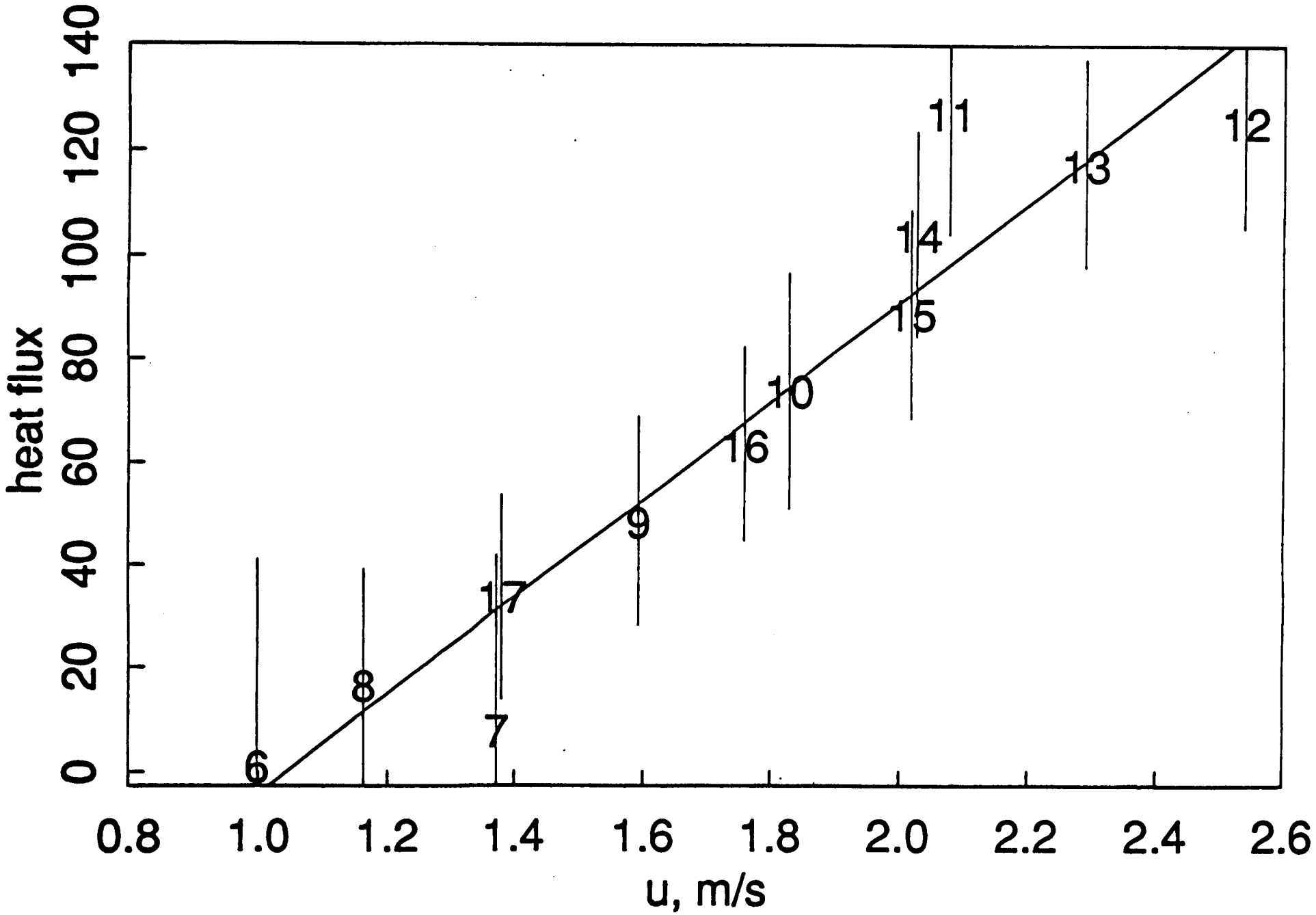
heat flux
0
20
40
60
80
100
120
140
0.8
1.0
1.2
1.4
1.6
1.8
2.0
2.2
2.4
2.6
u, m/s
6
8
7
17
9
16
10
15
14
11
13
12

FIG. 24

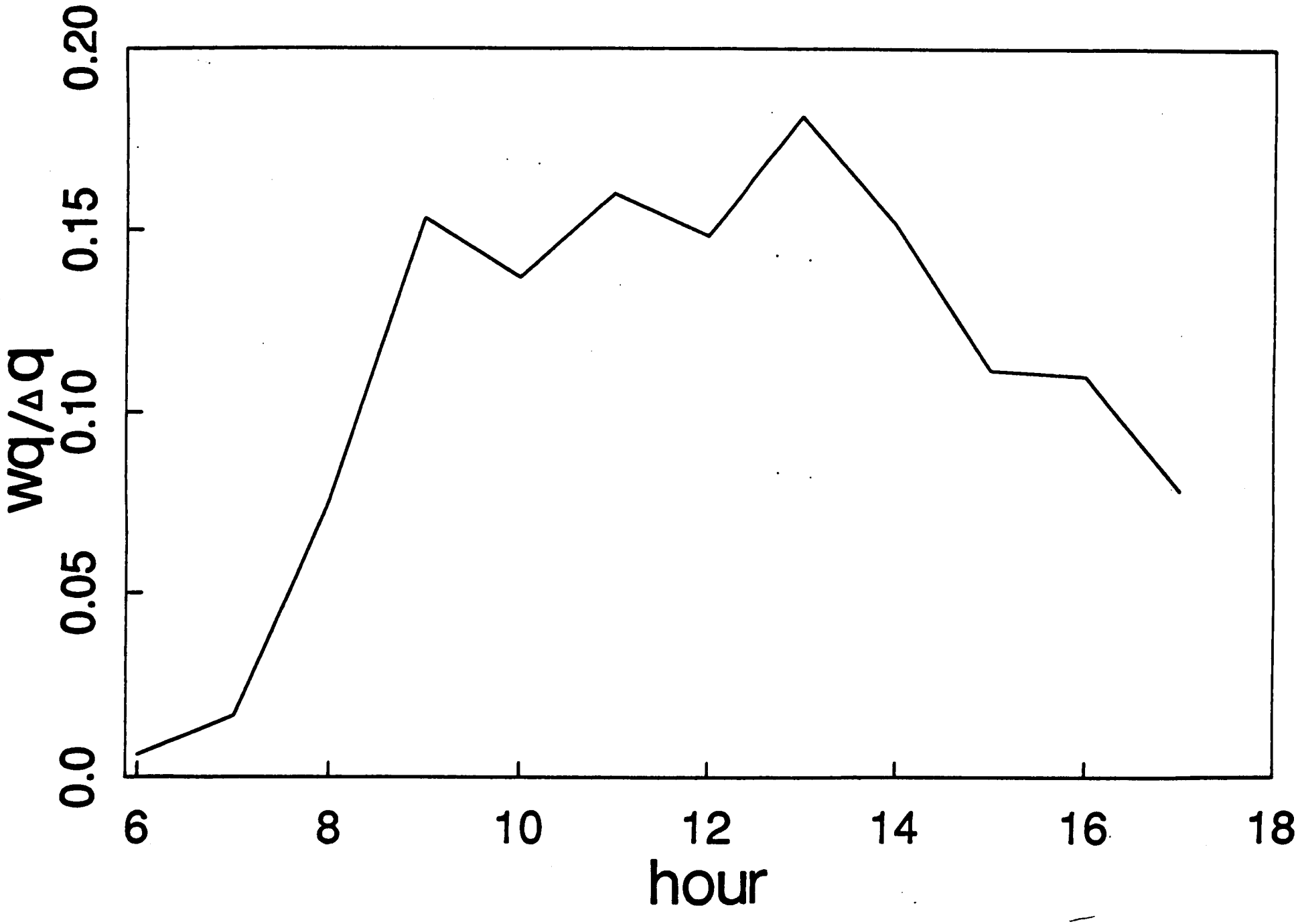

FIG. 25

Nocturnal exchange between rain forest and atmosphere

David R. Fitzjarrald and Kathleen E. Moore
Atmospheric Sciences Research Center
State University of New York at Albany
100 Fuller Road
Albany, N. Y. 12205

June 1989

ABSTRACT

Significant escape to the atmosphere of carbon dioxide concurrent with heat and moisture flux from the Amazon forest canopy are observed to occur during fifty-three events. Two prototypical mechanisms associated with the weakening of the stable nocturnal inversion at canopy top are identified. Two detailed case studies illustrate how abrupt onset of cloudiness leads to a period with lowered Richardson number and enhanced heat, moisture, and carbon dioxide fluxes. Two additional detailed cases illustrate how significant exchange between the forest canopy and the atmosphere occurs even on totally clear nights. Occasional nocturnal increases in the windspeed above the canopy exceeding a well-defined threshhold lead to wave motion in the canopy layer on these nights. A simple model is presented to support the postulate that the waves result from a resonant interaction, as vertical fluctuating pressure gradient forcing operates on the evolving stable layer near canopy top. Turbulent diffusion associated with increased winds deepens and weakens the stable layer at canopy top, lowering the buoyancy frequency in the canopy. Eventually, a period of resonance occurs. Model results indicate that the recovery of the layer takes approximately twice as long as the period of enhanced wind that produced the event.

1. Introduction

The exchange of heat and atmospheric trace gases between the rain forest canopy and the atmosphere depends not only on the degree and depth of turbulent mixing in the canopy, but also on the source level of emission (or deposition) of the substance considered. Because of changes in atmospheric static stability, coupling between the forest and the atmosphere is different during the night than it is during the daytime. Turbulent mixing can be associated with the extent to which momentum penetrates into the canopy. As the wind encounters the upper canopy, a spectrum of eddies shed from the many roughness elements enhances turbulent dissipation there. Thus, the most important canopy structural characteristics for exchange processes are leaf and branch area rather than the total biomass, relevant to the biomass heat storage problem (Moore and Fisch, 1986) or to the problem of estimating the net ecosystem productivity (Odum, 1971). At the Ducke Forest Reserve, near Manaus in the central Amazon basin (2°57'S, 59°57'W), the average height of the canopy is near 30 m, with the average leaf biomass remaining nearly constant down to 15 m (Fittkau and Klinge, 1973). The largest trees have much of their leaf and branch volume concentrated in the upper canopy. The appearance of the rain forest canopy from the air is that of a green carpet, punctuated at intervals by the presence of the occasional emergent tree. However, the top of the canopy is porous, and how this property is related to nocturnal exchanges of momentum and different gases between the forest and the atmosphere is our topic. A similar study of the daytime case appears in a companion article (Fitzjarrald *et al.*, 1989).

Although nocturnal exchanges do not play a major role in the heat and moisture budgets at canopy top in the Amazon (*i.e.*, Fitzjarrald *et al.* , 1988), the nighttime growth of carbon dioxide within the canopy is a standard way to estimate the respiration rate of the forest ecosystem (Whittaker, 1975, Woodwell and Dykeman, 1966). Nitrogen oxides and other radiatively active trace gases, believed to be important to climate change, also accumulate in the canopy during the night (Kaplan et al., 1988, Bakwin, et al.,1989). Conditions favorable for the transport or germination of certain fungal spores occur at night. In the Amazon, for example, development of commercial rubber plantations was thwarted by the presence of the fungus *Microcyclus ulei* (P. Henn.) Arx., whose spores germinate only after prolonged exposure to rain or dew (Thurston, 1984).

Although it seems reasonable that strong nocturnal radiative cooling at canopy top would effectively bar significant exchanges between the canopy below the crown and the atmosphere, Wofsy *et al.* (1988) reported that carbon dioxide concentrations there did not increase monotonically during the evening. Rather, mean concentrations reached a limiting value early in the evening,

indicating that transport is occurring, and we have taken this observation as a starting point for the present work. We believe that these transports occur during a series of sporadic mixing events. If this is true, then applying flux-mean gradient relations would be mechanistically incorrect.

In Section 2, we present a site description, with details of instumentation and the experimental design. Case studies of transports theat occurred during specific mixing events are presented in Section 3, and the wave-like character of some of these events is identified. Spectral analysis of the wave events is presented in Section 4, followed by a conceptual and model analysis of the waves in Section 5. Conclusions and suggestions for continuing work are in Section 6.

2. Instrumentation and Site

This study was conducted at the Ducke Forest Reserve during April and May in 1987, as part of the NASA ABLE-2b experiment. The Anglo-Brazilian micrometeorology program built the 45 m tower on which our instrumentation was mounted in 1983. The canopy and surrounding area at Ducke reserve are described in Shuttleworth *et al.* (1984). Fittkau and Klinge (1973) describe the general structure of the rain forest at a site very near to the Ducke Reserve.

Single-axis sonic anemometers were located at 45, 39 and 25 m on the tower, although for the most part only the 39m (above canopy) and the 25 m (below canopy) instruments functioned during this experiment. Fast-response temperature (fine-wire thermocouple) and humidity sensors (krypton hygrometers) were also located at these levels, providing for eddy-correlation estimates of the sensible and latent heat fluxes. All three sets of instruments were manufactured by Campbell Scientific, Inc. Information on their performance in a previous experiment at this site is given in Fitzjarrald *et al.* (1988), and details of instrument siting during this experiment are given in Fitzjarrald *et al.* (1989). It should be noted that these instruments provide measurements of fluctuations only, and not mean values of the vertical velocity, temperature, and specific humidity. A Gill propeller-vane anemometer was installed at 45 m. A Campbell Scientific datalogger recorded means, standard deviations, and correlations calculated for 20 minute periods, based on a 1-second sampling interval. These data were stored on cassette tape. A PDP 11/73 computer acquired data from the fast-response instruments at 10 Hz and performed calculations of the spectra and co-spectra. The raw 10 Hz data were stored on floppy disks. For the most part the results reported here are based on calculations done on these raw data, after the end of the experiment.

Profile measurements on the tower were done using instrumentation and data acquisition system operated by the team from the Instituto de Pesquisas Espaciais (INPE). This system is described in Shuttleworth *et al.* (1984). An important modification introduced for this experiment is that measurements of wet and dry-bulb temperature and wind speed were recorded every five minutes rather than the previous twenty minute rate. Aspirated psychrometers were mounted at

44.6, 40.9, 39.3, 35.6, 30.5, 23.3, 13.5, and 1.5 m. wind speed was measured at all of these levels except 1.5 m , and at 48.7 42.8 and 37.5 m. The lowest three windspeeds were obtained with newly installed low-threshold Thornthwaite cup anemometers.

Investigators from Harvard University (Fan *et al.*, 1989, Bakwin *et al.*, 1989), maintained chemical sampling instrumentation which included CO_2 concentration profiling at 45 minute intervals, and a fast-responses CO_2 sensor, the intake for which was at the 39 m level. Carbon dioxide fluxes in this paper, therefore, refer to the above-canopy flux.

3. Phenomena

a. Nocturnal conditions in the canopy

After 1630 LST, the sensible heat flux typically becomes negative over the Amazonian rain forest, resulting in a sharp stable potential temperature gradient at canopy top, apparently isolating the canopy from the atmosphere for long periods of time. During these periods gaseous products of ecosystem respiration build up inside the canopy; this is the basis for the traditional method of using CO_2 buildup to estimate the ecosystem respiration rate. On occasion, the stable layer breaks down and accumulated gases are released to the atmosphere in relatively large pulses. We identify two main ways in which the stable layer above the canopy may break down. First, there are cases when net radiative heat losses are sharply reduced at night, most likely because of increasing cloud cover. With reduced net radiation, there is eventually much reduced cooling at canopy top to maintain the stable potential temperature (Θ) gradient, and enhanced heat, momentum and CO_2 fluxes result. Second, there is occasional venting of the forest even on nights with no periods of reduced net radiation. This appears to be a dynamic effect, with apparent wave motion seen in the vertical velocity both above and within the canopy. Four examples, two of each type, illustrate these prototypical mixing episodes.

Time-height sections of virtual potential temperature (Figures 1-4) obtained from the INPE tower illustrate the formation and maintenance of the stable capping inversion in the canopy. At times when there are tethered balloon soundings, the above-canopy temperature profile matches the nearby tethered balloon profile to within 0.5K. The tethered balloon profiles indicate a continuation of the stable layer above the canopy, but the strongest inversion anywhere in the boundary layer is concentrated in a thin layer at canopy top. The depth and strength of the inversion is observed to change through the night, in response to the episodic turbulent heat flux and changes in net radiation. The inversion can disappear quickly when the net radiation is reduced (Figure 5). Below the canopy there exists a neutral to unstable layer. On April 27-28, no canopy wave events were observed. Intermittent clouds prevented the development of a deep stable layer in the canopy (Figure 1). The average wind speed was lower on this night than on most others (Table 1), but a small increase in wind speed around 0130 on April 28 (2530 in Figure 1) produced a CO_2 flux

peak. At the start of this event the entire canopy was neutral to unstable. As the heat flux above the canopy increased in magnitude, however, the stable layer grew down into the canopy. The earlier CO_2 escape, at 2200, was also associated with rising wind speed, followed by diffusion of the stable layer downward.

Clearly identifiable oscillations in vertical velocity and temperature fluctuations inside the canopy occurred from 19:50 to 2010 and from 2330 to 2343 on May 2. The large upward CO_2 flux after 0200 on May 3 (2600 in Figure 2) was associated with the disappearance of stable layer at canopy top due to cloud cover and rain. The downward diffusion of the canopy stable layer from 2330 to 2600 was a response to heat flux divergence in the upper canopy (Figure 2d), in turn driven by wind speed above the canopy.

The nights of May 4-5 and May 8-9 (Figures 3 and 4) contrast with the previous two examples in that the waves were observed frequently throughout both nights. The mean wind speed above the canopy in each of these cases was near or over 2 ms^{-1}, and the net radiation on these nights maintained the cooling rate at canopy top nearly continuously. On May 4-5 some clouds did interrrupt the cooling for a period after midnight, but the canopy stable layer remained strong.

The largest amplitude wave events on May 8-9 occurred from 1930-2000, 2100-2130, 2230-2300, 2400-2430 and from 2700-2745 (0300-0345 on May 9). This last event was the most significant in terms of CO_2 flux (Figure 4). An examination of 10-point averaged (1 Hz) time series for nighttime cases revealed the presence of regular oscillations in fluctuating quantities in the stable above-canopy and within-canopy layers (Figure 6). While easiest to detect at 25 m, inside the canopy, where vertical velocity often indicates oscillatory motion with modulated frequency and amplitude, these frequencies are also present at 39 m. The period of the wave varied from 65 to 80 seconds. On May 4-5 large amplitude wave events lasting longer than 10 minutes were also observed in the vertical velocity inside the canopy during the following periods: 2000-2030, 2230-2320,2500-2520 (i.e. 0100-0120 on May 5), and 2720-2740. These times correspond to peak CO_2 escape from the canopy.

Table 1 lists the 9 nights for which turbulent flux and profile data are available for all or part of the night, as well as a summary of flux episodes for each night. Flux calculations were based upon 6.8 minute (4096 points) time series with the 300 s running mean removed. The starting points for successive flux calculations were 5 minutes apart. The intermittent nature of these nocturnal exchanges dictated that some accuracy in the determination of flux quantities was sacrificed. That is, in order to document the existence of events lasting less than 20 minutes, we were required to make the averaging period relatively short. Standard errors of flux estimates are shown for one case in Figures 7A and 7B.

Following Wyngaard (1983), the accuracy, a, of a flux estimate $\overline{wx}$ made over an averaging time T_{ave} is:

$$a = 1.4\ [\ \sigma_{wx}/\overline{wx}][T_{wx}/T_{ave}]^{1/2} \quad ,$$

where T_{wx} is the integral time scale of the flux product, and σ_{wx} is the standard deviation of the flux estimate made during the averaging time. The integral time scale for the two flux measurements are 2-3 s.Greater instrumental noise in the eddy CO_2 sensor results in errors that are a larger fraction of the mean CO_2 flux than those for heat flux. By this method, $\sigma_{wx}/\overline{wx}$ =10 and a = 0.95 for the nighttime CO_2 flux. We can only estimate the CO_2 flux to within 95% of its ensemble mean value, in an averaging period of 6.8 minutes. The heat flux, by contrast, yields a = 0.36, during the same night time periods. These dismaying assessments point out one of the large difficulties with applying the tools of statistical turbulence analysis to phenomena charcterized by a series of individual events, for which the assumption of stationarity made when deriving the expression for a above is not really valid.

The coupling between the upper level and the within-canopy flow was episodic at night, being associated with a wind-speed threshold at the 45 m level. The threshold varied with the strength of the stability (Ri) but it was usually about 1.8 m/s. For example, more than half of the CO_2 flux for a given night occurs when the 45 m wind speed is from 1.7 to 2.0 m/s.

b. Characterization of Flux Events

Fluxes of heat, CO_2, momentum, and moisture were associated with these episodes, which occur from 4 to 8 times per night and last 10 minutes to 1 hour. Typical fluxes observed were sensible heat fluxes from 10-50 W/m^2, latent heat fluxes from 0-10 W/m^2, and CO_2 fluxes were from 10-30 ppm s-1. Temporary minima in CO_2 concentrations below the canopy could occasionally be associated with these flux episodes, but in general the chemical profiling rate was too coarse to detect the effect. The magnitude of the fluxes is 10 to 100 times greater during the peak of the episode than during intervening quiet periods.

To gain a measure of the intermittency of flux over a given night, CO_2 flux events were established as beginning when the flux exceeded 10 ppm cm/s and ending when the 6.8 minute average flux product dropped below 5 ppm cm/s. This technique takes much of the noise, as well as subjectivity, out of determining what an event is. By this measure CO_2 flux was observed to be very intermittent, since well over half the flux occurs , in most cases, in much less than half the time (Table 2). The length of time that a given event lasts is extremely variable. On most nights CO_2 flux occurred as a series of small episodes followed by a much larger, longer-lasting one occurring at some time from midnight to 0400 LST. In these cases the small events were each about 10% of the total measured flux for the night, whereas the large one would constitute 30-80% of the flux. Using these criteria for establishing the extistence of a flux event, the mean flux within events is more than double the mean flux overall.

While the flux magnitudes are small, as is expected in strong stability, the wave episodes

account for all of the flux when the canopy is strongly stable. On three nights, (4/27-28, 5/2-5/3, 5/6-5/7) this strong stability either did not develop, or it disappeared later in the night, due to cloud cover, allowing for much larger flux to occur. In these cases, the flux was not associated with wave motions within the canopy, but rather was characterized by turbulence, as deduced from examination of the time series and the autocorrelation functions .

4. Analysis of exchanges on nights with uninterrupted radiative cooling

Vertical motions within the canopy, day or night, are similar to those above, provided sufficient wind speed exists. The lower level vertical velocity signal appears as a filtered version of the upper level signal (Fitzjarrald *et al..*, 1989). There is a diurnal cycle in the correlation coefficient between vertical velocities at the two levels, which reaches a maximum of 0.45 at mid-day but drops to 0.2 on average during the night. This correlation is considerably higher during transient wave episodes. On average, the phase angle between upper and lower w spectra at their peak frequency is 10-20 degrees. Autocorrelation functions were found using the FFT method (Press, et al., 1986), using 1-hz (10-point averaged) data with a 300 s running mean removed. The autocorrelation functions above and below the canopy observed during wave episodes (Fig. 8) illustrate: 1) Evidence of wave motions at canopy top are obscured by the presence of high-frequency noise, and 2) A much clearer wave signal, with a period of approximately 60 s is present at the below-canopy level.

A measure of the integral scale is found by examining the lag at which the autocorrelation of the vertical velocity becomes zero (Lenschow and Stankov, 1986). There is a diurnal difference in integral scale of the 39 m vertical velocity, due to the difference in the mean wind speed, U, an average confirmation of Taylor's hypothesis. During the day this integral scale is typically 25 s (U = 2.4 m/s) above the canopy, while at night it is about 15 s (U= 1.4 m/s). The integral scale within the canopy, where the mean diurnal wind speed difference is small (Fitzjarrald *et al.*, 1989) is about 18 s day and night.

The 10-hz data were averaged over 5 points to create two-herz time series. Subsequently, a 600-point (300 s) running mean was removed from the data to produce the time series of fluctuating quantities. The 300 s running mean removal acts as a high-pass filter for the variance such that 90% of the variance remains at 0.003 hz , and 100% at 0.004 hz. Spectra of vertical velocity for upper and lower levels indicate the existence of an inertial subrange for both sensors, but also demonstrate the loss of energy in a certain frequency band within the canopy (Figure 9). This would suggest that the canopy elements are filtering out certain scales of motion in a "short-circuit" of the energy cascade, as suggested by Shaw and Seginer (1985). An alternative explanation for this characteristic shape of the canopy vertical velocity spectrum is that a buoyancy subrange is being exhibited. Similarity arguments provide a -2 power law for the variance spectrum in very

stably stratified environments, $kS(k) \approx k^{-2}$ at wave numbers between the wave energy source and the buoyancy wavenumber (Finnigan, et al., 1984).

To represent changes seen in power spectra seen over an entire night, we constructed time-frequency diagrams with contours of power spectral density in the following manner: A time series of the power spectra was produced by computing sequential 1024 point (512 s) power spectra on time series averaged to two Herz, each spaced 64 s apart. Each spectrum was logarithmically block-averaged into 30 frequency bands. The time series of power spectra was then smoothed first in the frequency dimension, and then the time dimension, using the median filter smoothing routine of Velleman and Hoaglin (1981). This routine utilizes a 3-point running median smoother followed by a "splitting operation" on flat spots in the data series. These two procedures are repeated, and then followed by a 3-point hanning operation. The smoothed spectra could be contour plotted (Figure 10) to illustrate changes in the amplitude and peak frequency of the fluctuations throughout the night. The transient episodes of variance appear as "hill" on this plot. In general, the peak frequency is close to the buoyancy (Brunt-Väisäilä) frequency for the 39-30 m layer, but in some cases, as on May 9, the canopy wave frequency appears to undergo modulation while the buoyancy frequency becomes lower in response to a turbulent heat flux divergence in the layer (Figure 10c). Tethered balloon profiles do not indicate the existence of a layer with higher N above the surface layer. Traditional techniques of time-series analysis are not well suited to presenting data for which there appears to be a coherent signal but whose frequency is continually modulated, as the wave data indicate. In the next section we address this difficulty by introducing a simple model of the wave phenomenon.

5. Toward a model of the resonant wave events

Nocturnal mixing during wave events, epitomized by the example in Figure 6, are always associated with transient periods of increased winds at canopy top. Enhanced winds at canopy top are likely the result of the breakdown in the nocturnal jet observed to occur in the Amazon stable boundary layer (Garstang *et al.*., 1989; Oliveira, personal communication). The origin and stability of these jets is currently under investigation, but a likely hypothesis is that they are a "river breeze" phenomenon, driven by the nocturnal river-land temperature discontinuity. If this hypothesis proves correct, jet formation and sporadic breakdown would be expected to occur on the clear nights with appreciable canopy top inversions that characterize the wave events we are discussing.

The waves seen in the vertical velocity and temperature traces inside the canopy appear to be predominantly of a single, frequency-modulated signal. This type of signal could conceivably result from a "beat frequency" produced as two higher frequency waves interfere. However, we believe that the occurrence of relatively high amplitude fluctuations in w and T are the result of a transient resonance phenomenon. If both the natural frequency of oscillation of the stable layer in

the upper canopy and the frequency of forcing above are changing simultaneously, then it is possible for the observed combination of shifting frequency and amplitude of the w fluctuations to result. Any type of resonance could lead one to observe relatively large responses, such as w oscillations, from very small but periodic forcing.

The interaction between the stable layer in the upper canopy and turbulent eddies impinging on it from above is similar in some ways to that identified by Carruthers and Hunt (1986) to explain gravity wave generation in the capping inversion above the convective boundary layer (CBL). Their hypothesis is that buoyant eddies impinging on the stable layer from below can supply energy to trapped wave modes within that layer. Subsequently these waves grow preferentially through this resonance, ultimately breaking to enhance stable layer mixing. Carruthers and Moeng (1987) showed that waves in the capping inversion predicted by linear theory actually occur in large eddy simulations of the CBL.

In the present case, we view the process that leads to the wave-like motions to consist of two stages. First, as the wind speed at canopy top increases, part of the turbulent energy in the above canopy layer leads to turbulent diffusion that makes the Θ inversion there weaken and penetrate deeper into the forest. This leads to an overall reduction in the buoyancy frequency, but at any fixed level below the initial inversion base inside the canopy, the stability increases with time during the event. Thus, the natural frequency of the "forest oscillator" decreases with time during the initial stages of the event. Second, we note that turbulent eddies that move across canopy top are associated not only with with small scale pressure fluctuations but also with pressure gradient fluctuations, as has been demonstrated by Sigmon *et al.* (1982, Fig. 2). If the characteristic wave number k of eddies in the layer just above the canopy remains essentially constant, determined perhaps by the physiognomy of forest top and the surrounding topography, then the frequency imposed by the turbulence at canopy top is $f_c \approx Uk$. As the horizontal wind speed increases, the forcing frequency eventually can reach the natural frequency of the near-canopy layer, and the wave begins to grow. Our previous work indicates that eddies with wavelengths from 30-100 m dominate heat transport just above the forest. Resonance occurs as the amplitude of the sympathetic oscillations in the upper canopy stable layer is enhanced during the interval when the forcing frequency and the buoyancy frequency are similar. After a time, the turbulent diffusion brought on by the increased winds leads to downward movement and weakening of the canopy stable layer. The resonance condition changes, the buoyancy frequency drops, and the wave amplitude falls off. Thus, the event begins by the forcing frequency being increased by the increasing wind speed to the resonance point and ends as the resonance is lost at constant forcing when the buoyancy frequency in the layer changes as turbulent mixing reduces $\partial\Theta/\partial z$. Note that the flux of CO_2 and sensible heat (Fig. 7a and 7b) drops *before* the horizontal wind speed at canopy top does. It is clear from Fig. 3a and Fig. 4a that the stable layer penetrates into the canopy with time and that the buoyancy

frequency drops. The negative correlation between N_b and wind speed during the event (Fig. 11) is consistent with our hypothesis that the buoyancy frequency in the upper canopy drops initially during the event, up to the moment that there is a pulse in the heat and CO_2 fluxes.

A simple physical model of the scheme just presented can be derived through consideration of the mean momentum and heat balance equations, to define the changing environment, and the simple Boussinesq equations for gravity waves, to describe the oscillations whose amplitude and frequency are changing with time. We assume that the fluctuations in the vertical velocity that were seen in the observations were gravity waves that consist of purely vertical motion. This assumption was made not only in the interest of obtaining a simple model, but also because we lack spatial data with which to assess any horizontal wave structure. It seems unlikely, however, that extensive horizontal wave development would occur, owing to the presence of so much vegetation. Rather, it seems more likely that narrow chimneys of air are oscillating. The pulses of CO_2, heat, and moisture fluxes observed during these events result from some kind of nonlinear wave-turbulence interaction in the above-canopy layer. This interaction is not addressed in the following simple model, which is designed to test the plausibility of the resonance hypothesis. Work on characterizing the nonlinear regime above canopy is currently in progress.

The changing environment is described in the model by integrating the momentum and heat balance equations in the vertical over the thickness of the stable layer and allowing the upper and lower limits of integration to vary with time. Details of the derivation of this model are given in the Appendix. Important assumptions made during the derivation are: 1) As the wind increases during an event, the local acceleration is balanced by an increase in the turbulent shear stress that is distributed downward into the canopy, roughly in agreement with the profiles of shear stress presented in Shaw *et al.* (1988). 2) Fluctuations in the perturbation vertical pressure gradient are characterized by a *constant* horizontal wave number, so that there is a fluctuating forcing term in the equation for the perturbation vertical velocity whose frequency is linearly proportional to the wind speed. 3) Profiles of mean wind and potential temperature in the canopy top stable layer have shapes that are similar during the event. We assume here (Appendix) here that they are linear, but this is not essential. 4) The event is forced by a wind speed *specified* to vary as a Gaussian in time. 5) Shear stress, wind speed, and turbulent heat flux go to zero at the bottom of the inversion. 6) For this presentation, diabatic terms from changes in the turbulent heat and radiative flux divergences are ignored. This simplification is discussed further in the Appendix. The parameters used in the model are shown along with profiles of virtual potential temperature made during the May 9 event given in Figure 12. The profiles illustrate the deepening and weakening of the inversion layer during the event.

The model equations were made dimensionless using $\Delta\Theta_o$ for potential temperature difference, Δh_o inversion layer thickness, σ_t (the dimensional standard deviation of the temporal

Gaussian that specifies the ambient wind, explained in the Appendix) for time, and U_{ao}, horizontal wind velocity. Subscript o refers to the state obtaining before and after the wind event. Constants C_i below are defined and interpreted in the Appendix. The dimensionless equations are:

specified wind speed at canopy top :

$$\hat{U}_a(t) = 1 + \hat{U}_m \exp[- (\hat{t} - \hat{t}_c)^2] \quad (1)$$

equivalent to

$$d\hat{U}_a/d\hat{t} = -2(\hat{U}_a - 1) (\hat{t} - \hat{t}_c) \quad (2)$$

This form is roughly in accord with the observed form of the period of enhanced wind (Fig. 6).

deepening of the inversion layer :

$$d\Delta\hat{h}/d\hat{t} = C_1 [\hat{U}_a - \Delta\hat{h}/\hat{U}_a] - [\Delta\hat{h} /\hat{U}_a] d\hat{U}_a/d\hat{t} \quad (3)$$

The first term on the right accounts for the deepening of the stable layer due to enhanced layer shear stress at canopy top. The second term on the right refers to the effect of making the layer thinner, so that the layer-averaged momentum is constant but the wind accelerates.

variation of the mean layer stability $\hat{\gamma} \equiv \Delta\hat{\theta}/ \Delta\hat{h}$:

$$d\hat{\gamma}/dt = -[\hat{\gamma}/\Delta\hat{h}] d\Delta\hat{h} /d\hat{t} \quad (4)$$

The term on the right shows decreasing stability as the layer deepens, reversing when the layer begins to thin.

The equations for the fluctuating quantities are standard for simple waves with only vertical motion.

vertical velocity fluctuation : $d\hat{w}/d\hat{t} - C_2 \theta = C_3 \sin (\hat{U}_a \hat{k} \hat{t}) - C_4 \hat{w} |\hat{w}|$ (5)

The forcing frequency increases with wind speed as explained above. The right side represents a parameterization of the fluctuating vertical pressure gradient across the canopy, less a damping term due to frictional resistance to vertical motion.

potential temperature perturbation : $d\hat{\theta}/d\hat{t} + \hat{\gamma} \hat{w} = 0$ (6)

Certain features of the observed wave resonance phenomena (i. e., Figs. 4 and 6) are well represented by this simple model (Fig. 13). The parameters C_i have been roughly adjusted to correspond to conditions shown in Fig.12. The modelled environment (top panel, Fig. 13) indicates that the recovery of the stable layer thickness $\Delta\hat{h}$ and stability $\hat{\gamma}$ goes on for an appreciable period

after the wind speed pulse is over. If one increases the dimensionless drag coefficient C_1, recovery of the system occurs more rapidly. The sensitivity of $\hat{\gamma}$ to more than doubling C_1 is shown by comparing $\hat{\gamma}_1$ and $\hat{\gamma}_2$. The $\Delta\hat{h}$ curve (not shown) corresponding to $\hat{\gamma}_1$ peaks at 4.2. If the drag coefficient is lowered sufficiently, it is clear from (3) that Δh may even decrease during an event. The stability minimum, near 0.1, predicted by the model with the given choice of parameters is smaller (< 0.2 compared to ≈ 0.4) than that observed (Fig. 12) and the maximum in $\Delta\hat{h}$ is larger (3.5 compared to ≈ 2).

The bottom two panels show the modelled response for vertical velocity and temperature fluctuations. The value of the ordinate on the $\hat{w}$ and $\hat{\theta}$ axes scales linearly with the amplitude of the fluctuating vertical pressure gradient forcing the system, and one may treat these scales as arbitrary. However, the value assumed for A (C_3 in the dimensionless form) in Fig. 13 is 0.06 m/s^2, corresponding to that presented in Sigmond *et al.* (1983). This value is certainly much too large for the present case. In dimensional terms, to obtain vertical velocity fluctuations with amplitude of 0.25 m/s and temperature oscillations of 0.5 K from this model, the fluctuating pressure gradient acceleration need only be 3×10^{-4} m/s^2, corresponding to pressure differences of only 10^{-3} mb over 10 m in the vertical. Such a fluctuating pressure gradient is a factor of 20 smaller than the reported by Sigmon *et al.* (1983). This illustrates how powerful the hypothesized resonant mechanism can be in producing large amplitude responses inside the forest to small amplitude forcing above, provided that there is appropriate stability near canopy top. Two periods with enhanced amplitude of w occur at $\hat{t} \approx -0.25$ and $t \approx 1$, but only the first pulse occasions a similar large amplitude response in $\hat{\Theta}$. The model appears to capture the qualitative features of concurrent frequency modulation with a double peak in amplitude seen in the observed w signal inside the canopy in Fig. 6. Some indications of the nonlinear character of the oscillator are seen in the irregular course of amplitude variations with time.

It is clear that the stable layer at canopy top, perhaps coincident with the layer over which momentum flux is still nonzero, should be a characteristic vertical scale for constructing stability indices rather than the total canopy thickness (Shaw *et al.*, 1988). The total canopy height becomes relevant only when the stable layer extends through the entire depth of the canopy. These model results, along with observational results presented in our companion paper (Fitzjarrald *et al.*, 1989), indicate that good physical information is needed about the ability of different types of forest canopies to distribute downward the momentum flux present at canopy top under non-neutral conditions. The likelihood of encountering repeated canopy resonance phenomena at other sites depends, in the simple analysis presented here, on the set of dimensionless parameters C_i that obtain there and the initial conditions, themselves indicators of the canopy structure.

Physical interactions essential to the understanding of the flux pulses associated with the flux events are not addressed with the model presented here. In particular, there is clear evidence

that the waves seen in w below the canopy can be seen, with noise, above the canopy in both the w and u signals there (Fig. 6). To model the breakdown of the waves induced by the resonance phenomenon, it will most likely be necessary to construct a model that includes explicitly wave-turbulence interactions as well as the diabatic heating and cooling terms. We view the present work as the first step in producing such a model, whose ultimate aim is to relate extreme wind speed events to total nocturnal canopy exchange.

6. Implications and Conclusions

The stable nocturnal temperature gradient in the canopy places a constraint on the escape of gases produced at the forest floor, for example, CO_2 and NO. While the concentrations of these gases do increase during the night, they do not do so monotonically. Barring large fluctuations in source strength, the reason for this is that episodic fluxes do occur in the canopy layer. The observed waves provide one mechanism for the transport of mass out of the subcanopy layer on clear nights with strong stability at canopy top. On a few occasions a temporary miminum in the CO_2 concentration could be associated with a flux episode, but for the most part the CO_2 profiling rate was too coarse in time , and the flux episodes too brief, to be able to make this association.

Since there is a threshold in wind speed that is required for CO_2 flux (Figure 14), the fraction of time that wind speed is greater than some threshold is a surrogate for or measure of the number of flux events occurring in a given night. We consider the hypothesis that the flux of CO_2 at the forest floor is constant over the night. Then one would suppose that the early morning maximum concentration of CO_2 would be related to the total amount of ventilation that occurred during the night. The maximum CO_2 concentration, plotted against the percentage of time that $u > 1.75$ m/s (derived from winds at the Ducke PAM station), indicates that there may be relationship between these quantities (Figure 15), though confirmation awaits a much larger set of data.

A further implication of the intermittency of flux is that the rate of dew deposition is likely to change with the flux episodes, since enhanced upward moisture flux above the canopy is a feature of these events. This is an important consideration from the point of view of microbiological agents such as fungal spores. For instance, the fungus *Microcyclus ulei* , cause of South American Leaf Blight of rubber, requires a period of 8 hours of free water for germination (Thurston, 1984). The flux episodes we have observed are drying periods, while the period of time between events would promote dew deposition. Thus the length of time between events could be an important determinant of conditions favorable for pathogenic spore germination. This problem bears more exploration, both in rain forest environments and in other canopies.

We arrive at the following conclusions:

1. The combination of radiative cooling and low windspeeds at night at canopy-top promotes

both the trapping of biogenic trace gases and the existence of a wave-supporting medium within the upper 10-15m of the canopy.

2. Occasional increases in the windspeed above the canopy, possibly associated with a nocturnal jet, cause resonant wave motion in the canopy layer. There is a windspeed threshold requirement on the presence of thesewaves. A simple model illustrates that the mechanism of the resonant interaction is plausible. The postulated mechanism is the following: Turbulent diffusion associated with increased winds deepens and weakens the stable layer at canopy top, lowering the buoyancy frequency in the canopy. Further, periodic forcing in the vertical occurs as a result of the fluctuating vertical pressure gradient induced as turbulent eddies move across canopy top. We postulate that the wavenumber of these eddies is determined by the canopy top structure, and thus the frequency of the forcing is increasing with wind speed while the buoyancy frequency of the upper canopy is decreasing. Eventually a period of resonance occurs. Model results indicate that the recovery of the layer takes approximately twice as long as the period of enhanced wind that produced the event. The model formulation indicates that the occurrence of interactions in other canopies depends on the degree to which long wave radiation and momentum are transmitted in the upper canopy.

3. During the canopy wave episodes, there is downward heat flux in the upper canopy, resulting in a diffusion of the stable layer deeper into the canopy, a weakening of the theta gradient and a decrease in the buoyancy frequency. Recovery of the gradient occurs with continued radiative cooling after the episode.

4. Significant escape of CO_2 from the canopy to the atmosphere occurs in conjunction with these episodes. The waves thus provide a mechanism for the escape of biogenic gases through the capping inversion from the neutral-to-unstable sub-canopy layer. With the present instrumentation, heat flux is a more reliable tracer for the amplifying waves.

There are several clear directions for continuing work on this type of problem. It is clear that to understand the mechanisms of canopy-atmosphere exchange, it is necessary to consider the dynamic interaction between the mean stability in the canopy and the turbulent fluxes. Resistor analogies of the canopy are not the only approach necessary in modelling this exchange. It appears that better measurements of the fluctuating vertical pressure gradient could confirm or deny our hypothesis about the resonant forcing. High speed wind fluctuation measurements with horizontal spatial resolution are needed to add to the understanding of the structure of waves in the upper canopy. Although the simple model we have presented appears to capture much of the physics of the wave events, a coupled wave-turbulence interaction will probably be necessary for estimates of the flux pulses to be obtained.

7. Acknowledgements

This work, part of the GTE ABLE-2b field mission, was supported by NASA Grant NAG-1-692 to the Atmospheric Sciences Research Center (ASRC) at the State University of New York at Albany and by the Instituto Nacional de Pesquisas Espaciais (INPE), the Brazilian Space Institute. G. G. Lala of ASRC helped with experiment planning and wrote the Datalogger acquisition program in the field. In Manaus, researchers from the Instituto Nacional de Pesquisas da Amazônia (INPA) and from INPE were very helpful. A. O. Manzi was extremely helpful in providing the Ducke tower mean temperature and wind profiles. Special thanks go to S. Wofsy, P. Bakwin, and S-M Fan, all of Harvard University, who not only went to extra trouble to help record the large amounts of raw data obtained during this experiment, but also graciously allowed us access to the high-speed CO_2 data. We thank Amauri P. Oliveira of ASRC and the University of São Paulo, who first noted the presence of the vertical velocity waves in the forest canopy during a class project and brought it to our attention.

8. Appendix

Derivation of a layer-averaged model to describe wave resonance events in the forest canopy.

The procedure is to integrate the equations of mean momentum and temperature from $h_b(t)$, inside the canopy, to $h_a(t)$, assumed to be just above the canopy. Terms are defined in Fig. 14. Integrating the equation for changes in the mean temperature in the layer, and taking into account the terms that result from applying Leibnitz' rule, results in:

$$d[\int \Theta \; dz] /dt + \Theta_b \, dh_b/dt - \Theta_a \, dh_a/dt = F_b - F_a + R_b - R_a \equiv D \,, \qquad \text{(A1)}$$

where F_b and F_a are the turbulent heat fluxes at h_b and h_a, R_a and R_b are net radiative fluxes, and D is shorthand for all of the diabatic terms. Assuming that the Θ profile is *similar* in the vertical, $\Theta(z) = \Theta_b \, \Delta h + \Delta\Theta \, \Delta h \int f(z')dz'$, where f is an (empirical) shape function and $z' = (z - h_b)/\Delta h$, $\Delta\Theta \equiv \Theta_a - \Theta_b$, $\Delta h \equiv h_a - h_b$. Integrals are all taken from h_b to h_a. Writing $\int f(z')dz' = F$, the expression $\int \Theta \, dz = F \, \Delta\Theta \, \Delta h + \Theta_b \Delta h$. For simplicity, we take the profiles to be linear here, implying that F=0.5. Defining $\gamma \equiv \Delta\Theta/\Delta h$, and rearranging terms, one arrives at the expression:

$$d\gamma /dt = -[2/\Delta h]\gamma \, d\Delta h /dt + 2D/(\Delta h)^2 + (2/\Delta h) \, d\Theta_b/dt - 2[(\Theta_a+\Theta_b)/(\Delta h)^2] \, dh_a/dt \qquad \text{(A2)}$$

The deep canopy temperature does not vary appreciably during an event and we assume that $d\Theta_b/dt \approx 0$. If we hypothesize that the top of the canopy essentially fixes the top level of the inversion, $dh_a/dt \approx 0$.The final prognostic equation for the layer stability γ is:

$$d\gamma /dt = -[2/\Delta h] \, \gamma \, \Delta h /dt + 2D/(\Delta h)^2 \quad . \qquad \text{(A3)}$$

It is clear that there is diabatic heating during the event, in the form of increased turbulent sensible heat flux, and this will tend to increase stability ($D > 0$). We encountered some difficulty finding simple parameterizations of this process that agree qualitatively with the observed pulse in heating. While understanding this pulse is ultimately of great importance, our results indicate that it is not critical to the description of the resonance interaction, and we have set $D = 0$ in model results presented here.

The equation for growth of the inversion thickness Δh derives from the mean horizontal momentum equation departure from an initial balance, and we hypothesize that the local acceleration in the wind above the canopy that gives rise to the layer deepening is balanced by an increase in the shear stress in the canopy. We assume that the wind speed and momentum flux vanish at the bottom level and further that this level is the same level where the turbulent heat flux is zero. The shear stress responds by both accelerating and deepening the stable layer. For this derivation, we assume

that the stress (τ) profiles are linear, though one could easily assume other similarity forms. According to our assumptions, the acceleration at any level is given by:

$$dU/dt = d(\tau_o - \tau) /dz, \qquad (A4)$$

where τ_o is the stress in the initial state. Integrating A4 from h_b to h_a, as before yields:

$$d\Delta h/dt = 2\tau_o \Delta h / (\Delta h_o U_a) - 2 \tau_a / U_a - (\Delta h/U_a)\, dU_a/dt \quad . \qquad (A5)$$

This can be further simplified by assuming that stress is given by the bulk aerodynamic formula, $\tau_a = - C_d U_a^2$, where C_d is a drag coefficient assumed here to be constant:

$$d\Delta h/dt = 2 C_d U_{ao} [U_a/U_{ao} - (\Delta h/ \Delta h_o)U_{ao}/U_a] - (\Delta h/U_a)\, dU_a/dt \qquad (A6)$$

with U_{ao} being the wind speed at canopy top at the beginning of the episode. Subscript o refers to the initial condition.

By assumption, the environment is forced by increased winds at the top of the canopy, and this time variation is specified in the model to be Gaussian:

$$U_a(t) = U_{ao} + U_m \exp [- (t - t_c)/\sigma_t^2] \ , \qquad (A7)$$

and the specified width of the Gaussian, σ_t, forms the time scale for making the equations dimensionless.

The equation for the vertical velocity is simply a linearized form of the vertical momentum balance.

$$dw/dt - \beta\theta = A \sin (U_a k t) - Kw |w| \quad , \qquad (A8)$$

where β is the buoyancy parameter [(g/Θ_{ref})], A is the amplitude of the assumed fluctuating vertical pressure gradient force, and K, with dimensions of 1/length, is an empirical damping coefficient. We have assumed here that it is equal roughly to $C_d/\Delta h_o$. The forcing frequency, $U_a k$, increases with wind speed, as described in the text. The right side represents a parameterization of the fluctuating vertical pressure gradient across the canopy, less a damping term due to frictional resistance to vertical motion.

The perturbation temperature is described by a simple linearized relation with no sources or sinks:

$$d\theta/dt + \gamma w = 0 \quad . \qquad (A9)$$

The model equations presented in the text were made dimensionless using $\Delta\Theta_o$, Δh_o, σ_t, U_{ao} for potential temperature difference, inversion layer thickness, time, and horizontal wind velocity, respectively. The fluctuating vertical velocity was made dimensionless by scaling by $\Delta h_o / \sigma_t$. The constants C_i referred to in the main text are:

$C_1 \equiv C_d U_{ao} \sigma_t / \Delta h_o$, a dimensionless drag coefficient.

$C_2 \equiv \Delta\Theta \sigma^2_t \beta / \Delta h_o$, a dimensionless buoyancy parameter.

$C_3 \equiv A \sigma^2_t / \Delta h_o$, a dimensionless amplitude of the vertical pressure gradient forcing.

$C_4 \equiv C_d$, a dimensionless value of a damping coefficient for vertical motion.

References

Bakwin, P. S., S. C. Wofsy, Song-Miao Fan, M. Keller, S. Trumbore, and J. Maria da Costa, Emission of Nitric Oxide (NO) from tropical forest soils and exchange of NO between the forest canopy and atmospheric boundary layers, *J. Geophys. Res.*, (submitted),1989.

Carruthers, D. J. and C.-H. Moeng, Waves in the overlying inversion of the convective boundary layer, *J. Atmos. Sci. 44,* 1801-1808, 1987.

Carruthers, D. J. and J. C. R. Hunt, Velocity fluctuations near an interface between a turbulent region and a stably stratified layer, *J. Fluid Mech. 165,* 475-501, 1986.

Fan, S.-M., P. S. Bakwin, S. C. Wofsy, D. R. Fitzjarrald and O. M. R. Cabral, Eddy correlation measurements of the exchange of CO_2 and O_3 between the Amazon forest and the atmosphere, *J. Geophys. Res.*, (submitted), 1989.

Fittkau, E. J. and H. Klinge, On biomass and trophic structure of the Central Amazonian rain forest ecosystem, *Biotropica 5*, 2-14, 1973.

Finnigan, J.J., F. Einaudi, and D. Fua , The interaction between an internal gravity wave and turbulence in the stably-stratified nocturnal boundary layer, *J. Atmos. Sci. 41(16),* 2409-2436, 1984.

Fitzjarrald, D. R. , B. L. Stormwind, G. Fisch, and O. M. R. Cabral, Turbulent transport observed just above the Amazon forest, *J. Geophys. Res. 93,* 1551-1563, 1988.

Fitzjarrald, D. R. , K. E. Moore, O. M. R. Cabral, J. Scolar, A. O. M. Manzi, and L. D. de Abreu Sá, Turbulence in and above the Amazon forest, *J. Geophys. Res.*, (submitted), 1989.

Garstang et al., The Amazon Boundary Layer Experiment (ABLE-2B): A meteorological perspective, *Bull. Am. Meteor. Soc.* (submitted), 1989.

Kaplan, W. A.. S. C. Wofsy, M. Keller, and J. Maria da Costa, Emission of NO and deposition of O_3 in a tropical forest system, *J. Geophys. Res., 93,* 1389-1395, 1988.

Lenschow, D. H. and B. B. Stankov, Length scales in the convective boundary layer, *J. Atmos.*

Sci., 12, 1198-1209, 1986.

Moore, C. J. and G. Fisch, Estimating heat storage in Amazonian tropical forest, *Agric. and Forest Meterol., 38,* 147-169, 1986.

Shaw, R. H. , G. den Hartog, and H. H. Neumann, Influence of foliar density and thermal stability on profiles of Reynolds stress and turbulence intensity in a deciduous forest, *Boundary-Layer Met., 45,* 391-409, 1988.

Shaw, R. H. and I. Seginer , The dissipation of turbulence in plant canopies, 7th Symposium on Turbulence and Diffusion, American Met. Soc., Boston, MA, pp200-203, 1985.

Shuttleworth, W. J. et al., Daily variations of temperature and humidity within and above Amazonian forest, *Weather 40(4),* 102-108, 1985.

Sigmon, J. T., K. R. Knoerr, E. J. Shaughnessy, Microscale pressure fluctuations in a mature deciduous forest, *Boundary-Layer Meteorol. 27,* 345-358, 1983.

Odum, E. P. , *Fundamentals of Ecology,* W. B. Saunders, Philadelphia, 574 pp., 1971.

Press, W. H., B. P. Flannery, S. A. Teuklosky, and W. T. Vetterling, *Numerical Recipes: The Art of Scientific Computing*, Cambridge U. Press, 818 pp., 1986.

Thurston, H. D., *Tropical Plant Diseases*, American Phytopathological Society, St. Paul, Mn. 208pp., 1984.

Velleman, P. F. and D. C. Hoaglin Applications, *Basics, and Computing of Exploratory Data Analysis*, Wadsworth, 354 pp. 1981.

Whittaker, R. H., *Communities and Ecosystems*, 2nd Edition, MacMillan, N.Y. 385 pp., 1975.

Wofsy, S. C., R. C. Harriss, W. A. Kaplan, Carbon Dioxide in the atmosphere over the Amazon basin, *J. Geophys. Res. 93,* 1377-1387, 1988.

Woodwell, G. M. and W. R. Dykeman, Respiration of a forest measured by CO_2 accumulation

during temperature inversions, *Science 154,* 1031-1034. 1966.

Wyngaard, J. C., Lectures on the planetary boundary layer, in *Mesoscale Meteorology-- Theories, Observations and Models,* D. K. Lilly and T. Gal-Chen (eds.), D. Reidel, Dordrecht, the Netherlands, 1983.

Table 1. List of nights for which fast-response data are available.

Date, Time	flux events	Rn, Wm^{-2}	q_{35m}-q_{30} K	u_{45m} ms^{-1}	wave events
4/26-27, 19:00-02:30	3	--	---	.88	3
4/27-28[1] 18:40-05:50	4	-30	0.45	1.35	0
4/28-29, 17:00-02:30	--	-45	1.0	1.84	2
4/29-30 17:00-06:00	7	-35	1.1	1.86	7
5/2-3[1] 19:00-05:00	8	-40(w)[2] -15(t)	1.0(w) 0.5(t)	1.52	3
5/4-5 17:00-04:20	7	-45	0.8	2.22	7
5/5-6 00:57-12:06	5	-40	1.0	1.95	3
5/6-7[1] 17:00-05:00	5	-40	0.5	1.75	1
5/7-8 17:00-23:20	4	-30	0.6	1.80	4
5/8-9 17:00-04:15	10	-45	1.0	1.97	1

[1] nights when above-canopy flux was not associated with wave activity at the 25 m level.

[2] waves occurred earlier in the evening, but turbulence without discernable waves predominated later.

Table 2. Characterization of CO2 flux events using the criteria described in the text. Total and average fluxes are given in ppm-10^{-2}m/s.

Date	# events	measured flux in events	measured flux total	avg. length of time	mean/ event	time fraction
4/26-27	3	334	447	38 mins	14.5	18%
4/27-28	6	1353	1494	61	22.2	54%
4/29-30	4	292	651	26	13.9	16%
5/2-3	6	1173	1332	33	35.6	25%
5/4-5	7	879	1105	47	13.3	66%
5/6-7	5	1492	1688	59	25.7	44%
5/7-8	4	275	376	31	11.0	32%
5/8-9	5	277	58	25	11.1	21%

Figure Captions

Figure 1. For the night of April 27-28:

A. Time-height sections of virtual potential temperature derived from the tower data. The 301 (left) and 299 (right) isotherms are bold. The contour interval is 0.2K.

B. Net Radiation (Wm^{-2}).

C. CO2 flux (ppm-cm/s).

D. Heat flux (Wm^{-2}) at 39 m (solid line) and 25 m (dashed line).

Figure 2. Same as Figure 1, but for May 2-3. Rain began at 02:00. The 301 and 300 isotherms are bold.

Figure 3. Same as Figure 1, but for May 4-5. Resonant waves in the canopy were observed on this night. The 301 and 299 isotherms are bold.

Figure 4. Same as Figure 1, but for May 8-9. Resonant waves in the canopy were observed on this night. The 301 and 303 isotherms are bold.

Figure 5. Gradient Richardson number over time on May 2-3. Ri is plotted on a log scale. Horizontal line is drawn at Ri=0.25.

Figure 6. Time series of one-second-averages 10 herz data from the 45 m gill anemometer (*u* and phi, top), 39- m *w* (middle) and 25 m *w* (bottom), showing oscillations developing as windspeed at 45 m goes over 2 m/s.

Figure 7A. Heat and moisture fluxes (ms^{-1}-K, ms^{-1}-gkg^{-1}) associated with a canopy wave event on the morning of May 9. Solid lines are heat fluxes, dotted are moisture. Vertical bars indicate standard error of the mean.

B. CO2 flux at 39 m during same event as in A.

Figure 8. Autocorrelation functions for 39 m and 25 m vertical velocity signals on May 4 at 23:00.

Figure 9. Mean power spectra for 39 m and 25 m vertical velocity over the night of May 8-9. Inertial subrange (-2/3) and buoyancy range (-2) slopes are illustrated.

Figure 10. A Contour plot of smoothed 25 m vertical velocity power spectra over time, on May 4-5. Solid line is the buoyancy frequency (N) computed in the 35 to 23 m layer. Inertial subrange is indicated by bar at left.

B. as in A, for May 8-9.

C. 39 m w,T cospectrum contour plot on May 8-9 . Heat flux above canopy is associated with the power spectrum peaks below canopy shown in B.

Figure 11. Plot of the buoyancy frequency vs. wind speed during the wave event on the morning of May 9. Local time is indicated. The time of maximum flux is indicated by the star.

Figure 12. Profiles of potential temperature at the start (0248 LST) and near the end (asterisks, 0330) of the canopy mixing event o May 9 shown in Fig. 6. Definitions of the model parameters Δh (thickness of the canopy inversion) and $\Delta\Theta$ (the temperature difference across the inversion) are also illustrated.

Figure 13. Results of the canopy mixing model. At top, the cahnge in dimensionless evironmental parameters is shown, varying with the dimensionless time ($t = t/\sigma_t$). U_a is the wind speed at canopy top, scaled by its constant initial background value, Δh is the thickness of the canopy inversion, scaled by its initial value, and $\gamma = \Delta\Theta/\Delta h$. Results for two values of the dimensionless drag coefficient are shown: γ_1 corresponds to $C_1 = 2.4$; γ_2 corresponds to $C_1 = 1.1$. The other parameters used are $C_2 = 4752$, $C_3 = 8640$, and $C_4 = 0.005$. The two lower panels show the modelled perturbation vertical velocity, w, and potential temperature, θ, corresponding to the forcing and environment consistent with that shown above. Scaling of these quantities depends linearly on the assumed value of the amplitude of the perturbation pressure gradient forcing, C_3.

Figure 14. A. Fraction of total CO2 flux measured on the night of May 4-5 by windspeed category (m/s).

B. As in A, except for May 8-9.

Figure 15. Maximum CO2 concentration observed in the early morning as function of the fraction of time during the previous night that the windspeed at 45 m was greater than 1.75 m/s. Plotted points are designated by the date of the morning CO2 concentration.

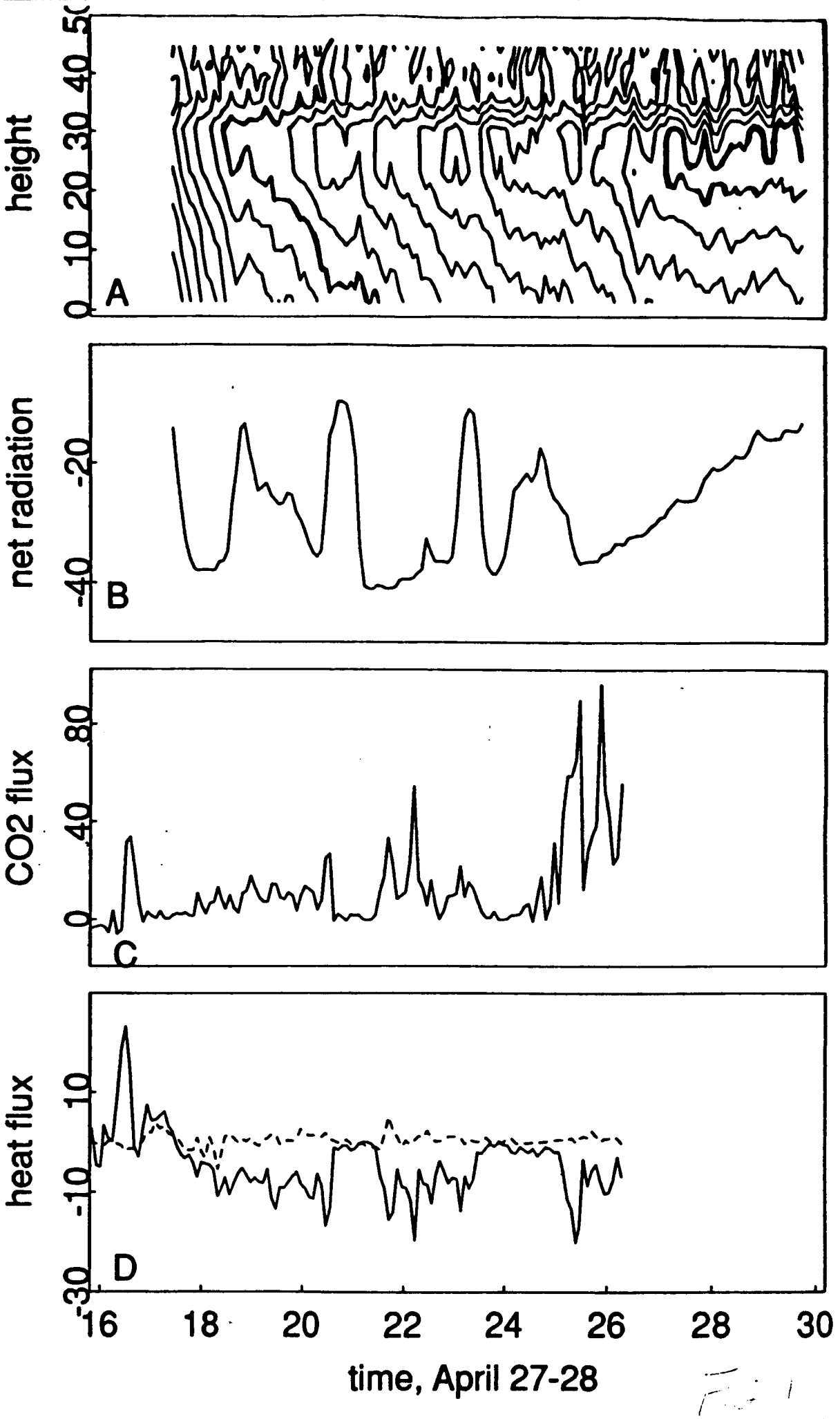
height
0
10
20
30
40
A
net radiation
-20
-40
B
CO2 flux
0
40
80
C
heat flux
10
-10
-30
D
16
18
20
22
24
26
28
30
time, April 27-28

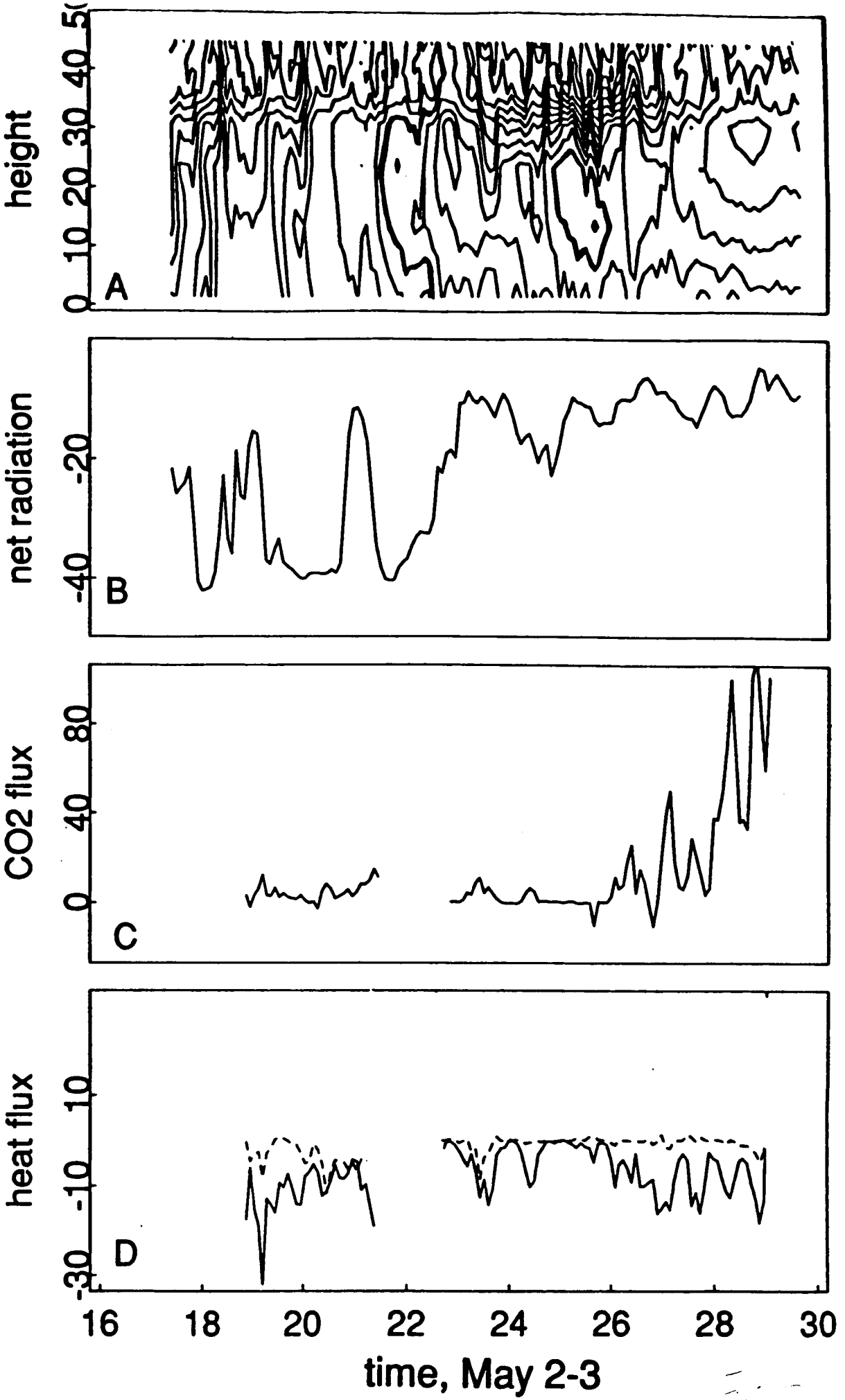
height
0
10
20
30
40
A
net radiation
-40
-20
B
CO2 flux
0
40
80
C
heat flux
-30
-10
10
D
16
18
20
22
24
26
28
30
time, May 2-3

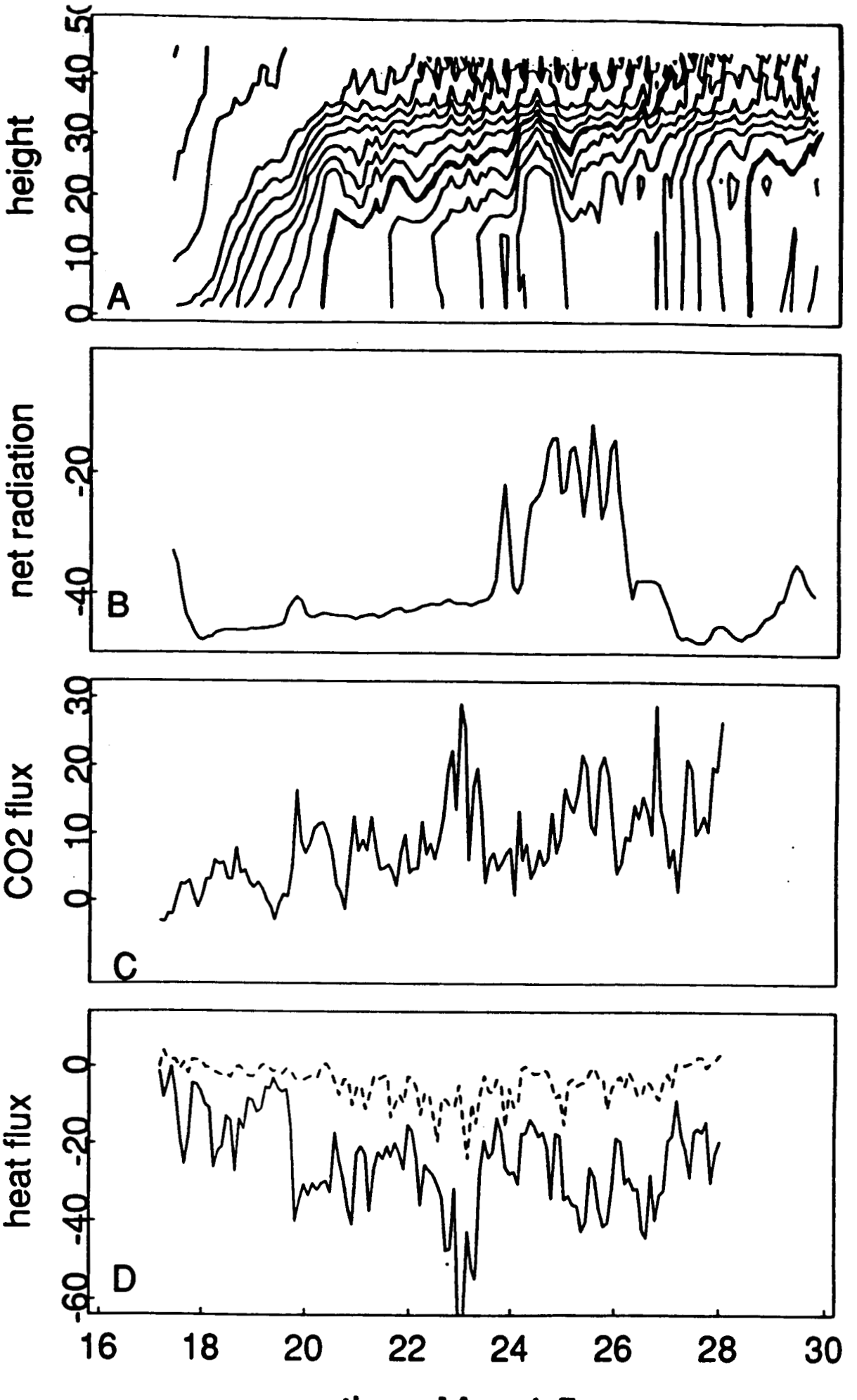
height
0 10 20 30 40 5(
A
net radiation
-20
-40
B
CO2 flux
0 10 20 30
C
heat flux
0
-20
-40
-60
D
16 18 20 22 24 26 28 30
time, May 4-5

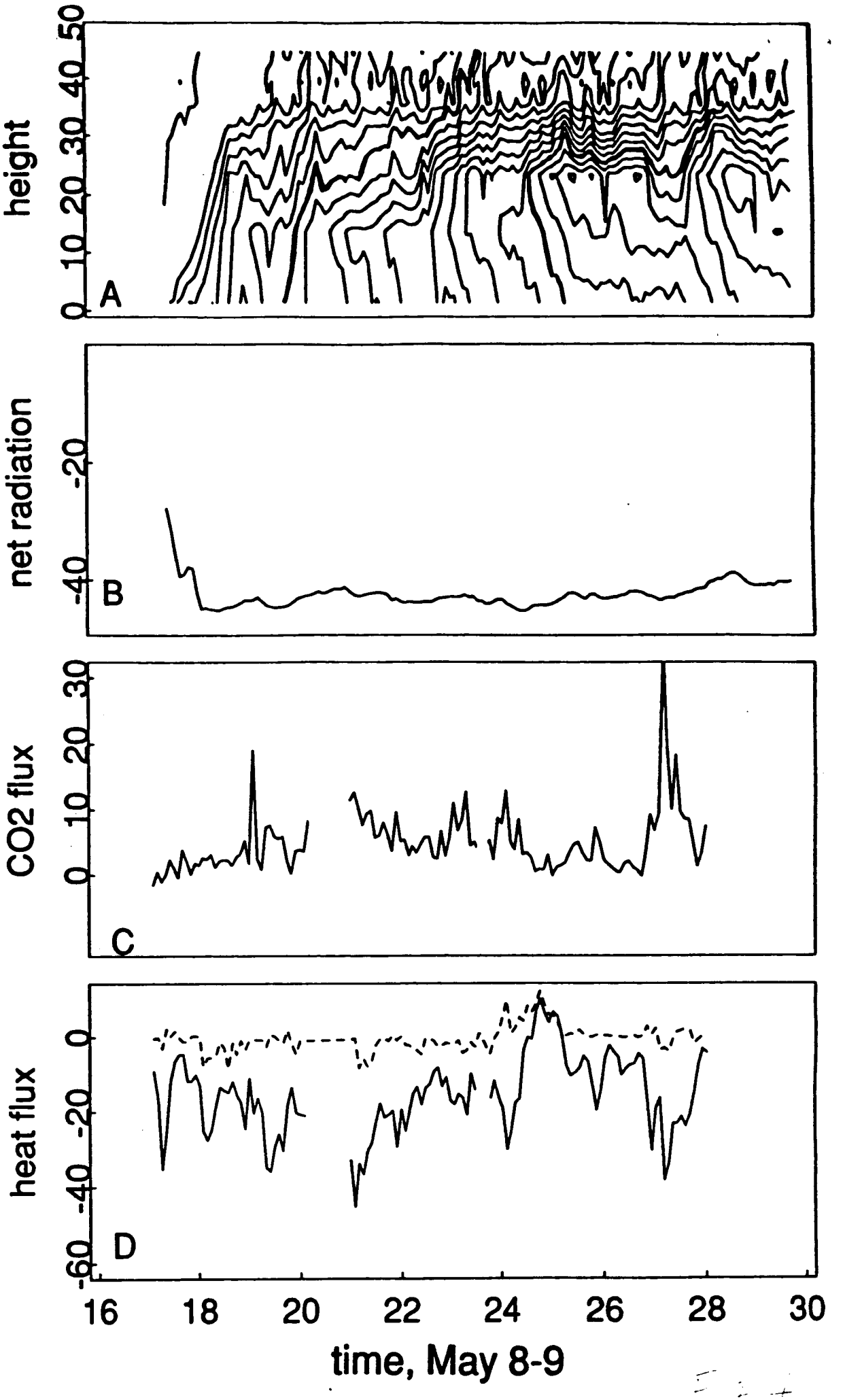
height
0 10 20 30 40 50
A
net radiation
-20
-40
B
CO2 flux
0 10 20 30
C
heat flux
0 -20 -40 -60
D
16 18 20 22 24 26 28 30
time, May 8-9

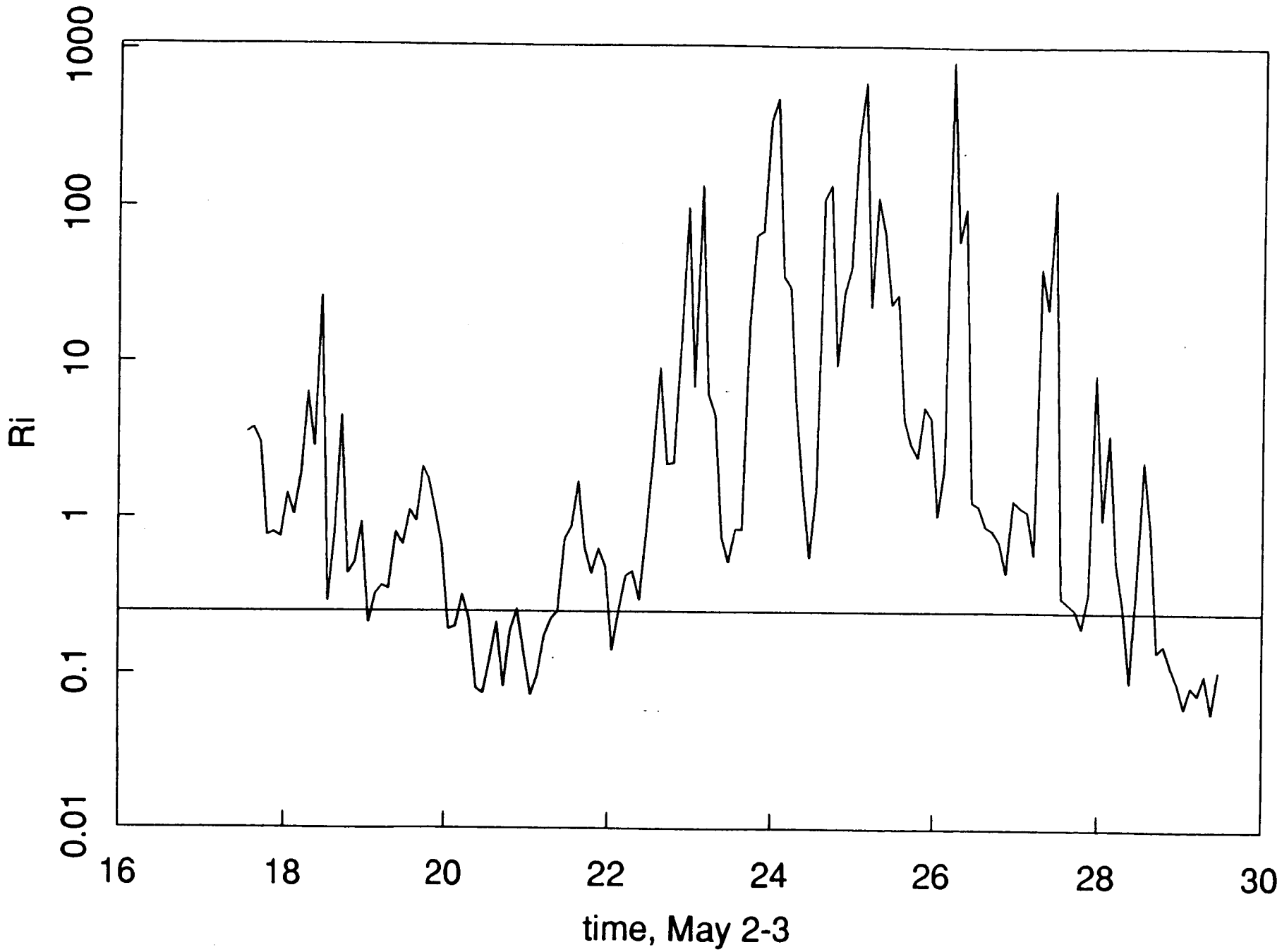

Fig. 5

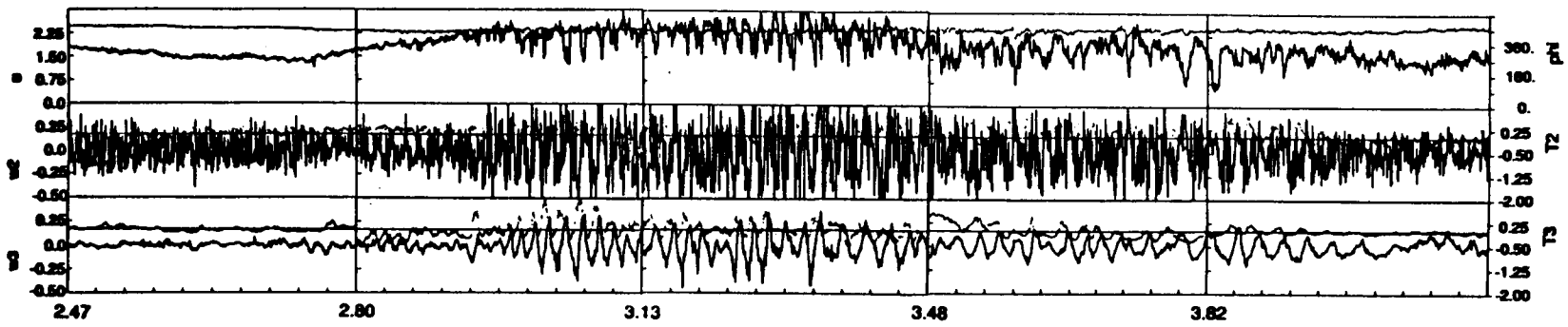
2.25
1.50
0.75
0.0
0.25
0.0
-0.25
-0.50
0.25
0.0
-0.25
-0.50
360.
180.
0.
0.25
-0.50
-1.25
-2.00
0.25
-0.50
-1.25
-2.00
T1
T2
T3
2.47
2.80
3.13
3.48
3.82

FIG. C

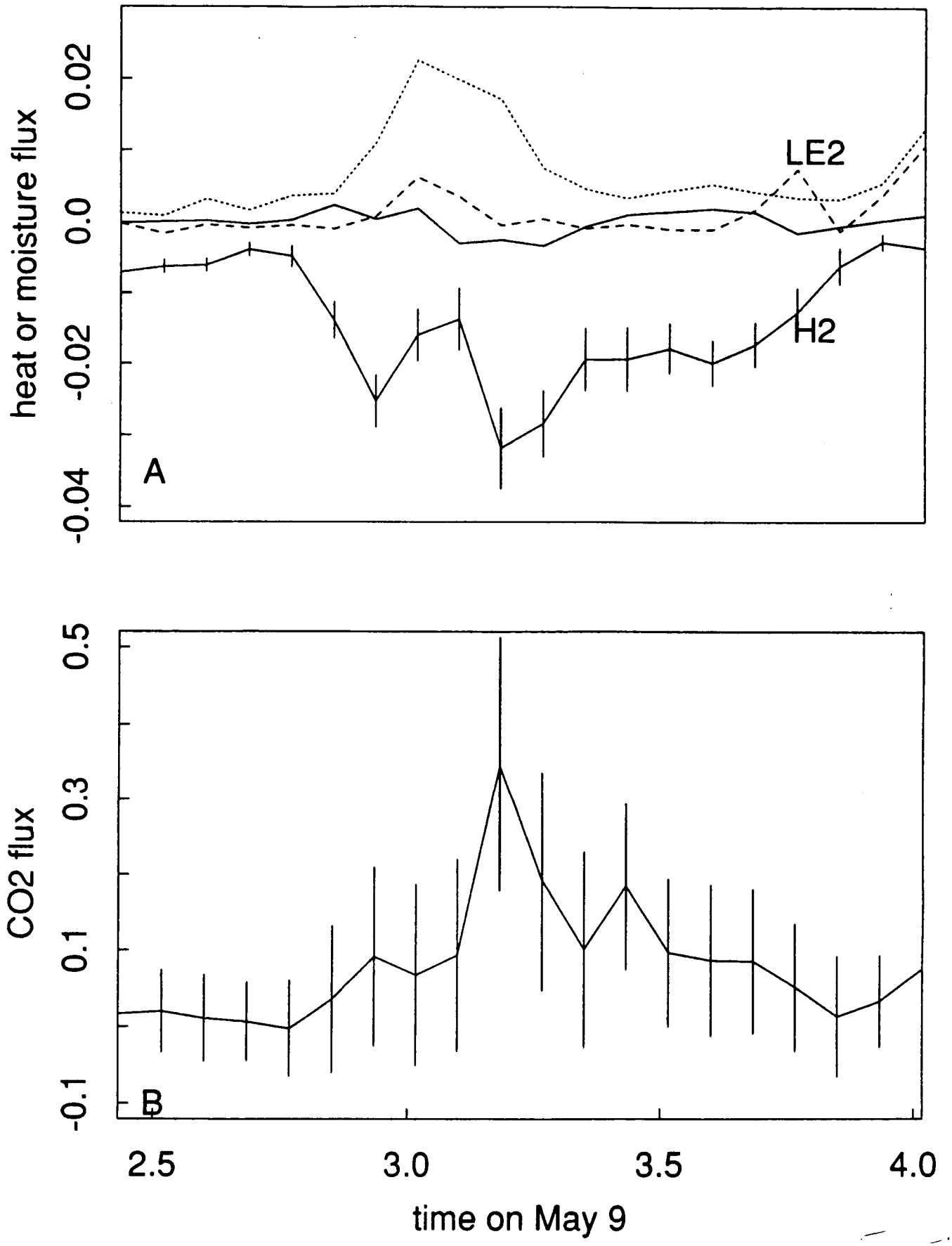
heat or moisture flux
0.02
0.0
-0.02
-0.04
LE2
H2
A
CO2 flux
0.5
0.3
0.1
-0.1
B
2.5
3.0
3.5
4.0
time on May 9

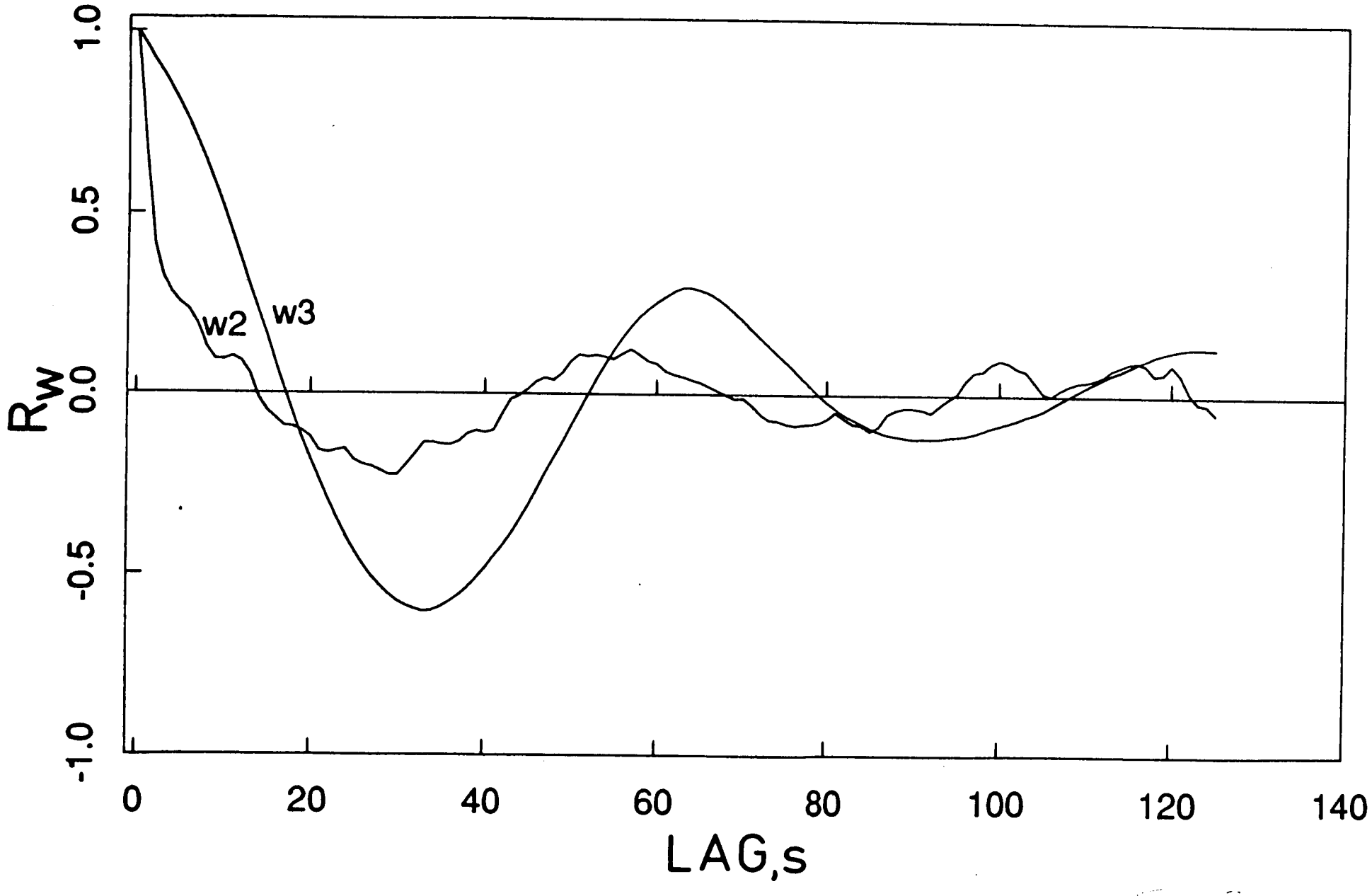
1.0
0.5
0.0
-0.5
-1.0
R_W
w2
w3
0
20
40
60
80
100
120
140
LAG,s

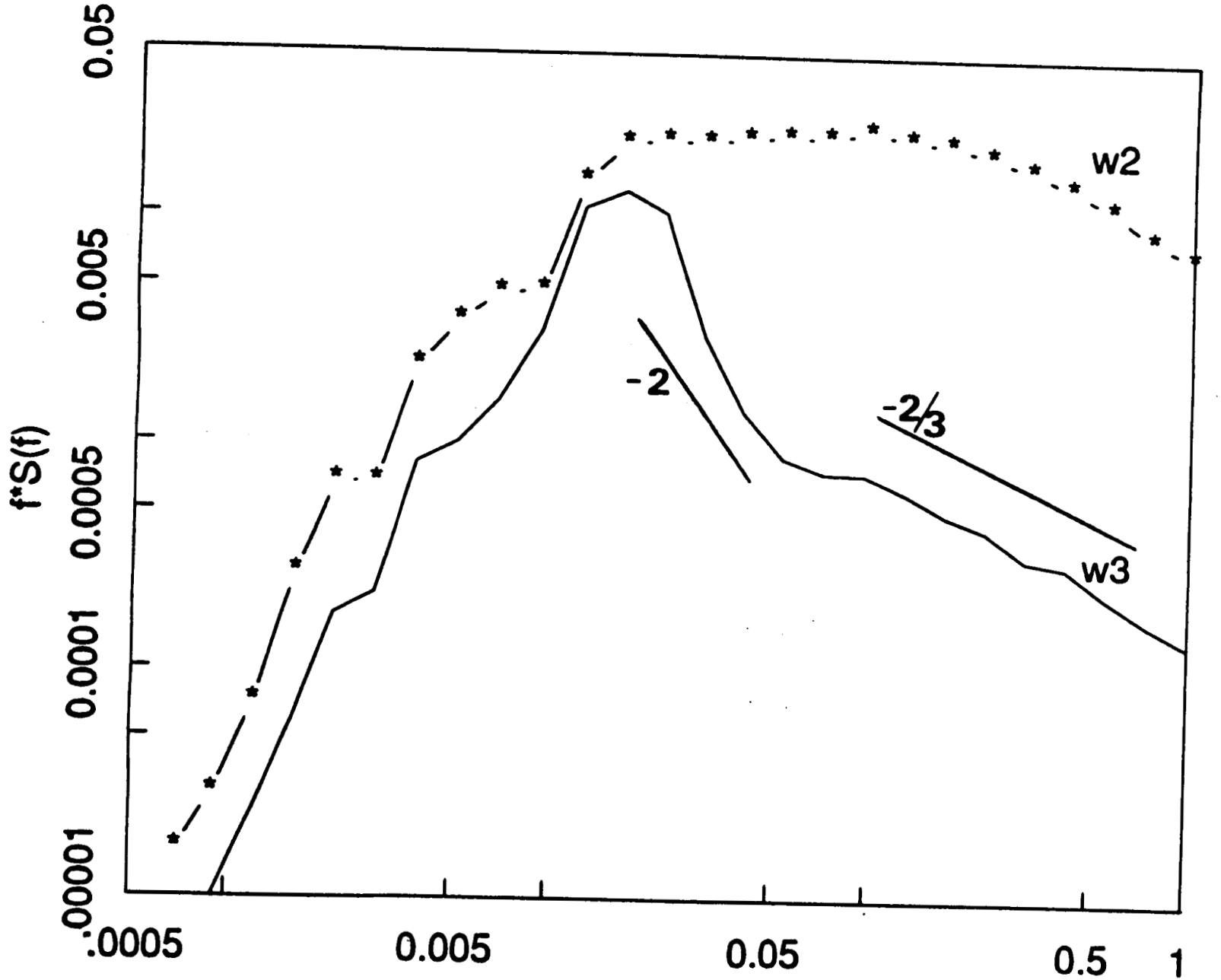

Fig. 9

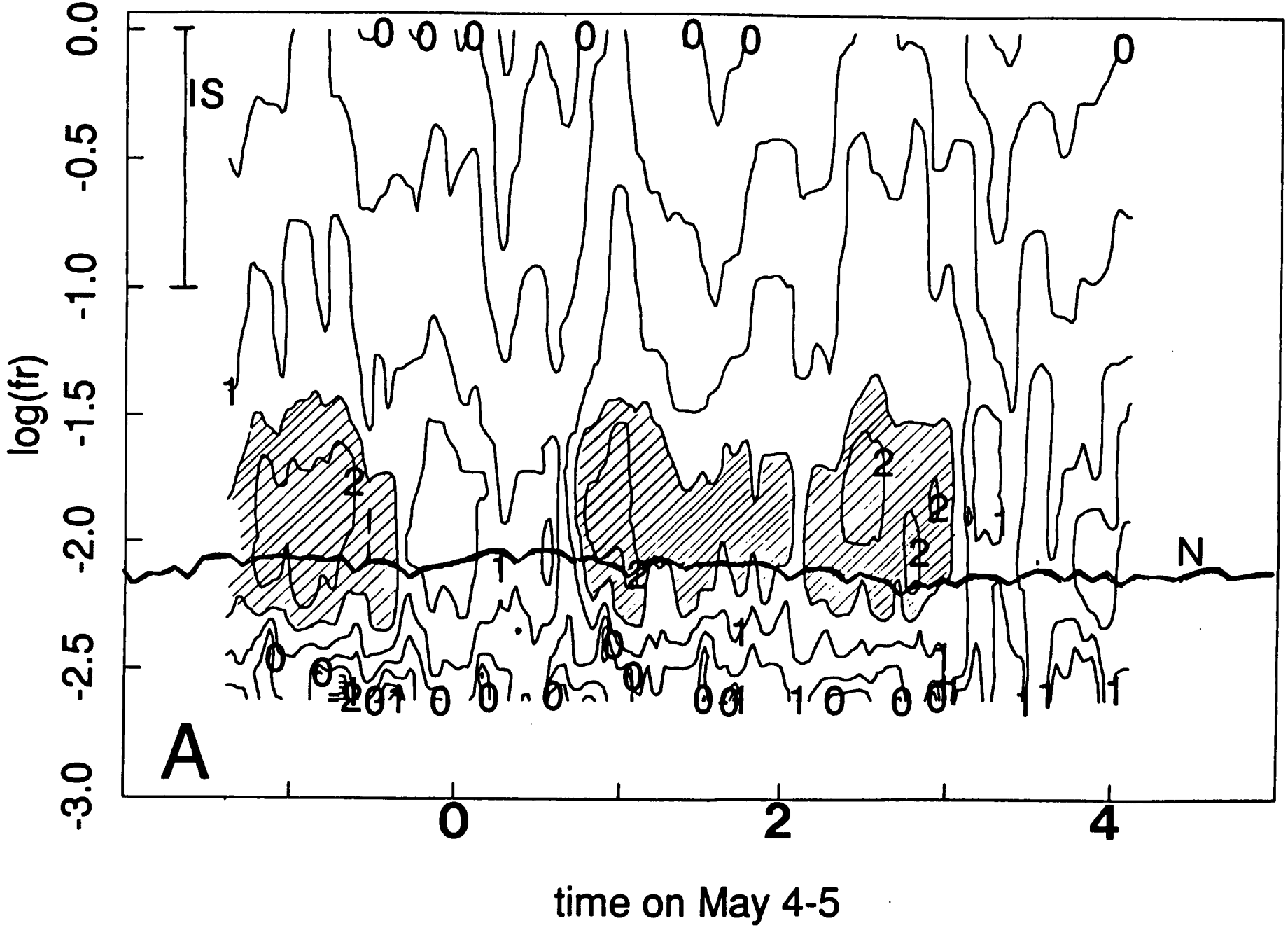
log(fr)
0.0
-0.5
-1.0
-1.5
-2.0
-2.5
-3.0
1S
N
A
0
2
4
time on May 4-5

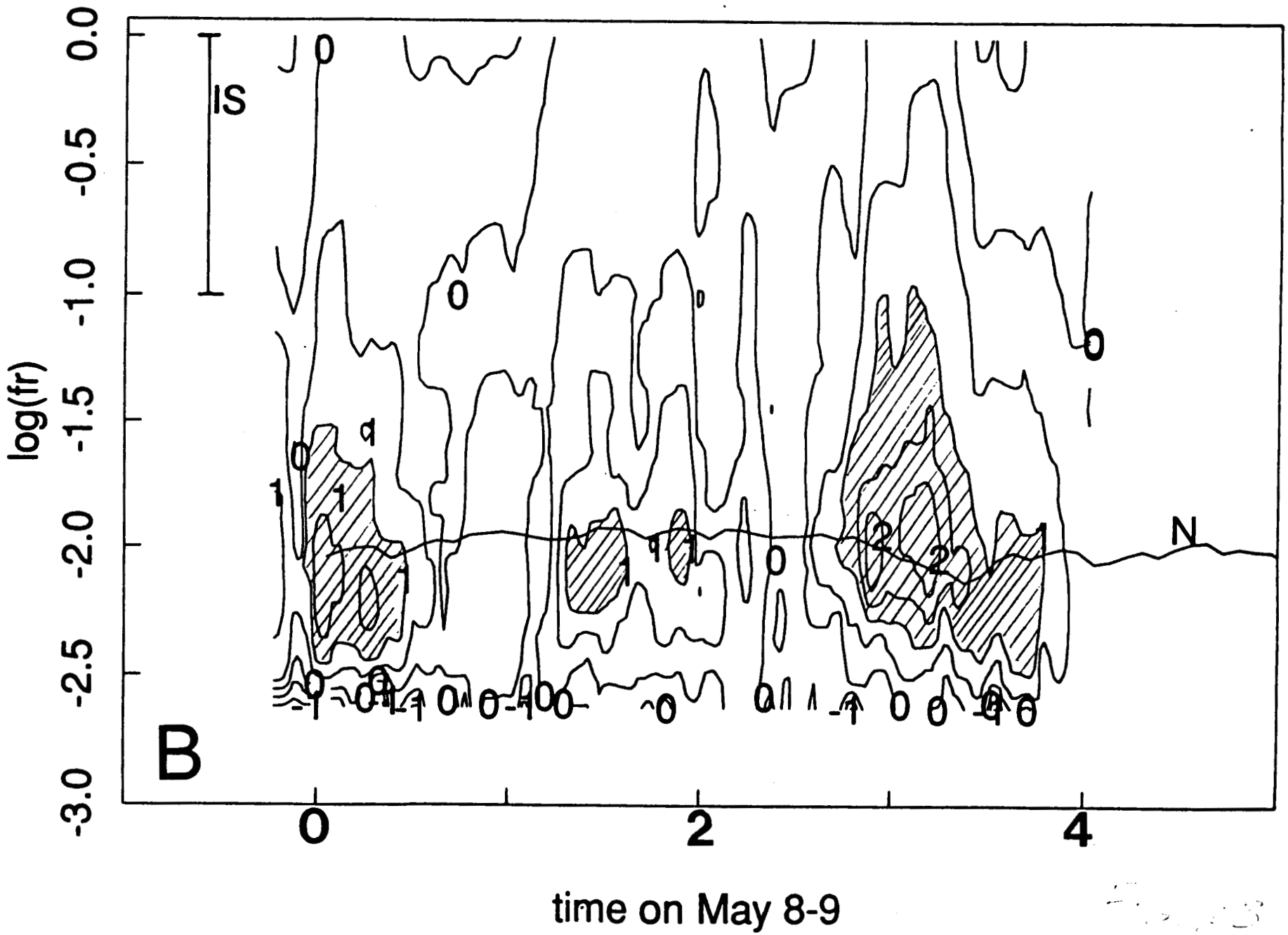
log(fr)
0.0
-0.5
-1.0
-1.5
-2.0
-2.5
-3.0
0
2
4
time on May 8-9
B
S
N

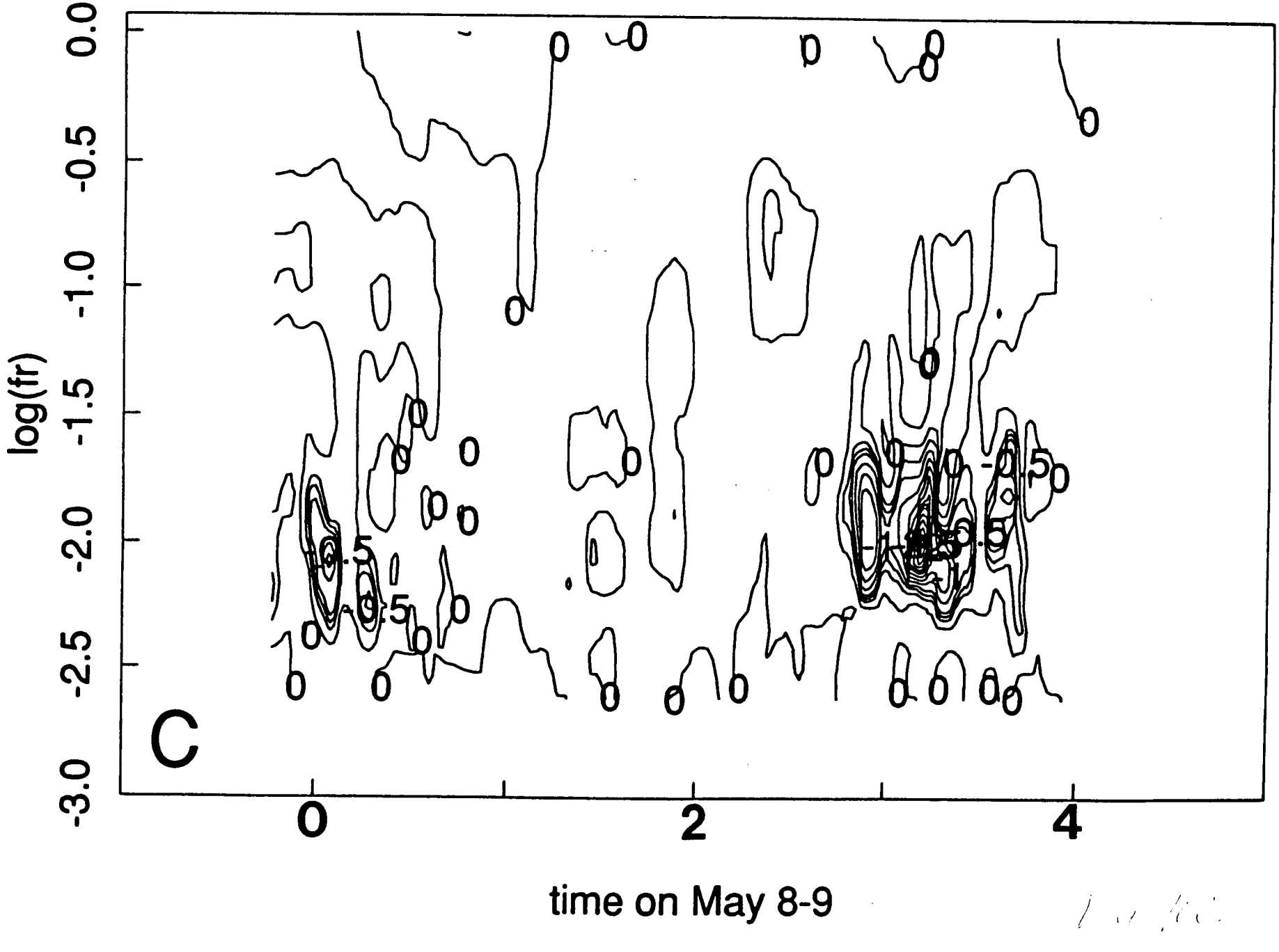
log(fr)
0.0
-0.5
-1.0
-1.5
-2.0
-2.5
-3.0
0
2
4
time on May 8-9
C

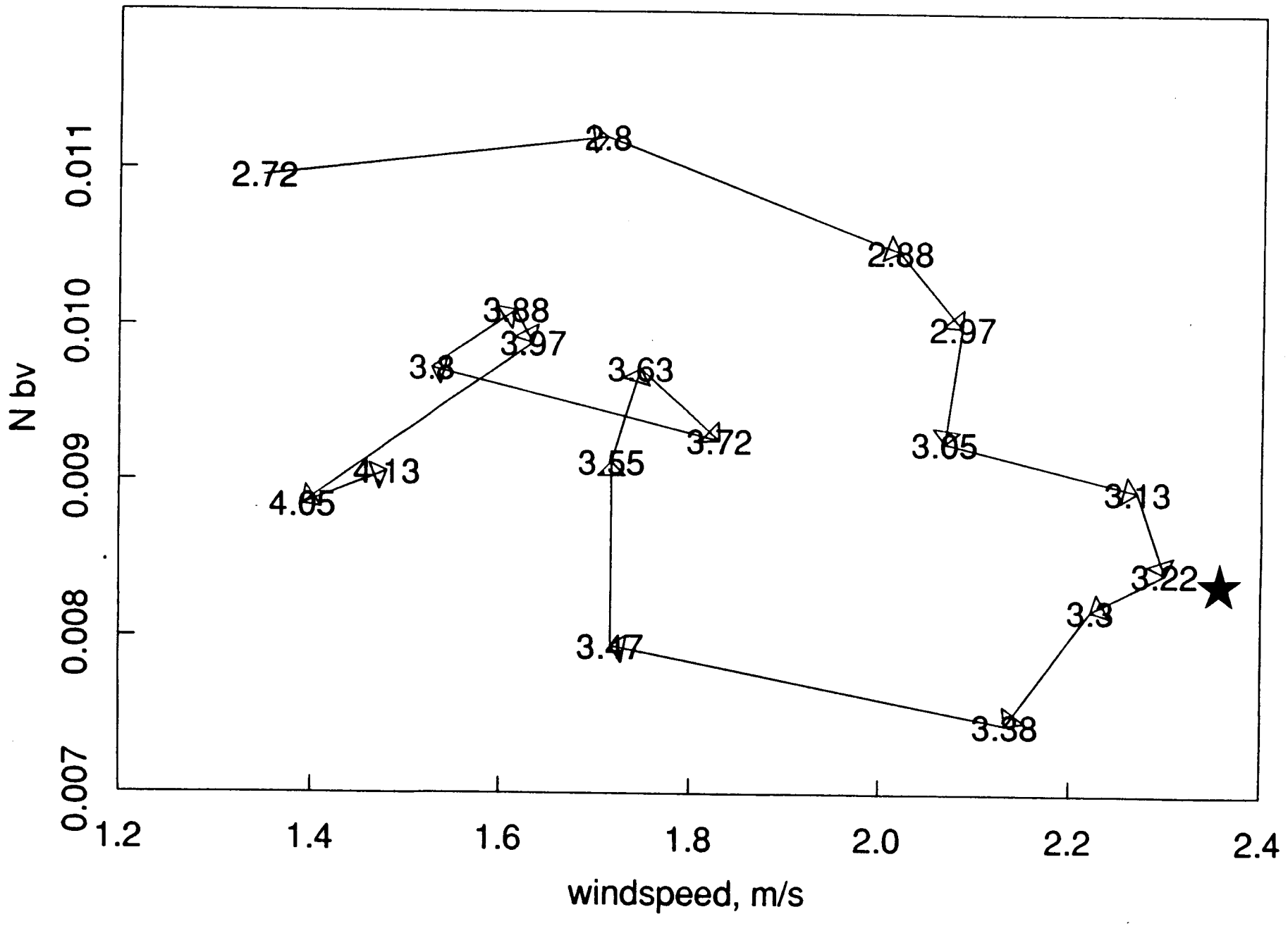
N bv
0.007
0.008
0.009
0.010
0.011
1.2
1.4
1.6
1.8
2.0
2.2
2.4
windspeed, m/s
2.72
2.8
2.88
2.97
3.05
3.13
3.22
3.38
3.47
3.55
3.63
3.72
3.88
3.97
4.13
4.65

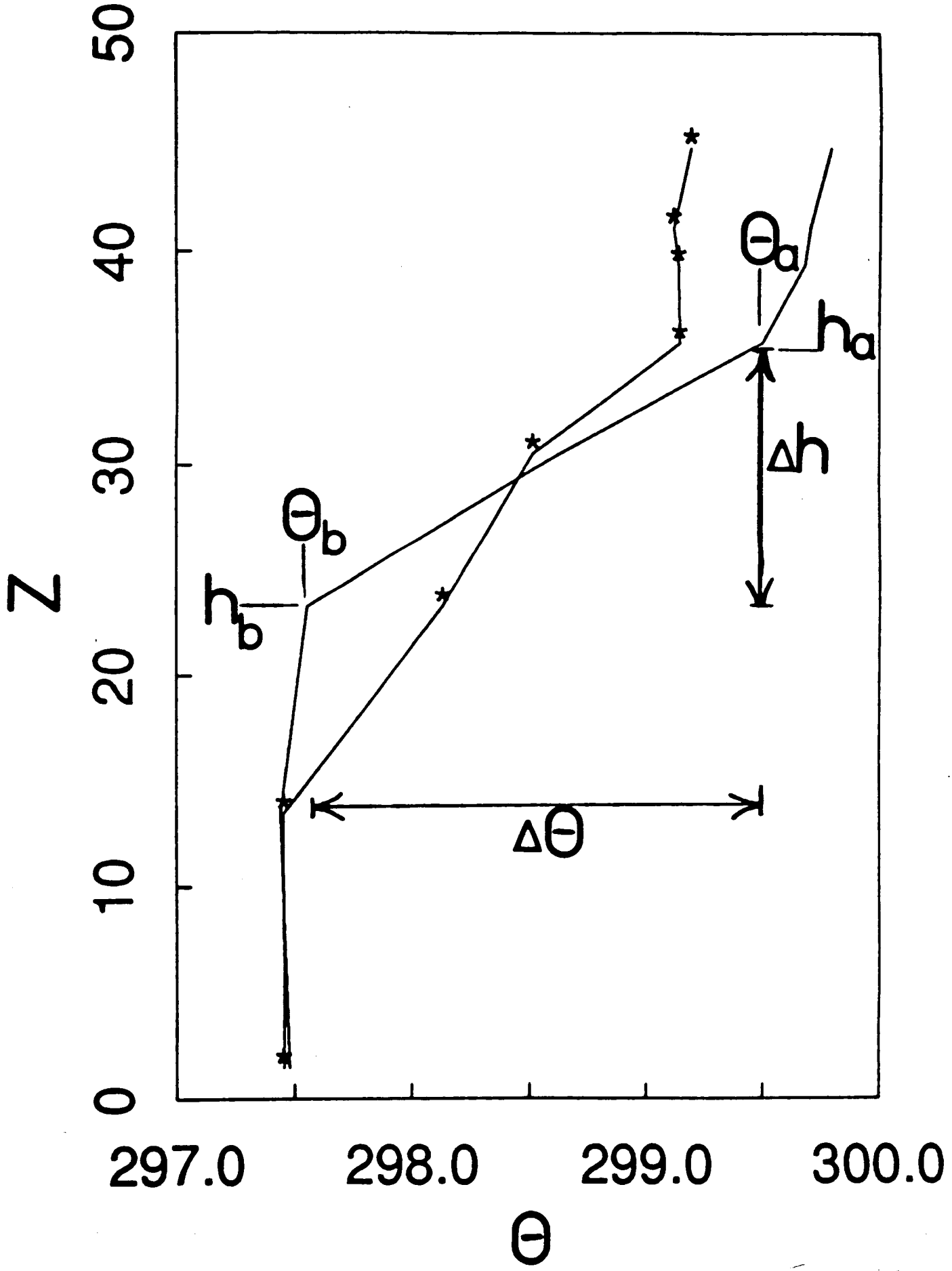
50
40
30
20
10
0
Z
297.0
298.0
299.0
300.0
θ
θa
ha
Δh
θb
hb
Δθ

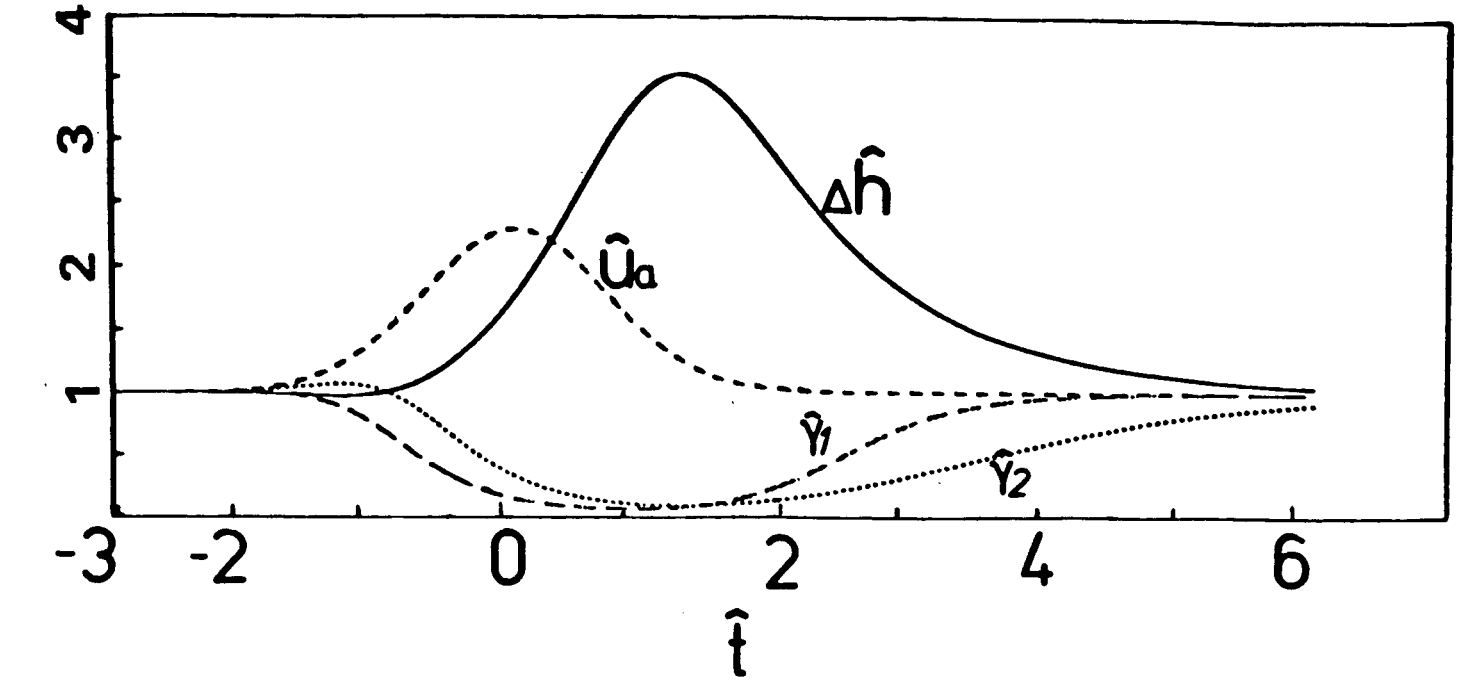
4
3
2
1
$\Delta\hat{h}$
$\hat{U}_a$
$\hat{\gamma}_1$
$\hat{\gamma}_2$
-3
-2
0
2
4
6
$\hat{t}$

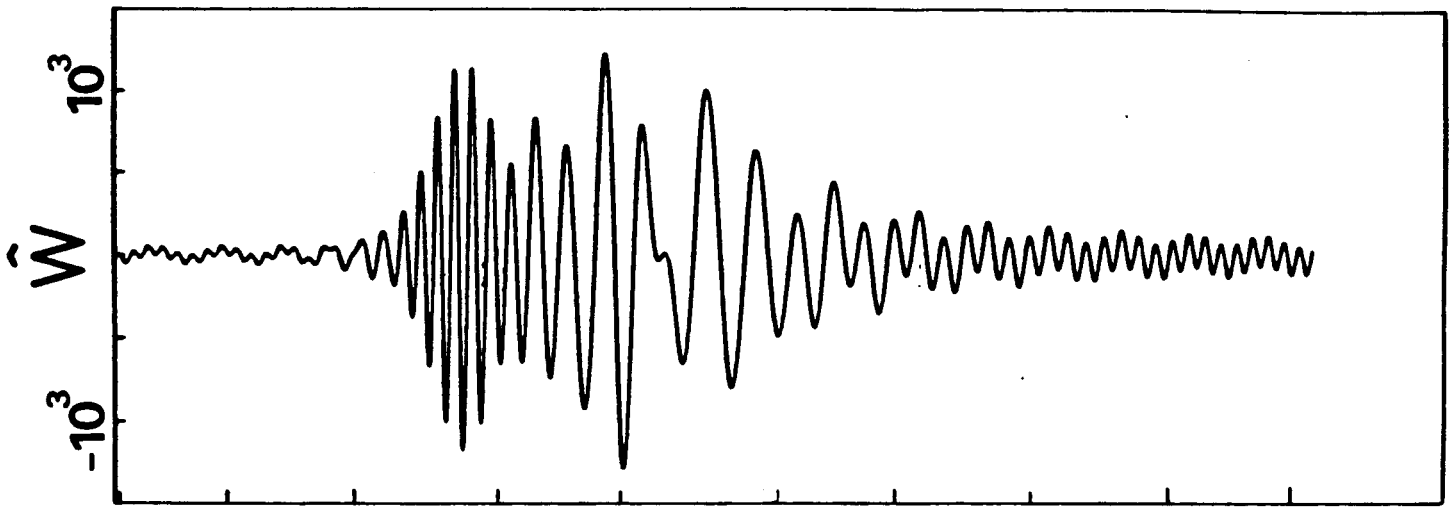
$\hat{W}$
10^3
-10^3

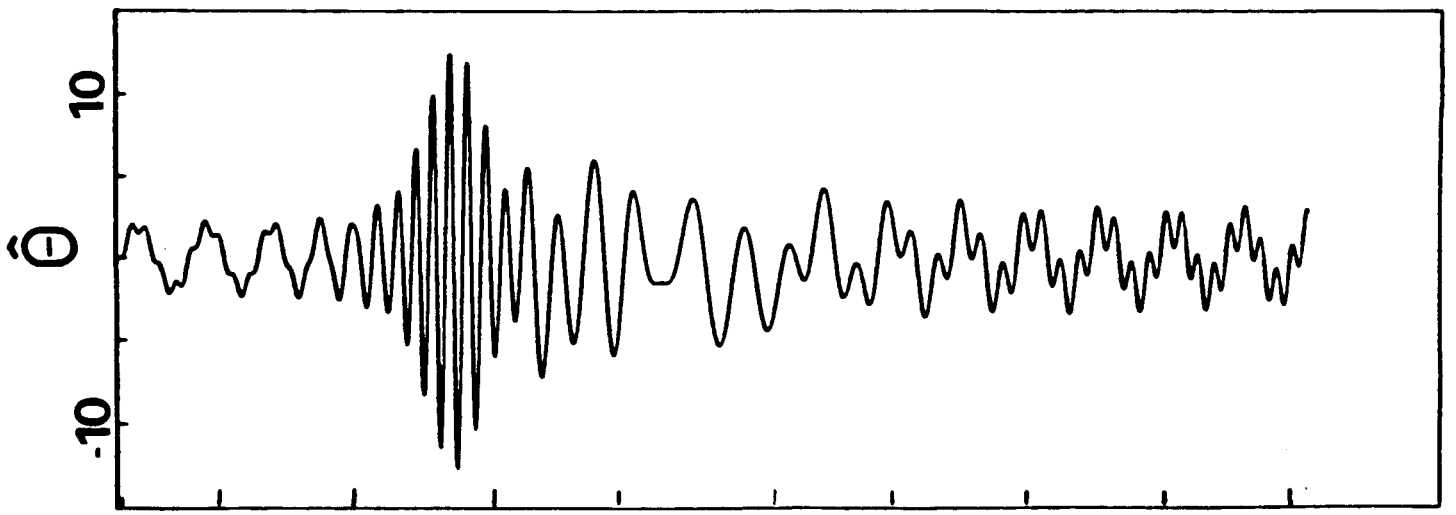
$\hat{\Theta}$
10
-10

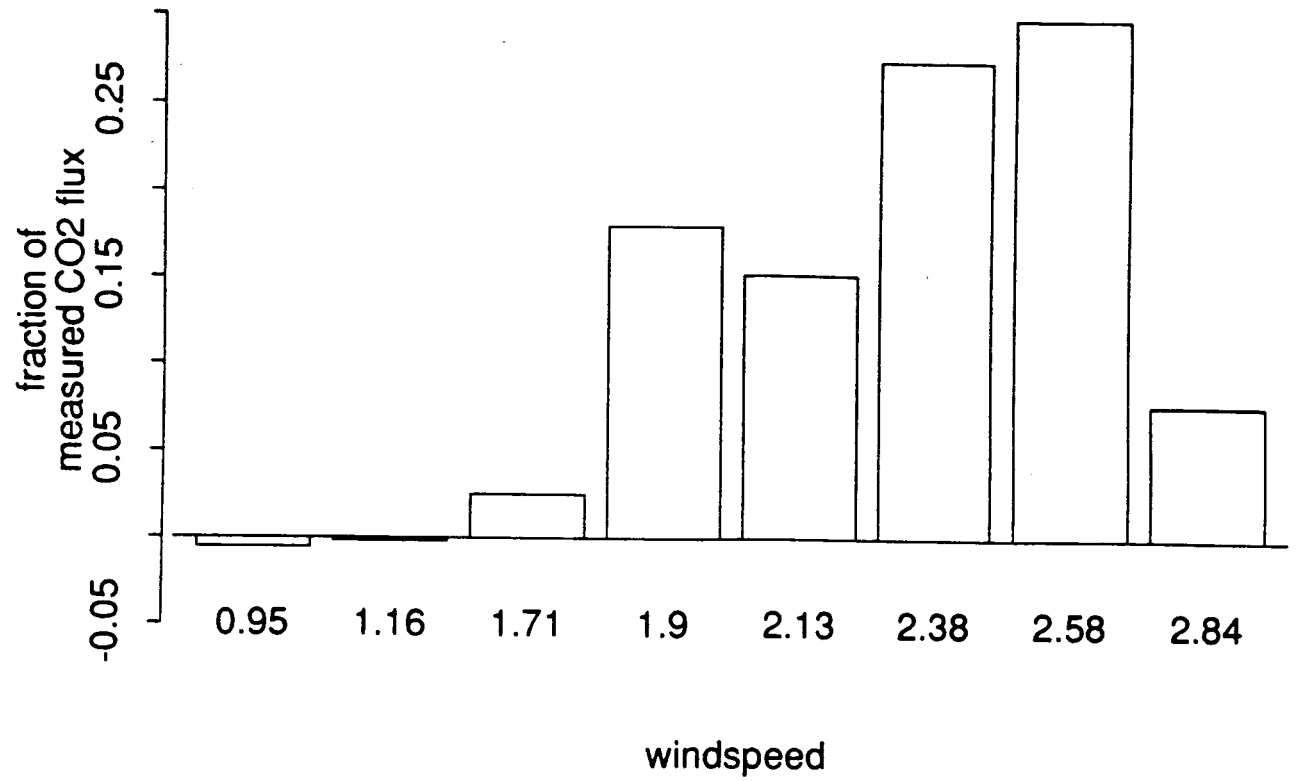
fraction of measured CO2 flux
-0.05
0.05
0.15
0.25
0.95
1.16
1.71
1.9
2.13
2.38
2.58
2.84
windspeed

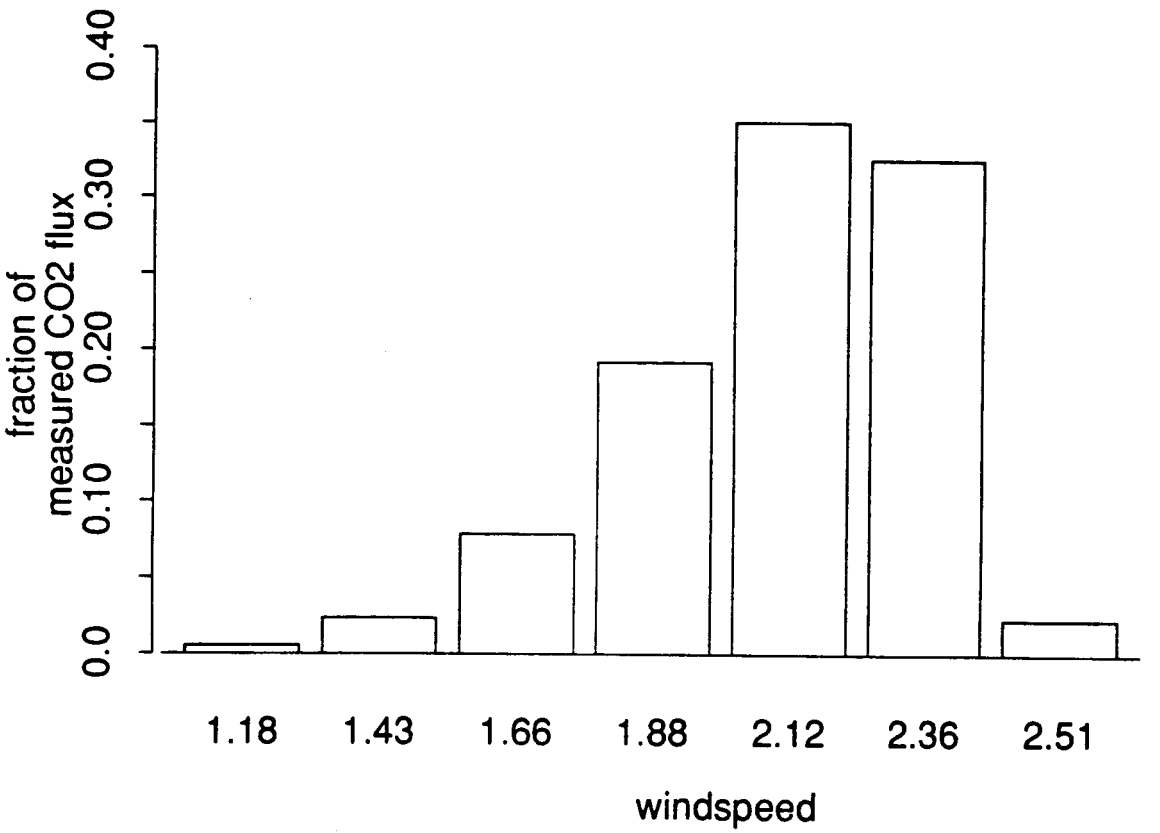
fraction of measured CO2 flux
0.0
0.10
0.20
0.30
0.40
1.18
1.43
1.66
1.88
2.12
2.36
2.51
windspeed

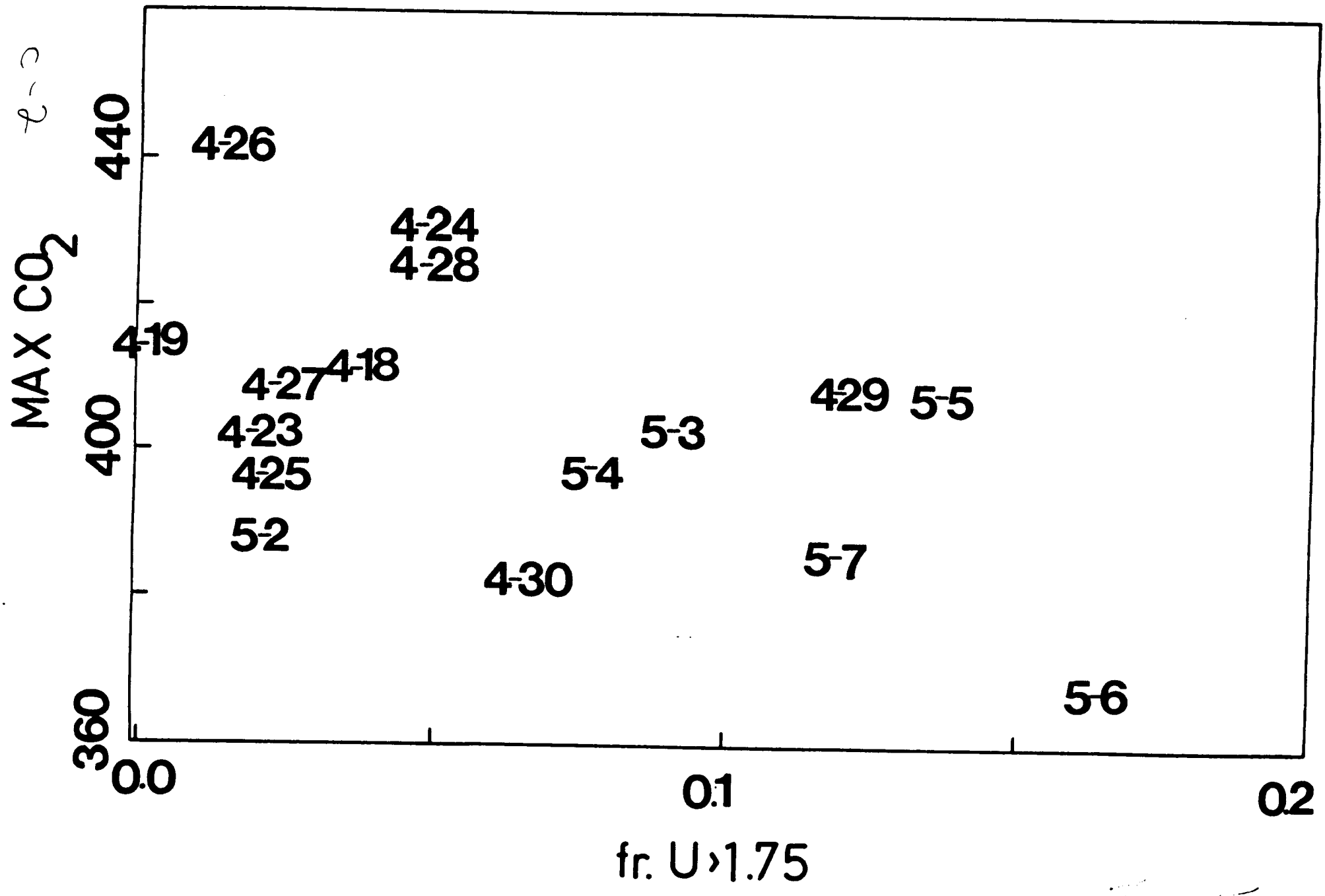
MAX CO_2
440
400
360
0.0
0.1
0.2
fr. U>1.75
4-26
4-24
4-28
4-19
4-18
4-27
4-23
4-25
5-2
4-30
5-4
5-3
4-29
5-5
5-7
5-6